UNIVERSIDAD AUTONOMA DE MADRID

Facultad de Ciencias

Departamento de Biología Molecular

Reconstitution of redox enzymes on gold electrodes mimicking their natural environment

Óscar Gutiérrez-Sanz

Madrid, 2014

Departamento de Biología Molecular

Facultad de Ciencias

Reconstitution of redox enzymes on gold electrodes mimicking their natural environment

Institute of Catalysis and Petrochemistry

Spanish Council for Scientific Research (CSIC)

Óscar Gutiérrez-Sanz (Ldo. Bioquímica)

Director: Dr. Antonio López de Lacey

Madrid, 2014

ANTONIO LÓPEZ DE LACEY, DR. EN CIENCIAS QUÍMICAS, INVESTIGADOR CIENTÍFICO DEL C.S.I.C EN EL INSTITUTO DE CATÁLISIS Y PETROLEOQUÍMICA

CERTIFICA: Que el presente trabajo "Reconstitution of redox enzymes on gold electrodes mimicking their natural environment", que constituye la Memoria que presenta el Licenciado en Bioquímica por la Universidad de Córdoba, Óscar Gutiérrez Sanz, ha sido realizado bajo su dirección en el Departamento de Biocatálisis del Instituto de Catálisis y Petroleoquímica del C.S.I.C., Campus de Excelencia Internacional UAM + CSIC, Madrid.

Para que conste, firma el presente certificado a 27 de Noviembre de 2014.

Dr. Antonio López de Lacey

Agradecimientos

Quisiera organizar este pequeño apartado por orden cronológico.

Por eso, empezaré dando las gracias a Eva Pérez por sus múltiples consejos, todos los buenos momentos y por acercarme al grupo de investigación del Dr. Conrado Moreno, quién me ofreció la primera oportunidad de participar en un proyecto de investigación, muchas gracias. De esta manera, entré a formar parte de mi primera pequeña familia científica, en la que he de agradecer a Lola, Víctor, Lara, Isa, Jesi y Mari Paz todo el tiempo que dedicaron a enseñarme y su amistad.

Quisiera agradecer al Dr. Antonio López de Lacey, la oportunidad de poder llevar a cabo la presente tesis doctoral. Ha sido un verdadero placer realizarla bajo la dirección de un gran científico y buen maestro. Muchísimas gracias. A Cris Gutiérrez, quien me adoptó al llegar a Madrid, por todo (son muchas cosas las que agradecerte). A Marcos Pita, gracias por todos los consejos y discusiones científicas así como los buenos ratos en los cafés. Al Dr. Víctor M. Fernández por enseñarme la historia de cómo llegaron todos los instrumentos al laboratorio y por su constante simpatía y buenas palabras. A todos los amigos que me he ido encontrando por el camino; Álvaro I y II, Ile, Musta, Lucía, Bárbara, Mónica, Marco, Caio, Nieves, David, Óscar, Rafa, Jesús, Bernardo, Gofu, Paco, Ana, Marta, Isa, Cris, Chiara, José, Esteban, Alejandro, María, Lara, Asier y un largo etcétera.

De mis estancias en el extranjero me gustaría agradecer a Marta Marques, Dr. Inês Pereira, Dr. Olaf Rüdiger, Dr. Manuela Pereira, Dr. Ana Batista, Profesor Lubitz, Dr. Ingo Zebger y al Profesor Hildebrandt todas las discusiones científicas y su gran hospitalidad.

Para terminar, y rompiendo el prometido orden cronológico, quería agradecer a Carmen el haberme tirado a la cara una solución de cobalto nada mas conocernos. Ha sido el mejor “accidente” de laboratorio que he tenido nunca. Gracias por no dejarme pasar un solo día sin reírme. Y como no, a mi familia, que gracias a su apoyo y cariño han hecho que la distancia nunca haya sido una barrera.

Muchas gracias a todos

Summary

The interface between artificial and living world has been for many years a source of inspiration of many ideas. The goal of bionanoelectronics is to achieve a superior functionality with a device combining man-made and biological machines. Redox enzymes are ideal to reach this purpose as their activity can be controlled and measured electrochemically when they are immobilized on electrodes. The methodology of globular proteins immobilization has advanced much faster than the one for membrane proteins, in which their natural environment is mimicked on electrodes. In this sense, this thesis has been focused in the functional and oriented immobilization of membrane proteins on electrodes in supported phospholipid bilayers. Two related membrane enzymes have been used for this purpose: the membrane-bound NiFeSe hydrogenase from *Desulfovibrio vulgaris* and the Respiratory Complex I from *Rhodotermus marinus*.

The isotopic H/D exchange activity of the hydrogenase has been studied by mass spectrometry in this thesis. The conclusion from this work is that the protein structure surrounding the active site modulates its catalytic function, which is in agreement with the so called "cage effect". Then, a characterization by SEIRAS combined with electrochemistry of two different configurations of its immobilization on an electrode with a supported phospholipid bilayer was performed. This study together with a previous characterization by AFM allowed to choose the most suitable configuration for creating and controlling electro-enzymatically a proton gradient in the bilayer/electrode interface.

Respiratory Complex I performs two different activities: electron and proton transport across the cellular membrane. Here it is presented the first functional reconstitution of this enzyme on a gold electrode embedded in a supported phospholipid bilayer. This construction has been characterized by AFM, Impedance Spectroscopy and by SEIRAS combined with electrochemistry.

The reconstitution of CpI and the membrane bound NiFeSe hydrogenase mimicking their natural environments on electrodes may open new doors to possible future applications.

Resumen

La unión de lo artificial y lo orgánico ha sido y sigue siendo una fuente de inspiración de muchas ideas. El objetivo de la bionanoelectrónica es lograr una funcionalidad superior con un dispositivo en el que se combine una parte biológica y otra fabricada por el hombre. Las enzimas redox son ideales para alcanzar este propósito gracias a que su actividad puede ser controlada electroquímicamente si se inmovilizan en electrodos. En este campo, la metodología referente a la inmovilización de proteínas hidrosolubles ha avanzado más rápido que la metodología para inmovilizar proteínas de membrana en electrodos. Siendo esto así, la presente tesis se ha centrado en la inmovilización funcional y orientada de proteínas de la membrana en electrodos utilizando bicapas fosfolipídicas soportadas. Dos proteínas de membrana han sido utilizadas para este propósito. la hidrogenasa NiFeSe de *Desulfovibrio vulgaris* y el Complejo Respiratorio I de *Rhodotermus marinus*.

Un primer estudio de la actividad de intercambio isotópico de la hidrogenasa NiFeSe por espectrometría de masas ha permitido concluir que la estructura de la proteína que rodea el sitio activo de la misma modula su actividad catalítica, lo que apoya la existencia del llamado "efecto de jaula". Tras esta primera caracterización de la hidrogenasa se procedió a caracterizar por SEIRAS electroquímico las dos diferentes configuraciones de la inmovilización de esta enzima que se habían descrito previamente sobre electrodos con bicapas de fosfolípidos soportadas. Este estudio unido a la previa caracterización por AFM permitió elegir la configuración más adecuada para conseguir controlar electroenzimáticamente la formación de un gradiente de protones en la interfaz bicapa / electrodo.

El Complejo Respiratorio I realiza dos actividades diferentes; el transporte de electrones y de protones. En esta tesis se presenta la primera reconstitución funcional y orientada de esta enzima embebida en una bicapa de fosfolípidica soportada sobre un electrodo de oro. Esta construcción se ha caracterizado por AFM, Espectroscopia de Impedancia y por SEIRAS electroquímico.

La reconstitución funcional de las dos proteínas utilizando membranas fosfolipídicas soportadas puede abrir nuevas puertas a posibles futuras aplicaciones.

Index

Abbreviations

- **4-ATP:** 4-Aminothiophenol
- **AFM:** Atomic Force Microscopy
- **Bil:** Bilayer
- **CpI:** Respiratory Complex I or NADH:ubiquinone oxidoreductase
- **CV:** Cyclic Voltammetry/Voltammogram
- **DDM:** n-dodecyl-β-D-maltopyranoside
- **DMN:** 2,3-Dimethyl-1,4-naphthoquinone
- **DPV:** Differential Pulse Voltammetry
- **EDC:** 1-Ethyl-3-(3-dimethylaminopropyl)carbodiimide
- **Hase:** hydrogenase
- **MV:** Methyl Viologen
- **NADH:** Nicotinamide Adenine Dinucleotide
- **NHS:** N-Hydroxysuccinimide
- **O.D:** Optical Density
- **SAM:** Self-assembled monolayer
- **SEIRAS:** Surface Enhanced Infrared Spectroscopy
- **SHE:** Standard Hydrogen Electrode

1. Introduction

1.1 Bionanoelectronics

Nature is complex. We only have to take a look of a single cell; the simplest one performs a great number of functions using a vast number of proteins, which are not simple at all. Enzymes are able to catalyse chemical reactions which require high costs and extreme conditions when performed industrially in non-catalyzed processes or with non-biological catalysts.

As well as nature is complex, the artificial world created by mankind is getting more and more complex. This artificial reality is nowadays almost completely dependent on electricity. The humankind knows electricity since a long time ago, but it was Maxwell´s equations in 1865, which describe how electric and magnetic fields propagate, interact, and how they are influenced by objects, which meant the beginning of the fast technology evolution still going on nowadays.

The interface between artificial and living world has been for many years a source of inspiration of many ideas and science-fiction stories about beings created by organic and biomechatronic parts (cyborgs), as "The bicentennial man" of Isaac Asimov (Asimov 1978). Thanks to development of the nanotechnology we can tailor materials in the protein scale length with high precision. In this sense, the continuous development of the bionanoelectronics field is decreasing the gap between real science and science-fiction faster than we can imagine.

The goal of bionanoelectronics is to achieve a superior functionality with a device combining man-made and biological machines. The first mismatch for the practical realization of bionanoelectronics is the absence of an adequate interface that enables to couple correctly biological and inorganic components in a biomimetic environment. The device should provide good fidelity and a good signal to noise ratio, while being at the same time simple and versatile in order to achieve substantial technological impact at a reasonable cost. Thus, we could affirm that the aim of bioelectronics is the ability to

create architectures that enable bidirectional flow of information between the living systems and man-made structures (Noy 2011).

The activity of redox enzymes can be controlled and monitored by electrochemistry, thus, the application of these proteins into bionanoelectronics seems to be ideal (Léger, Elliott et al. 2003). They shuttle electrons and catalyse redox reactions in various vital processes in the cell, including photosynthesis and energy metabolism. It was in the 1980s when works reporting the immobilization of redox proteins on "protein-friendly" electrode surfaces and the interchange of electrons between both began to appear (Armstrong, Hill et al. 1984, Yaropolov, Karyakin et al. 1984). The problem is that many of these enzymes perform their *in vivo* function in relation with a membrane, as usually electron transport chains are allocated in membranes. The advances in the bioelectrochemistry field have been less for membrane proteins than for soluble ones (Léger, Elliott et al. 2003). The reason of this fact is because to achieve a biomimetic environment for a globular protein immobilized on an electrode is easier than for membrane proteins. Nevertheless, the importance of redox membrane enzymes and the high potential of electrochemical studies for understanding and obtaining benefit from these proteins make this field amazing and fascinating.

1.2 Supported phospholipid bilayers

In order to achieve a biomimetic environment for membrane proteins, various membrane models and different methods of supported phospholipid bilayers formation at metals surfaces have been developed.

The first method consists on the transfer of a monolayer of phospholipids from the air–solution interface onto the metal-solution interface of a mercury drop electrode (Coldrick, Steenson et al. 2009). In order to achieve phospholipid bilayers at freshly cut surfaces of metals such as Pt, Au, Ag, Cu, Ni, they were exposed to solutions of phospholipids in organic solvents and then, were soaked in an aqueous solution (Salamon, Wang et al. 1994).

Another method consists in the modification of the metal surface by a self-assembled monolayer (SAM) of thiols, over which is deposited a monolayer of phospholipids in

order to form a hybrid bilayer (Buoninsegni, Herrero et al. 1998). The supported membranes formed by these methods have excellent barrier properties. However, they are not useful for reconstitution of membrane proteins which require a few nm thick surface/bilayer interface as a separation to preserve their native state (Lipkowski 2010).

The called "tethered bilayer lipid membranes" (tBLMs) were developed in order to solve the commented handicap. This type of supported membranes consists in two parts; (1) a first layer formed by thiolipid, a synthetic molecule consisting of a hydrophilic spacer terminated with a thiol or dithiol group, which is anchored to the metal and covalently attached to the polar group of a phospholipid and (2) a second layer which consists of a monolayer of phospholipids over the first thiolipid monolayer to complete the bilayer (Schiller, Naumann et al. 2003). From this method, various related methods have been developed (Lipkowski 2010).

1.3 Techniques

In order to study proteins reconstituted in phospholipid bilayers supported on different surfaces a battery of different techniques are usually used:

1.3.1 Atomic Force Microscopy (AFM): Since its invention in 1986, AFM has become to be a multifunctional tool in membrane proteins research. This technique consists in a combination of the principles of the scanning tunneling microscope and the stylus profilometer (Binnig, Quate et al. 1986). Various methods have been established for investigating structure, assembly, folding and interactions of membrane proteins. AFM-based single-molecule force spectroscopy (SMFS) has been used to detect inter- and intra-molecular interactions of membrane proteins and to determine their unfolding pathways (Bippes and Muller 2011).

1.3.2 Electrochemistry: Several electrochemical techniques can be used to transduce the biological functions occurring at an electrode:

1.3.2.1 Amperometry: It allows detecting changes in the current under redox potential control. Cyclic Voltammetry (CV) is a useful technique to study the catalytic activity of redox enzymes. It consists in the measurement of the

current associated to the scan of potentials between two different values in both directions. An extension of cyclic voltammetry is the Differential Pulse Voltammetry (DPV). In this technique the current is measured immediately before each potential pulse and a short time after, and the current increment is plotted versus the potential. DPV allows decreasing the charging current, and thus a more sensitive detection of faradaic process (Léger, Elliott et al. 2003).

1.3.2.2 Potentiometric titrations: The application of different potentials to a redox enzyme immobilized on an electrode or in a thin layer cell induces changes in its state and functionality. Redox titrations of the different states of enzyme can be performed by different spectro-electrochemical techniques (Hellwig, Scheide et al. 2000, Dementin, Belle et al. 2006). These allow determining the redox equilibria between the different states of the active site, kinetic barriers for activation/inactivation of function and catalytic mechanisms.

1.3.2.3 Electrochemical impedance spectroscopy: An impedance analysis allows demonstrating the ability of a circuit to resist the flow of electrical current. This resistance is represented by two terms, the "real impedance" and the "imaginary resistance". This technique has been used has been used in the field to investigate vesicules deposition and phospholipid bilayer formation on electrodes, ion channels and proton translocation (Jeuken, Weiss et al. 2008, Kozuch, Steinem et al. 2012, Khan, Dosoky et al. 2013).

1.3.2.4 Field effect transistor (FET): a FET consists of three terminals: the source, drain, and gate. The voltage between the source and drain of the FET regulates the current flow in the gate voltage. It is possible to use as the gate terminal molecular receptors or ion-selective membranes for biosensor applications (Lee, Kim et al. 2009).

1.3.3 Piezoelectric transduction: Quartz crystal microbalance measures a mass per area unit area by measuring the change in frequency of a quartz crystal resonator. It has been shown to be a sensitive technique to study the formation of biomimetic membranes (Keller and Kasemo 1998) and membrane protein interactions (Cho, Frank et al. 2010).

1.3.4 Fluorescence: Techniques based in fluorescence have been used since the late 1960s to study different aspects of membrane-related phenomena. Mainly, these studies are related to lipid-lipid and lipid-protein interactions. Fluorescence spectroscopy approaches provide valuable structurally and dynamically related information on membranes. A handicap of these approaches is that they generally generate mean parameters from data collected on bulk solutions of many vesicles, and for this reason, direct information on the spatial organization at the single membranes level is not obtained (Bagatolli 2009).

1.3.5 Vibrational Spectroscopy: Oscillation of an atom within a molecule via its chemical bond is periodic, it occurs in a precise manner. These oscillations of molecular bonds are the probes of vibrational spectroscopy. There are two main techniques used to obtain vibrational spectra, Infrared (IR) and Raman spectroscopy (Siebert and Hildebrandt 2008).

1.3.5.1 In **Raman spectroscopy** the vibrational transitions are induced upon inelastic scattering of monochromatic light by the molecule, such that the frequency of the scattered light is shifted by the frequency of the molecular vibration (Siebert and Hildebrandt 2008). This technique has been used to study mainly hydrosoluble proteins or membrane proteins in solution or deposited on an electrode in presence of a detergent (Todorovic, Verissimo et al. 2008), but not in a biomimetic environment.

1.3.5.2 In **IR spectroscopy**, molecules are exposed to a continuum of IR radiation and those photons that have energies corresponding to the frequencies of the normal modes can be absorbed to excite the respective vibrations (Siebert and Hildebrandt 2008). A variation of the conventional IR spectroscopy is the **Surface Enhancement Infrared Absorption Spectroscopy (SEIRAS)**. The 'surface enhancement effect' leads to the increase of signal intensity by two orders of magnitude. The effective range of signal enhancement is only observed in the immediate vicinity of the metal surface (≈ 10 nm) because the plasmonic field of the metal significantly contributes to the enhancement effect. Another characteristic of SEIRAS is that vibrational bands are enhanced or weakened

depending on the orientation of their dipole moment changes relative to the surface (Wang, Jiang Xiu et al. 2012).

The use of the solid support as an electrode allows to apply a membrane potential or to directly inject electrons into the system. The combination of electrochemical methodologies with in situ vibrational spectroscopy provides new experimental opportunities to study the function of membrane proteins (Ataka, Stripp et al. 2013).

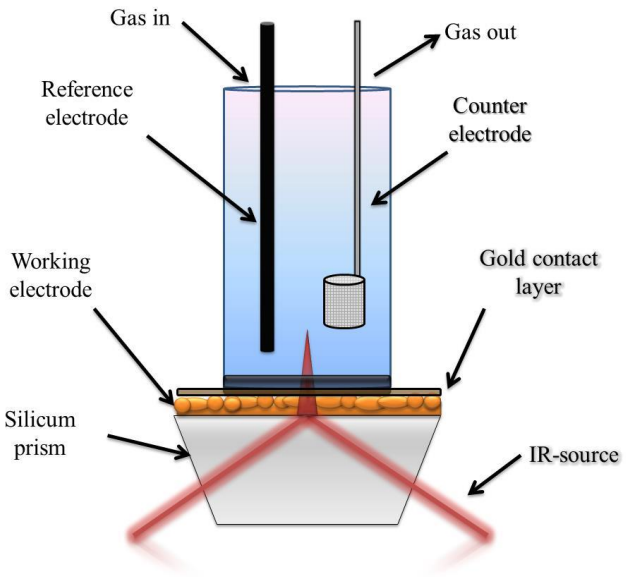

Figure 1.1: *Schematic representation of a typical Electrochemical-SEIRA setup. An IR-transparent silicon prism is used as support of the gold thin, which is the working electrode (WE) as well as the responsible of the SEIRA effect. The cell should be equipped with a water jacket to control the temperature during the experiment. A Pt mesh is used as counterelectrode (CE) and a Ag/AgCl as reference electrode (RE).*

1.3.6 Nanodiscs: This technology allows making different biophysical studies of membrane proteins in a controlled biomimetic environment. It is based in nanodiscs, which are discoidal phospholipid bilayers surrounded and stabilized by two molecules of a membrane scaffold protein (MSP). Membrane protein reconstitution in nanodiscs is regulated by the MSP to lipid ratio and the length of the MSP. Using the correct ratio of lipid to MSP achieve to obtain homogeneous and monodisperse entities. By using

nanodisc technology reconstituted membrane proteins can be treated like soluble proteins, which is a great advantage in order to avoid the difficulties of working with membrane proteins. In this way, different functional studies in solution have been carried out demonstrating the potentiality and versatility that the nanodiscs technology provides for the study of membrane proteins (Inagaki, Ghirlando et al. 2013).

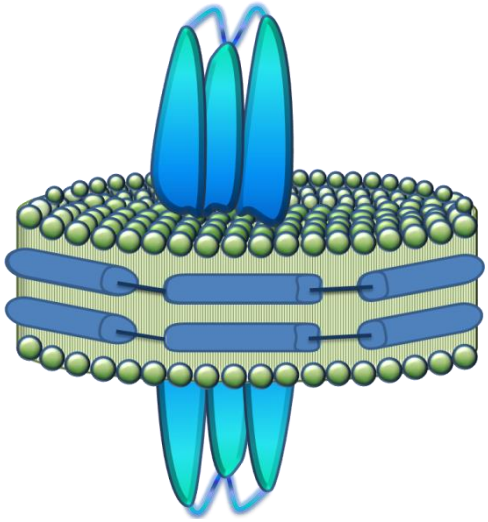

Figure 1.2: *Schematic representation of a nanodisc with an incorporated membrane protein. The canonical shapes in dark blue represent the membrane scaffold proteins (MSP). The green disc shape represents a lipid bilayer where the protein is embedded.*

1.4 Membrane-associated energy transduction

Common to bacteria and archea is the underlying principle of primary energy conservation, the chemiosmotic mechanism generating a electrochemical potential of ions across the membrane on expense of the energy derived from membrane-associated fermentative, redox or light-driven processes. Two of these, oxygen respiration and oxygenic photosynthesis, were transferred to eukaryotes by endosimbiosis uptake of putative ancient bacteria, the precursors of mithocondria and chloroplasts. Secondary process of membrane associated energy transduction, such as ATP synthesis, are consumers of the electrochemical ion gradient generated by primary energy (Schäfer 2004).

Membrane-associated energy transduction proceeds by linking an exergonic process catalyzed by a membrane-residing enzyme (or protein complex) to the simultaneous vectorial translocation of charge (electrons or ions) across this membrane by the same enzyme. This principle is common to bacteria and archea. Typical processes can be metabolic substrate conversions like redox reactions or decarboxylation, respiratory electron transport from a low potential donor to a high-potential acceptor (respiratory chains), or the decay from an energized state of a molecule generated by absorption of light to the low-energy ground state (Schäfer 2004).

We can find various examples of energy transduction in nature: Fermentation, Anaerobic respiration (denitrification, fumarate and sulfur respiration as well as ferric ion reduction), oxygen respiration (aerobic organotrophs and aerobic chemolithotrophs) and photosynthesis (Schäfer 2004).

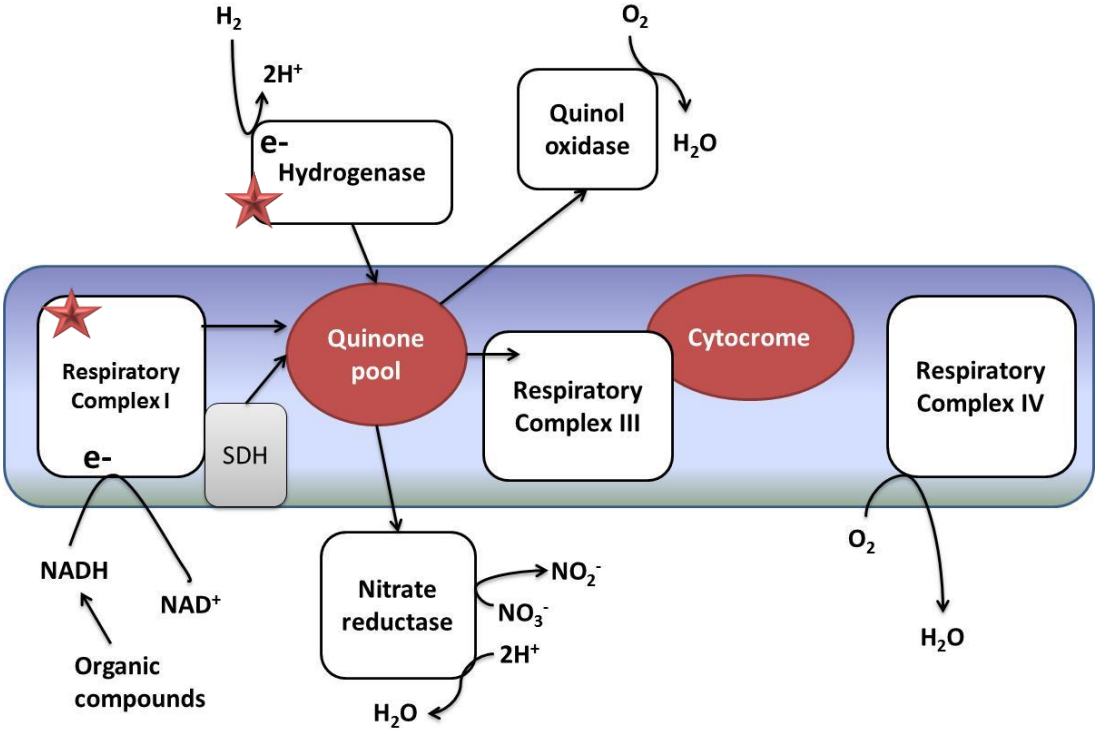

Figure 1.3: *Schematic illustration of the diversity of energy-transducing membrane systems in bacteria and archea. All boxed or encircled components are membrane-integral or membrane-associated .White boxes are proton pumps. The blue block symbolizes a regular and complete aerobic respiratory chain. The linear arrows represent the electron flux in the chain. SDH; succinate dehydrogenase, so called Respiratory Complex II (grey box). Stars indicate the enzymes that are object of study in this thesis.*

1.5 Enzymes

Both enzymes object of study in this thesis are redox membrane proteins involved in the electron transport (directly or indirectly) to a quinone pool, as well as in the regulation of proton concentration.

1.5.1 Hydrogenases (Hases)

Hases are a group of metalloenzymes that catalyze the simplest reaction in nature; the oxidation of dihydrogen to protons and electrons and the reverse reaction (Vignais, Billoud et al. 2001):

$$H_2 \rightleftharpoons 2H^+ + 2e^-$$

The oxidation reaction is performed in a buried bimetallic active site, where the H_2 binds to. The binding to the active site increases the acidity of the substrate, leading to its heterolytic splitting that is facilitated by the presence of a nearby base (a cysteine residue or a secondary amine). The dihydrogen formation reaction involves the respective coupling of H^+ and H^- at the active site (Alvin 1979).

Hases have a key role in the energy metabolism of several microorganisms including bacteria, archaea and lower eukaryotes. They consume hydrogen as an energy source or they produce it in order to dispose of an excess of reducing equivalents (Vignais, Billoud et al. 2001).

Hases can be classified in three groups according to the metal ion composition of their active site: NiFe; FeFe, and Fe Hases. In the two main groups of Hases, Fe-Fe and Ni-Fe, the metallic atoms that form the active are able to acquire several stable redox states, catalytically active or inactive. This behaviour can be due to the combination of different types of ligands coordinating to the metals: thiolates (good π-donors), cyanides (good σ-donors) and carbonyls (good π-acceptors). This special coordination makes easier the entry and exit of electrons in the active site due, as the ligands work as an electronic buffer. The different redox states of the active site of Hases have been

identified by redox titrations of Hases followed by different spectroscopic techniques. EPR and FTIR spectroscopy are the most common used. By FTIR all redox states of the active site can be detected by this technique, using*in situ* spectroelectrochemistry. Other spectroscopic techniques, such as EXAFS, ENDOR, and Mössbauer are useful to achieve information on structural and electronic aspects of the active site (De Lacey, Fernández et al. 2007). A common characteristic of the structure of Hases is their buried active site and the presence of gas channels that allow dihydrogen molecules transport into the buried active site or towards the outside (Montet, Amara et al. 1997).

1.5.1.1 NiFe Hases

The NiFe Hases are the most abundant group of Hases and are composed by a minimum of two subunits. The catalytic subunit contains the active site (large subunit) and the electron-transferring subunit contains one or more iron–sulphur clusters (small subunit). In the large subunit (typically ~63 kDa), the binuclear active site is formed by one Fe atom and one Ni atom coordinated by four cysteine residues. Two of these residues bridge both metals and the other two coordinate exclusively the Ni atom. The Fe atom is also coordinated by three diatomic ligands which are essential in FTIR characterization of these Hases; two CN^- and one CO. The small subunit is commonly ~29 kDa. This subunit is usually extended in the C-terminal region of membrane Hases by an α-helical transmembrane which attaches to the physiological partner, which is cytochrome b (Baltazar, Marques et al. 2011, Lubitz, Ogata et al. 2014).

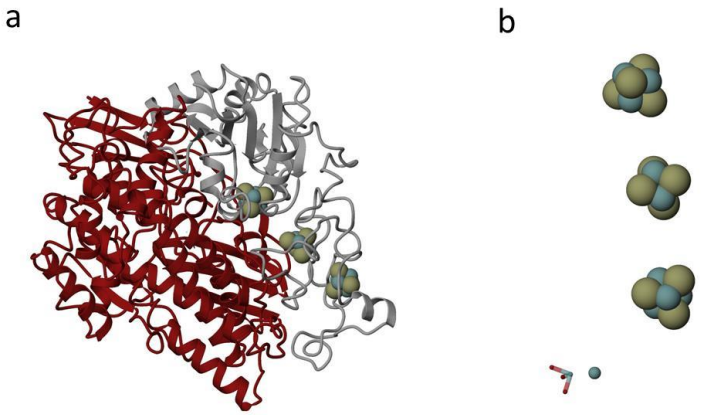

Figure 1.4: *Crystal structure of the standard NiFe Hase from Desulfovibrio gigas PDB ID: 1FRV. (a) The two subunits of a typical NiFe Hase are observable; the large subunit of 60 kDa (in red) where the bimetallic active site is allocated and the small subunit of 28 kDa (in grey) where are disposed three iron sulphur clusters responsible of the electron transfer. (b) From top*

to the bottom 4Fe-4S, 3Fe-4S, and 4Fe-4S clusters. The last cluster is called "proximal" due to its position closest to the Ni atom (shown at the bottom) from the active site. The Fe atom of the active site coordinated by two CO and one CN groups is also shown.

Inside the group of NiFe Hases we can find four different subgroups attending to a phylogenetic analysis of the two core subunits (Vignais, Billoud et al. 2001). The first group includes the periplasmic H_2-uptake Hases, which oxidize hydrogen and transfer the electrons resulting of this oxidation to the quinone pool. This group of Hases contains a characteristic signal peptide in the small subunit involved in translocation of the two mature subunits to the periplasm. The greater part of group 1 Hases are associated with an additional subunit responsible for transfer the electrons to the respiratory chain; cytochrome b or cytochrome c (Matias, Pereira et al. 2005). Group 2 includes the cytoplasmic and the cyanobacterial uptake Hases, as well as the H_2 sensors (Tamagnini, Axelsson et al. 2002). In group 3 are included cytoplasmatic Hases that bind cofactors as NAD(P) and F420 (heterodisulfide reductase associated Hases are also included in this group. The last group (4) is formed by multimeric complexes energy converting membrane-associated Hases, whose subunits are closely related to the Respiratory Complex I ones (CpI) (Forzi, Koch et al. 2005, Marreiros, Batista et al. 2013).

Thanks to the combination of different methods, the catalytic mechanism of Hases containing a NiFe active site has been elucidated. The simplest catalytic cycle contains three states; Ni-SI_a, Ni-C, and Ni-R (**Figure 1.5**). The Ni-SI_a contains no additional bridging ligand between the metals and the Ni is four-coordinated. The oxidation of the H_2 begins with its polarization at the Ni atom of Ni-SI_a, where it is split heterolytically. The produced Ni-R state brings the H^- between Ni(II) and Fe(II) and the H^+ is attached to a sulphur of a terminal cysteine. The exit from the active site of a proton and an electron generates the paramagnetic Ni-C state, which also has a hydride bridge between the metals. The loss of another electron and a proton (from the hydride bridge) closes the cycle generating again Ni-Si_a (Lubitz, Ogata et al. 2014). In the case of the oxidized inactive states there are still open questions. For Ni-B (ready oxidized state) it is established that an O-H is bridging the Ni and Fe atoms (De-Lacey, Fernandez et al. 2007), whereas for the Ni-A (unready oxidized state) there is an oxidized cysteine ligand (to sulfenate) besides the O-H bridging ligand (Volbeda, Martin et al. 2014)

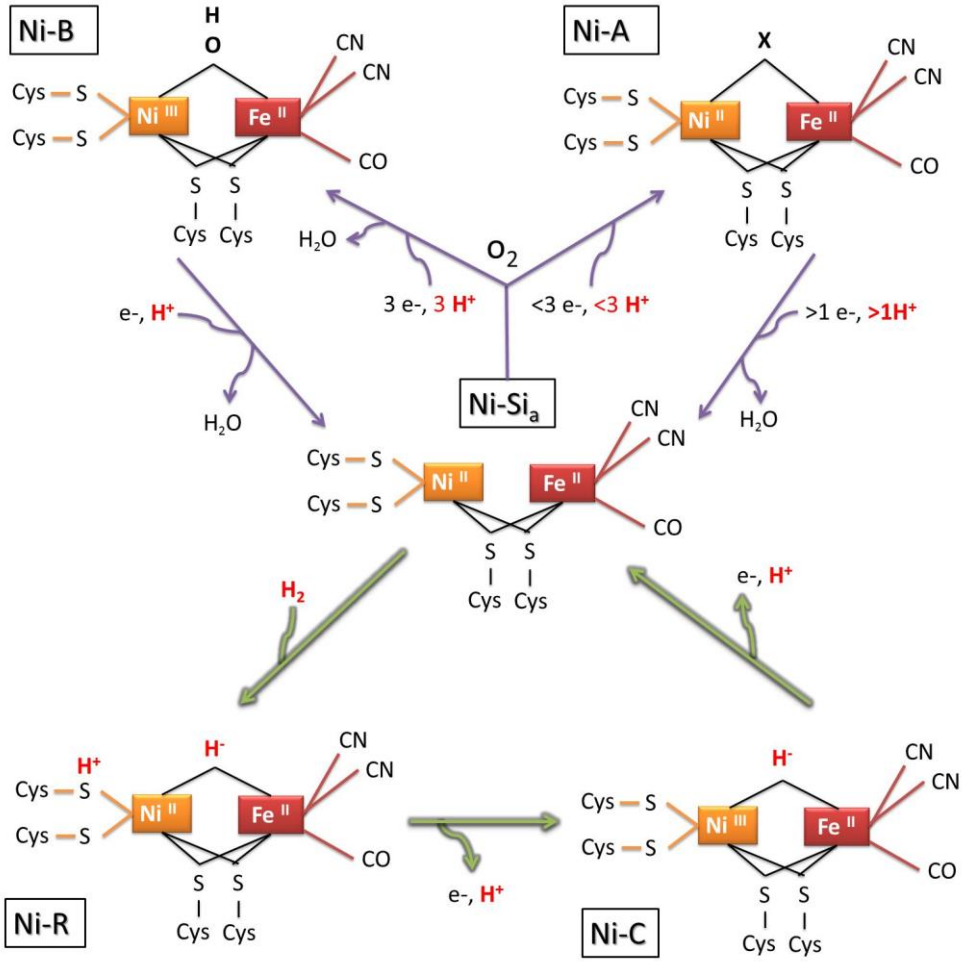

Figure 1.5: *Schematic representation of the H_2 oxitation catalytic cycle and inactivation/reactivation mechanism for NiFe Hases proposed by Lubitz et al (Lubitz, Ogata et al. 2014). The Ni-Fe active site is represented by two squares indicating the main characteristics of each state. The catalytic reaction of Hase is represented at the triangle formed at the bottom by the states Ni-Si_a, Ni-R and Ni-C. These states are connected by green arrows which indicate the direction of the reaction as well as its inputs and outputs. The inactivation/reactivation processes are represented by the triangle formed at the upper part by Ni-Si_a, Ni-A and Ni-B, which are connected by purple arrows indicating the possible reactions that can occur between them. When enough electrons are available at the active site, the formation of Ni-B state is favoured in presence of oxygen. This state (Ni-B) can be rapidly reactivated with one electron and one proton to the Ni-SI_a state by releasing a molecule of water. In standard oxygen-sensitive NiFe Hases, the Ni-A state is also formed in presence of oxygen. The Ni-A state requires low potentials and long reactivation times to form Ni-Si_a. Very recently, the bridging ligand X in the Ni-A state has been identified by X-ray cristallography as also OH^-, but one of the bridging cysteines is oxidized to a sulfenate (Volbeda, Martin et al. 2014).*

In some Hases of this group, one of the S atoms (from a cysteine residue) that coordinates the Ni atom is replaced by a Se atom (from a Selenocysteine residue). This family is called NiFeSe Hases. The Sec and Cys amino acids are structurally identical; the only change is a selenium atom replacing the sulphur atom (Baltazar, Marques et al. 2011). Sec amino acid is designated as the 21st genetically encoded amino acid because it is co-translationally added into proteins at an in-frame UGA codon. There are plenty of selenoenzymes wide spread in nature, but most of them are enzymes that can be inhibited by oxygen. In this sense, there is a hypothesis that proposes that these enzymes evolved to resist oxygen inactivation. This behaviour seems in principle incongruous due to the fact that a selenol is oxidized much faster than a thiol. Furthermore, the selenol/diselenide redox couple presents a lower redox potential than the thiol/disulphide couple (Snider, Ruggles et al. 2013). However, the advantage of Se versus S is that the oxidized states of the Se can be reduced easily to selenol (due to the electrophilic character of a selenoate), in contrast to the higher kinetic barrier of the oxidized states of the thiol to be reduced. In summary, the high nucleophilicity and the high electrophilicity of Se in its different redox states make this element a good option for the enzymes that need to be highly resistant to inactivation by oxygen (Snider, Ruggles et al. 2013).

1.5.1.2 Fe-Fe Hases

The active site of this family of Hases does not contain nickel. It consists of a dinuclear iron cluster which is only attached to the protein backbone by just a sulphur atom from a cysteine, which bridges to a 4Fe-4S cluster (De Lacey, Fernández et al. 2007). In this family, the active site is also coordinated by CO and CN^- groups and both iron atoms are bridged by an alkyl chain containing a secondary amino group (Zheng, Wang et al. 2014). In this sense, as Ni-Fe and Fe-Fe Hases are not phylogenetically linked, convergent evolution to achieve a low spin Fe(II) with CO and CN^- coordination indicates that these elements are essential to biological Hase activity (De-Lacey, Fernandez et al. 2007).

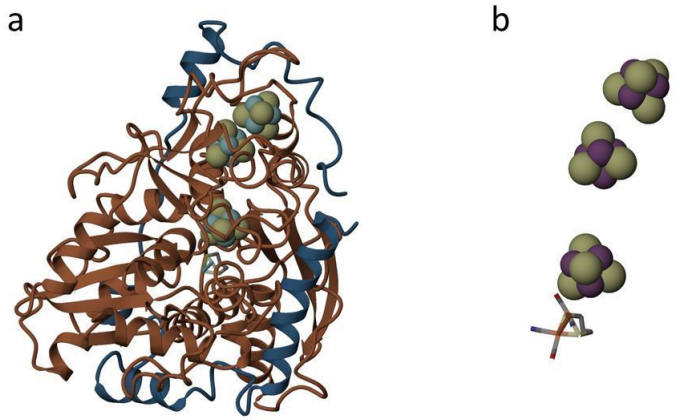

Figure 1.6: *Crystal structure of the standard FeFe Hase from Desulfovibrio desulfuricans PDB ID: 1HFE. (a) Two subunits are observable; a large subunit of 42 kDa (in red) where are allocated the bimetallic active site and three iron sulphur clusters, and a small subunit of 11 kDa (in blue) which is embracing the large subunit (b) Three 4Fe-4S clusters form the intramolecular electron transfer pathway. The bottom cluster (proximal) is bound to the active site (represented by sticks) through a cysteine residue, forming the called H-cluster.*

The catalytic activity of these enzymes depends on the redox states of the H-cluster. Both the proximal 4Fe-4S and the bimetallic active site are redox active. The cubane part has two possible redox states; the oxidized $(4Fe\text{-}4S)^{2+}$ and the reduced $(4Fe\text{-}4S)^{+}$ state. The bimetallic active site part has three possible states: doubly oxidized Fe(II)Fe(II), mixed valence Fe(II)Fe(I) and doubly reduced (Fe(I)Fe(I)).Therefore, there are six possible redox states for the complete H-cluster. Under physiological conditions only a fraction of these states is present (Lubitz and Tumas 2007).

Two common states of all FeFe Hases are the "active oxidized" state Hox ($(4Fe\text{-}4S)^{2+}$-Fe(I)Fe(II)) and the "active reduced state" state H_{red} ($(4Fe\text{-}4S)^{2+}$-Fe(I)Fe(I)), which participate in the catalytic cycle (**Figure 1.7**). It has been suggested that the cubane may play a crucial role in the different possible intermediate redox states, as well as in the catalytic cycle (Adamska, Silakov et al. 2012).

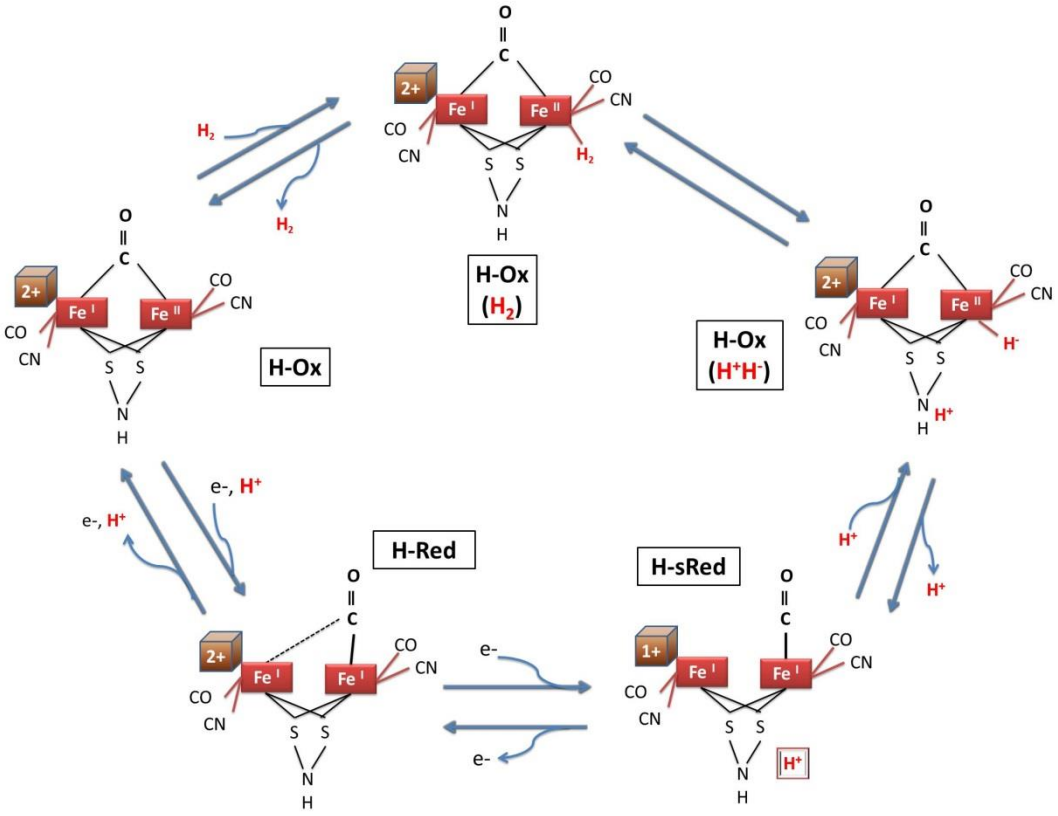

Figure 1.7: *Model of the catalytic cycle of FeFe Hases including the "Hsred" proposed by Adamska et al. (Adamska, Silakov et al. 2012). The H-cluster is represented by three squares, two red ones that represent the bimetallic active site and one brown which represents the proximal iron-sulphur cluster bound to the bimetallic active site by a cysteine. The hydrogen oxidation catalytic cycle may begin by the* H_{ox} *state (as "active oxidized state") and* continues in the clockwise direction. *The* H_{sred} *state is the proposed starting point for proton reduction in the reaction cycle of FeFe Hases (Adamska, Silakov et al. 2012).*

1.5.1.3 Fe-Hases

[Fe] Hases have been reported only in methanogenic archaea. In these organisms this family of Hases is only expressed under conditions with low nickel concentrations (Thauer, Kaster et al. 2010).

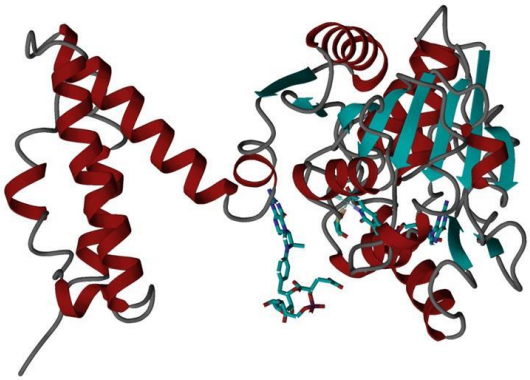

Figure 1.8: *Crystal structure of a monomer of the Fe Hase from Methanocaldococcus jannaschii PDB ID: 3H65. The structure of the FeGP-cofactor bound to the backbone of the protein and the substrate methenyltetrahydromethanopterin (methenyl-H_4MPT) can be observed.*

These Hases catalyze the reversible reduction of the substrate methenyltetrahydromethanopterin (methenyl-H4MPT)$^+$ to methylene-H_4MPT by H_2. They are able to catalyze H^+/D^+ exchange but only in presence of methenyl-H_4MPT$^+$, which indicates that H_2 activation can only be achieved in the presence of the substrate (Hiromoto, Warkentin et al. 2009). Fe-Hases are homodimers of 76 kDa which contain a single Fe atom in each subunit and do not contain iron-sulphur clusters, in contrast to rest of the known Hases. For this reason they are named iron-sulphur-cluster-free Hases (Thauer, Kaster et al. 2010). Another characteristic of these Hases is that their structures harbour an unique Fe cofactor (Fe-guanylylpyrodinol, Fe-GP), which plays a crucial role in its catalytic mechanism (Vogt, Lyon et al. 2008).

As commented above, the catalytic reaction mechanism of [Fe] Hase requires a second substrate, in contrast to the NiFe and [FeFe] Hases. The first step of the catalytical mechanism is the sequential binding of two methenyl-H_4MPT$^+$ molecules to an "open form" of the enzyme. The binding of the second substrate molecule induces the "closed form" between the two domains. Then, H_2 can access into the active site through a narrow hydrophobic tunnel. In the next step, the Fe-GP cofactor is activated and a hydrogen molecule binds to the open coordination site of the iron, facilitating its heterolytical cleavage, and then the hydride is transferred to the methenyl-H_4MPT$^+$ (Yang and Hall 2009).

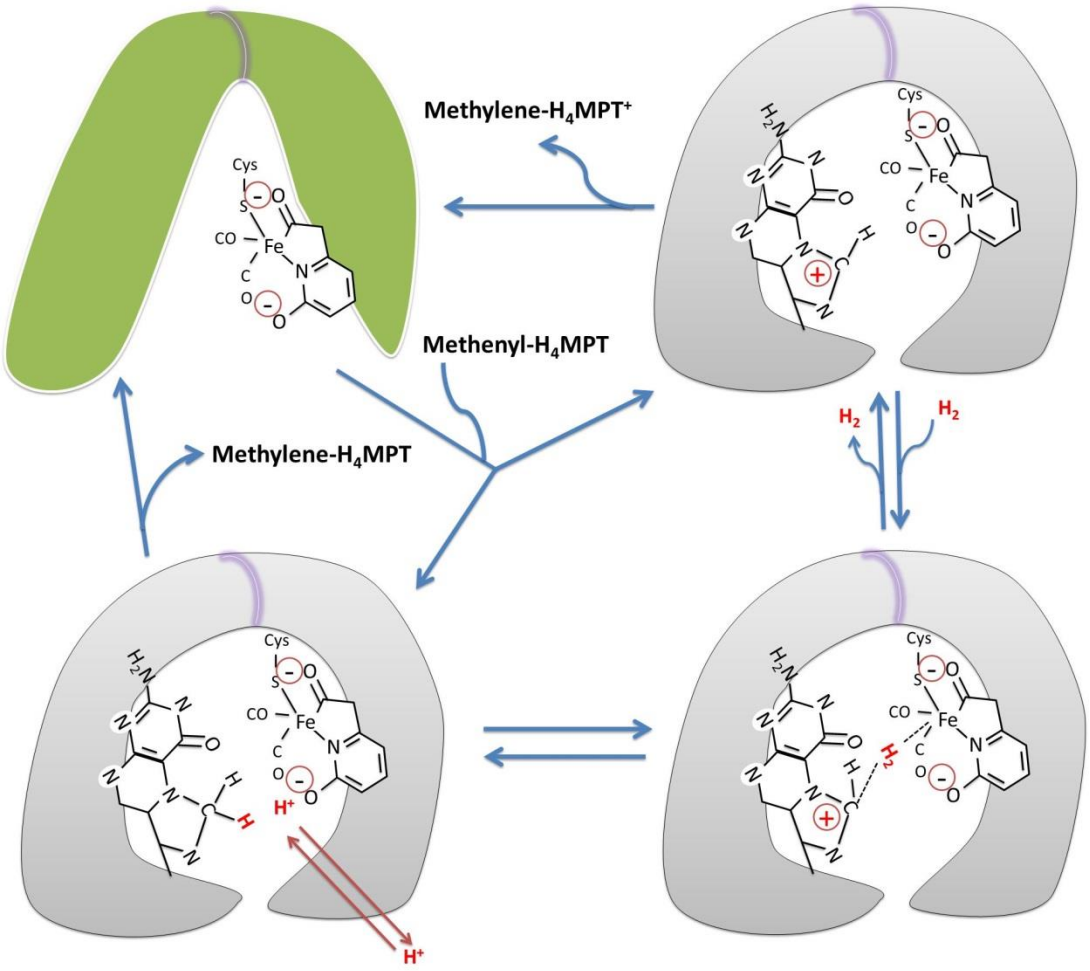

Figure 1.9: Schematic representation of the p*roposed catalytic mechanism of [Fe]-Hase involving the open/closed conformational transition by Hiromoto et al. (Hiromoto, Warkentin et al. 2009). The first state of the catalytic cycle is the "open conformation" represented in green where the Fe-GP cofactor is observable. The addition of methenyl-H_4MPT induces the "close conformation" indicated in grey colour. H_2 can access into the active site through the hydrophobic channel and binds to Fe as represented in the scheme. Then, the methenyl-H_4MPT^+ can accept the hydride generating methylene-H_4MPT, and the proton obtained from the dihydrogen cleavage is quickly exchanged with protons in bulk solvent via a proton relay pathway.*

1.5.2 Respiratory Complex I (CpI)

The proton-pumping NADH:ubiquinone oxidoreductase, also called Complex I, is the first enzyme of the respiratory transfer chain. It is responsible of accepting electrons from NADH and transferring them to a quinone, which will transport these electrons to the next step of the respiratory chain. In addition to this electron transfer activity, CpI translocates protons across the membrane in order to induce an electrochemical membrane potential (Walker 1992).

Bacterial complex I is a simplified model of the mitochondrial enzyme (Carroll, Fearnley et al. 2006). It has an L-shaped assembly normally consisting of 14 "core" subunits (7 hydrophilic and 7 hydrophobic ones, ~550 kDa combined mass), named as NuoA to NuoN or as Nqo1 to Nqo14. These subunits are conserved from bacteria to humans, where the mitochondrial enzyme is constituted by more than 40 subunits, bringing its total molecular mass to ~1MDa. Two structural/functional domains are differentiated in CpI, the hydrophilic peripheral arm and the membrane part (Walker 1992, Carroll, Fearnley et al. 2006).

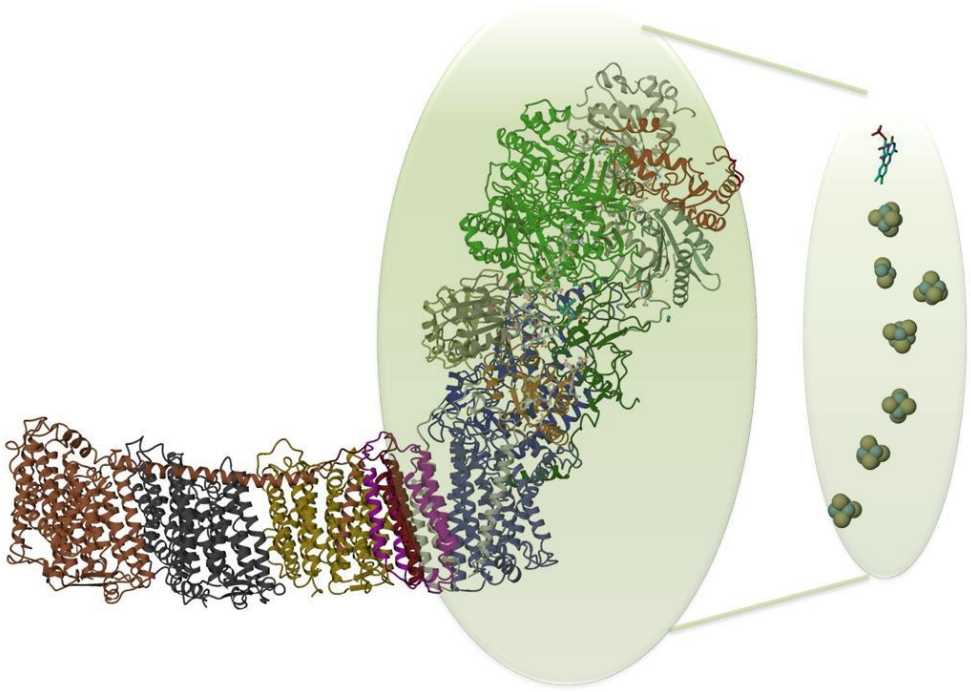

Figure 1.10: *Crystal structure of Respiratory Complex I from Thermus thermophiles PDB ID: 4HEA. The "L" shape with both domains of the enzyme is observable. The horizontal part of the*

enzyme is the membrane domain, formed by multiple vertical-orientated helices where the proton transport activity is allocated. The vertical part corresponds to the peripheral domain, where the iron- sulphur clusters and the FMN group that are shown at the right of the structure are allocated. From the FMN group (at the top) the electrons are transferred to the quinone substrate along seven iron-sulphur clusters allocated along the peripheral arm.

The membrane part of CpI has a curved shape with a total length of 180 Å and is constituted by seven subunits (NuoA, H, J to N). NuoH is the subunit that connects the two domains of the enzyme (Marreiros, Batista et al. 2013). The membrane domain is the responsible of the proton transport activity. The subunits NuoK to N are homologous to the subunits of Mrp Na^+/H^+ antiporters. In this sense, it is logical to find in CpI an Na^+/H^+ transport activity, as observed in *Rhodotermus marinus* and *Escherichia coli* (Batista and Pereira 2011).

The bacterial peripheral arm has a Y shape, a length of 130 Å and is composed of seven subunits (NuoB to G and NuoI). The branches of the Y are formed by three domains; NuoE and NuoF form one branch and the other is formed by the C-terminal domain of NuoG. Both branches are connected by the N-terminal domain of NuoG and by the subunits NuoC and NuoI. These subunits are supported on NuoD and NuoB, which form an interface with the membrane domain (Baradaran, Berrisford et al. 2013). Subunits NuoE, F and G are the entry gate for electrons. These subunits, with the exception of the C-terminal domain of NuoG, are homologous to soluble NAD^+ reducing Hases. The C-terminal domain of NuoG is homologous to molybdopterin-containing enzymes, such as formate dehydrogenase (Sazanov and Hinchliffe 2006). The subunits NuoB, C, D, I and H are homologous to subunits of the membrane-bound NiFe Hases (Mathiesen and Hägerhäll 2003). The peripheral arm contains from 8 (in mitochondria) to 9 (in *T. thermophilus*, *E. coli*) or 10 (in *A. aeolicus*) iron-sulphur clusters responsible of the electron transfer along the arm, and a flavin mononucleotide which receives the electrons directly from NADH (Fernandes, Sousa et al. 2006). The NADH and quinone binding sites are separated by the distance of nearly 100 Å. The electrons are transferred from NADH to the FMN group and then, one by one along the chain of iron-sulphur clusters N3→N1b→N4→N5→N6a→N6b→N2 to the quinone. The quinone substrate binds to a cavity formed between subunits Nqo4, 6 and 8 (Baradaran et al. 2013). The redox centres in the chain are separated within 14Å, the

maximal distance described for physiological electron transfer (Page, Moser et al. 1999). All redox clusters of the peripheral arm that are EPR-visible are equipotential (E_{m7} −250 mV), with the exception of the high-potential cluster N2 (E_{m7} −100 mV) (Fernandes, Sousa et al. 2006). This cluster has been shown to be coordinated in an unfavourable geometry by two consecutive cysteines. The reduction of this cluster leads to disconnection of one of the two cysteines. This non-common coordination may be responsible of the cluster´s redox state effect on the protein conformation, as part of the coupling mechanism between both activities of CpI (Baradaran, Berrisford et al. 2013, Sazanov 2014).

The first crystal structure of an entire Cp I revealed a surprising structural feature about the quinone reaction chamber (Q). It is a 30 Å cage completely enclosed from the solvent, with only a small apparent entry point for the quinone. This cage is formed by hydrophilic residues, and the cavity "front" is mostly negatively charged, while the "back" is neutral and the "top" (near the cluster N2) is positively charged. The ionisable residues conforming the chamber are highly conserved and mutations of many of these residues have been shown to be directly related to the loss of CpI activity and to human diseases. Since the Q chamber is long and narrow, it will restrict the quinone tail to an extended conformation. The passage around the entry of the cage is narrower than the rest of the cavity, so the quinone tail blocks solvent access to the cavity. Previously to the publication of this structure many authors suggested the presence of a second quinone binding site in CpI, but structural data argues strongly against its existence (Baradaran, Berrisford et al. 2013).

Currently, one of the key questions in CpI research is how it couples transfer electron activity and proton translocation, since both processes occur in different parts of the enzyme separated by large distances. As commented above, the structure of the entire enzyme shows that the quinone-binding site in CpI is unique: elongated, enclosed and reaching far out of the membrane towards cluster N2. It has been suggested that this quinone binding site allows the protein to fully control the protonation of the quinone as the essential part of the coupling mechanism (Sazanov 2014). The midpoint redox potential (E_{m7}) of NADH at pH 7 is about −320 mV, those of the Fe-S clusters around -250 mV, that of cluster N2 near -150 mV and the one of the Q/QH2 pair is around +100 mV (for ubiquinone) (Efremov and Sazanov 2012).Therefore, during CpI activity

most of the redox energy from NADH is used to reduce the quinone and some of it would be also used to reduce the N2 cluster, which produces the reported shifts of helices at the interface with the membrane domain (Baradaran, Berrisford et al. 2013). These two points of energy release in CpI may play a crucial role in the coupling mechanism (Sazanov 2014), but until now this question is still open.

2. Objectives

Functional reconstitution of membrane proteins on supported biomimetic bilayers has been the aim of this thesis. Two related enzymes have been chosen to develop this objective; membrane bound NiFeSe hydrogenase from *Desulfovibrio vulgaris* and Respiratory Complex I from *Rhodotermus marinus*. Both are redox enzymes that regulate the proton concentration of different parts in biological systems and play a crucial role in energy transduction. In order to reach the proposed global objective, different partial objectives were approached:

- To understand the catalytic mechanism of the membrane bound NiFeSe Hase from *D. vulgaris,* in particular the role that the Se atom confers to the active site of hydrogenases.

- To functionally reconstitute the membrane bound NiFeSe Hase from *D. vulgaris* on a gold electrode and characterize the biomimetic construction by electrochemical methods, Atomic Force Microscopy (AFM) and Surface Enhanced Infrared Spectroscopy (SEIRAS).

- To control and monitor the proton concentration generated by the enzyme in the interface bilayer/electrode interface by electrochemistry.

- To functionally reconstitute the Respiratory Complex I from *Rhodotermus marinus* on a gold electrode, measuring electrochemically both its NADH oxidation and proton translocation activities and characterizing the biomimetic construction by Atomic Force Microscopy (AFM) and Surface Enhanced Infrared Spectroscopy (SEIRAS).

3. Materials and Methods

3.1 Enzymes Purification:

The enzymes studied in this thesis were purified by two different groups from the ITQB (Instituto de Tecnologia Química e Biológica) Universidade Nova de Lisboa, Portugal. The PhD applicant has participated in one of the multiple purifications of the NiFeSe hydrogenase from *Desulfovibrio vulgaris* Hildenborough during a short stay at the laboratory of Dr. Ines Pereira. The process of purification of both proteins is described, although the hydrogenase purification is explained more in detail because of the above reason.

3.1.1 **Hydrogenase NiFeSe from *Desulfovibrio vulgaris* Hildenborough** (NiFeSe Hase) was purified in the laboratory of Dr. Ines Pereira. *Desulfovibrio vulgaris* Hildenborough (DSM 644) was grown in lactate/sulphate medium as previously described (Le Gall, Payne et al. 1994). The preparation of the membrane extract was performed as in a previous work (Valente, Saraiva et al. 2001). The membranes were washed twice with 10 mM Tris–HCl buffer, pH 7.6, to remove soluble and weakly bound proteins, and membrane proteins were extracted by homogenising twice the membrane pellet in 20 mM Tris–HCl buffer, pH 7.6, with 2% (w/v) Zwittergent 3–12 (N-dodecyl-N,N-di-methyl-3-ammonio-1-propansulphonate), followed by centrifugation at 140,000· g for 1 h.

3.1.2 All purification procedures were performed at pH 7.6 and at 4ºC, and in the presence of 0.2% (w/v) Zwittergent 3–12. The detergent extract was loaded on a DEAE Sepharose Fast Flow column (Pharmacia, 5·40 cm) equilibrated with 20 mM Tris–HCl buffer, and a linear gradient of 0–400 mM NaCl (2.4 L) in the same buffer was applied. The fraction eluted at around 300 mM NaCl with hydrogenase activity was concentrated by ultrafiltration and dialysed to lower the ionic strength. This fraction was then passed through a Pharmacia Q-Sepharose HP column (Hiload 26/10, flow rate 5 mL/min) equilibrated with 50 mM Tris–HCl, and eluted with a stepwise gradient of NaCl. The fraction eluted at 350 mM NaCl was concentrated, and the membrane-bound NiFeSe Hase

([NiFeSe]m) was finally purified on a Pharmacia Q-Sepharose HP column (HiLoad 16/10) equilibrated with 20 mM Tris-HCl and 0.1% n-Dodecyl b-D-maltoside (DDM, Sigma). This column yielded pure the NiFeSe Hase, confirmed by the SDS-PAGE and activity-stained native gel.

3.1.3 Respiratory Complex I from *Rhodotermus marinus* was purified in the laboratory of Dra. Manuela Pereira from the ITQB.- *Rhodothermus marinus* growth, membrane preparation, and membrane protein solubilization were done as described previously (Pereira, Carita et al. 1999), except that the growth medium contained 100 mM glutamate. Respiratory NADH:menaquinone oxidoreductase (Complex I) was purified according to an established procedure (Fernandes, Sousa et al. 2006), optimized by introducing a further chromatographic step with a Mono-Q column (GE-Healthcare). Briefly, the sample was submitted to two successive High Performance Q-Sepharose columns, using as buffer 20 mM Tris–HCl (pH 8.0), 1 mM phenylmethanesulfonyl fluoride (PMSF, Roth), and 0.1% DDM (Glycon Biochemicals GmbH), and was eluted in a linear gradient, 0 to 1 M NaCl. The fraction containing Complex-I was then applied to a gel filtration S200 column, eluted with 20 mM Tris–HCl (pH 8.0), 1 mM PMSF, 0.1% DDM, and 150 mM NaCl, and finally applied on a Mono Q column using 20 mM Tris–HCl (pH 8.0), 1 mM PMSF, and 0.1% DDM as buffer. The complex I was eluted in a linear gradient, 0 to 1 M NaCl.

3.2 Preparation of liposomes

For the preparation of the liposomes an Avanti extruder was used. We parted from commercial lipids that were kept at -20ºC in a 1:1 chloroform:methanol solution until its utilization. From this solution the desired quantity of lipids was taken and the chloroform was evaporated. Once the lipids were dry, a water solution was prepared. To dissolve the lipids, the solution was subjected to ultrasounds. In order to achieve a quasi-monodisperse suspension of unilamelar vesicles, the vesicles suspension was passed several times across a porous membrane using an extruder as shown in **Figure 3.1** (MacDonald, MacDonald et al. 1991).

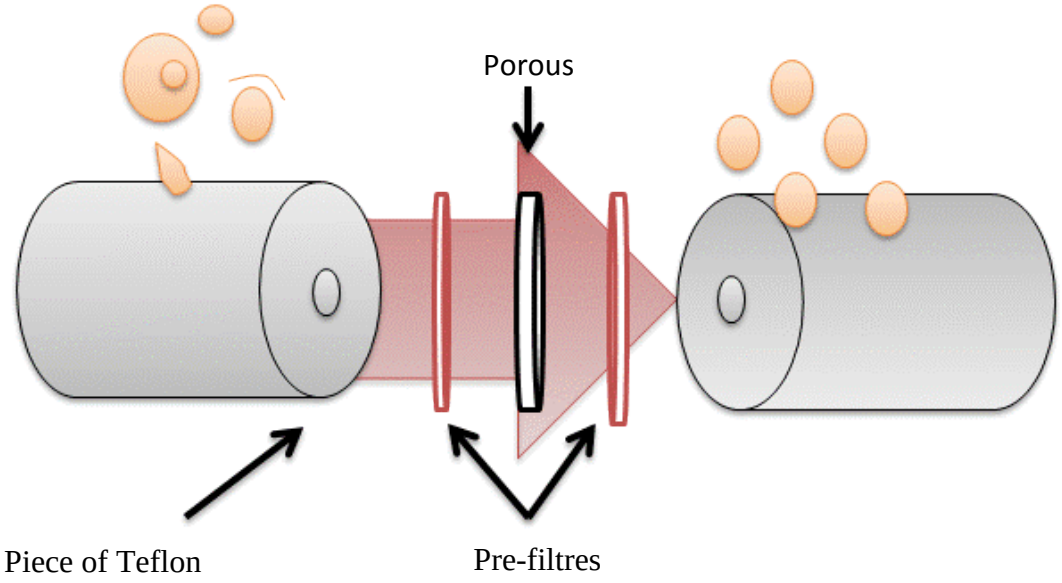

***Figure 3.1**: Schematic representation of the main parts of the extruder used to prepare the liposomes.*

Two different types of liposomes were prepared depending on the enzyme immobilized.

3.2.1 NiFeSe Hase immobilization:

E. coli polar fraction phospholipids (Avanti) solution in chloroform was evaporated using N_2. 10 mM MES buffer at pH 5 was then added in order to form a 4 mg/mL suspension of phospholipids that was subjected to ultrasounds for 15 min. The suspension was then extruded with the extruder equipped with a porous membrane (pores diameter of 300 nm). After this process, the dispersion was diluted to 0.6 mg/mL with 10 mM MES buffer at pH 5.

3.2.2 Complex I from *R. marinus* immobilization:

A 200 µL chloroform solution of 10 mg/mL egg phosphatidylcholine (PC, Avanti) was mixed with 180 µL of 1 mg/mL egg phosphatidic acid (PA, Avanti) in the same solvent. In order to achieve liposomes including quinone, 35 µl of 1.5 mg/mL 2,3-dimethyl-1,4-naphthoquinone (DMN) in ethanol was then added. The solution was shaken 10 min in a vortex and afterwards evaporated under N_2 flow. pH 5.5, 0.1 M phosphate buffer was added to form a 2 mg/mL suspension of phospholipids that was immersed in an ultrasound bath for 15 min. The

suspension was passed 21 times across an Avanti extruder equipped with a porous membrane (1 µm pores diameter). These lipids were also used in some hydrogenase experiments (indicated in the text).

3.3 Mass spectrometry measurements

The H/D isotope exchange activity of the NiFeSe Hase were measured by membrane-inlet mass spectrometry, in which a thermostated 37°C anaerobic vessel with magnetic stirring was connected through a 14-µm Teflon membrane to a mass spectrometer (Pfeiffer Prisma), as shown in Figure 1 (Jouanneau, Kelley et al. 1980).

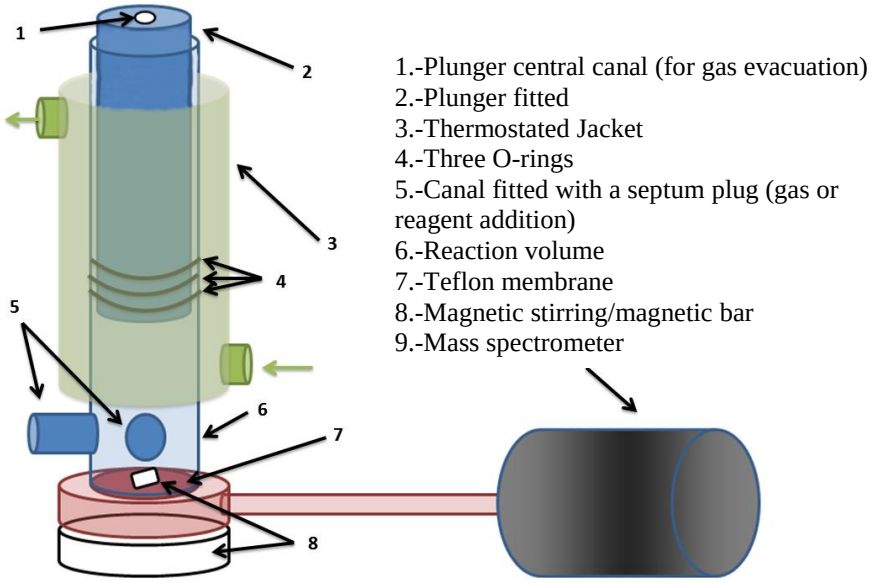

Figure 3.2: *Schematic representation of the reaction vessel connected to a mass spectrometer.*

The output signal of the spectrometer for each mass value is proportional to the partial pressure of the corresponding gas in the reaction vessel (Vignais, Cournac et al. 2002). The output signal was first calibrated by saturating the reactor solution with 100 % H_2 and then with 20 % D_2 in 80 % Ar (Air Liquide).

The D_2/H_2 assays were performed in a volume of 10 mL of buffered H_2O solutions in the pH range 3–10. Before the measurement the buffered H_2O was purged with argon (Air Liquide, 99.999 %) to replace the air. Once the oxygen level was not detected by the mass spectrometer, the solution was gassed with initial concentrations of D_2 that

ranged from 4 to 100 µM. For this, D_2 was bubbled through the solution in the reactor until the desired value of the mass 4 signal was reached. After reaching the desired value, the reactor lid was closed so that no gas phase was left in the reactor. The enzymatic reaction was started by adding through a rubber septum with gastight syringes (Alltech):

1.-100 µL of 1 % DDM
2.-1 µl of 1 M sodium dithionite
3.-25 µl of 0.1 µM NiFeSe Hase

During the measurement, masses 2 (H_2), 3 (HD), 4 (D_2) and 32 (O_2) were scanned (1 amu/s). The H_2 and HD production rates were determined from the difference in the slopes after and before the addition of hydrogenase and were expressed in micromoles per minute per milligram of protein. At least three independent measurements were used to obtain the main data.

The H_2/D_2 assays were carried in the reactor containing 10 mL of 20 mM phosphate buffer in D_2O (99.9 %, Sigma-Aldrich), pD 7.0, with initial H_2 concentrations that ranged between 7 and 450 µM. In order to exchange the enzyme's protons for deuterons, 1 µl of 100 µM hydrogenase sample was incubated overnight in 999 µL of D_2O-buffered solution at 4 ^oC. The other parameters of the experiment were the same as in the D_2/H_2 assays.

Taking into account the possibility of the presence of residual H_2O in the deuterated solution, a control experiment was performed. It was checked that H_2 and HD production was negligible in the D_2/D_2O system.

3.4 Preparation and modification of gold surfaces

Three types of gold surfaces were used:

3.4.1 Gold wires:

Au wires of 0.25 mm radius (Goodfellow Cambridge Limited) were used to perform electrochemical experiments. In order to clean and get a (111) surface the wires were submitted to: 1.-Cleaning with piranha solution (3:1 H_2SO_4

98%:H_2O_2 30%) followed by rinsing with Milli Q water (*Caution! Piranha solution is especially dangerous!*). 2.-Then, the wires were annealed to an orange glow for a few seconds in a propane flame (5 times). This treatment generates Au (111) terraces of a few micrometers radius. 3.- Au (111) wires were then submitted to an electrochemical cleaning (25 cycles in 0.5 M NaOH from -0.2V to -1.7 V at 0.5V/s followed by 25 cycles in 0.1 M H_2SO_4 from -0.2V to 1.3V at the same scan speed).

3.4.2 Au-coated substrates:

These substrates were used for AFM measurements. Au-coated surfaces (Metallhandel Schröer) consisted in a square (1 x 1 cm^2) of one layer of Au (200 nm) supported over Cr prepared on borosilicate glass. These substrates were submitted to: 1.-Piranha cleaning by adding a drop of piranha solution on the gold surface. 2.-Then, the substrates were annealed following the same process than the Au wires.

3.4.3 Gold film deposited on silicon:

The silicon prism used for SEIRAS experiments was treated following these steps: 1.- The reflecting plane of the prism (on which gold is deposited) was polished for one minute with successively finer grade alumina slurries down to 0.03 µm. 2.-Then, after rinsing carefully with mili-Q water, the prism was immersed in 40% NH_4F solution for two minutes. 3.- After removing the oxide layer on the Si surface, the prism was cleaned, dried and deposited in a water bath at 60ºC leaving the reflecting plane at the air. 4.- Once the prism was at 60ºC and the surface was completely dry, a drop of 200 µL of the platting solution (0.015 M $NaAuCl_4 \cdot 2H_2O$ + 0.15 M Na_2SO_3 + 0:05 M $Na_2S_2O_3 \cdot 5H_2O$ + 0.05 M NH_4Cl) mixed with 2% HF (2:1 in volume) was deposited on the surface. The reaction on the surface was stopped by adding water one minute after.

In order to modify the surface of the gold, a Self-Assembled-Monolayer (SAM) of 4-Aminothiophenol (Sigma) (4-ATP) was formed by incubating it overnight in a 1mM 4-ATP solution in ethanol.

3.5 Electrochemical measurements

The electrochemical measurements were run in three-electrode glass cells. A Ag/AgCl (3M NaCl) electrode from BAS or a saturated calomel electrode from Radiometer were used as reference electrode. All the results are shown vs. the Normal Hydrogen Electrode, NHE. A platinum wire from Goodfellow Cambridge Limited was used as a counter electrode. All the measurements were performed using an Autolab PGSTAT30 potentiostat/galvanostat, a μ-Autolab III electrochemical analyzer controlled by GPES 4.9 software (Eco Chemie), or a VersaStat 4-400 potentiostat (Princeton Applied Research). When anaerobic conditions were required the experiments were performed inside an anaerobic chamber (MBraun Unilab) filled with N_2 (oxygen concentration less than 0.1 ppm).

Different types of electrochemical measurements were carried in order to obtain the different types of information needed in each experiment:

3.5.1 Cyclic Voltammetry:

Different potentials in ramp were applied to the working electrode at a specific scan rate (V/s). The current associated at each potential was plotted in the voltammogram. It was used for electrode cleaning, electrode chemical modification and electrocatalytic measurements. The parameters used for these measurements are specified for each experiment.

3.5.2 Chronoamperometry:

A stepped potential was applied to the working electrode while the faradaic current was plotted versus time. This technique was used to study the effects of different conditions on the electroenzymatic activity. The applied potentials and conditions used are specified for each experiment.

3.5.3 Differential Pulse Voltammetry (DPV):

This technique was used for minimizing the effect of the charging current during potential scanning, thus allowing a more sensitive detection of faradaic

processes. The working electrode is subjected to different step potential pulses separated by a relaxation period. The current is measured immediately before the potential pulse and after the relaxation period. The increment of the current is plotted as function of the applied potential. The parameters used for these measurements were: a modulation time of 0.05s, an interval time of 0.1s and a modulation amplitude of 0.01V.

3.5.4 Impedance spectroscopy:

This technique has been used in order to obtain information about the effect of the different chemical modifications performed in the gold wires electrodes. Impedance can be defined as a complex resistance encountered when current flows through a circuit composed of various resistors, capacitors, and inductors. Faradaic impedance spectra were recorded using FRA 4.9 software (Eco Chemie) while applying +0.44 V (vs. NHE) bias potential and using 10 mV alternative voltage in the frequency range 10 kHz –100 mHz. The experimental impedance spectra were fitted using electronic equivalent circuits (Randles and Ershler model) in order to derive the electron-transfer resistance, R_{et}, values. An equimolecular solution of 2.5 mM $K_4[Fe(CN)_6]$ and 2.5 mM $K_3[Fe(CN)_6]$ was used as electrochemical probe in 0.1M phosphate buffer at pH 7. The measurements were carried out at room temperature (23 ± 2 °C).

3.6 Membrane enzymes reconstitution on/in biomimetic membranes on gold electrodes

The immobilization strategy of the different enzymes was developed taking into account the published structures. In both cases the adequate orientation of the enzymes was essential in order to achieve its functional immobilization.

3.6.1 NiFeSe Hase

Three different strategies were followed to achieve the oriented immobilization of the hydrogenase:

3.6.1.1 In order to achieve the configuration in which the lipid tail of the hydrogenase is embedded in the bilayer supported on the electrode (**Figure 5.1** (a)), the liposome suspension from *E. coli* polar extract 0.6 mg/mL in 10 mM MES buffer at pH 5 was incubated over gold for 45 minutes at room temperature. Then, the SEIRAS cell was cleaned carefully with MES buffer 10 mM at pH 7. 100 µl of 27 µM hydrogenase in MES buffer 10 mM at pH 7 were added over residual buffer. In order to remove the detergent present in hydrogenase sample, 48 mg of dry CALBIOSORB adsorbent were added to the solution inside a metallic mesh for 1.5 hours.

3.6.1.2 In order to achieve the configuration in which the protein is immobilized directly on the modified gold surface and the membrane is formed over the protein (**Figure 5.1** (b)), the liposome suspension (200 µl) was incubated together with the hydrogenase sample (100 µl) and the CALBIOSORB adsorbent (48 mg) for 1.5 hours. Then, the cell was cleaned very carefully with 10 mM MES buffer at pH 7 and incubated 30 minutes in a 11.6 mM N-(3-dimethylaminopropyl)-N´-ethylcarbodiimide hydrochloride (EDC) (Sigma) in 10 mM MES buffer at pH 6.

3.6.1.3 To improve the immobilization described in 2.6.1.2 for the SEIRAS measurements, a different strategy was developed. Instead of mixing hydrogenase and liposomes in one step, the immobilization was carried out “step by step”. Firstly, 100 µM (50 µl) hydrogenase sample was added to 150µl of 10 mM MES buffer at pH 5 with 0.1% of DDM. After 45 minutes incubation the protein that was not adsorbed on the surface was removed by rinsing carefully with 10 mM MES buffer at pH 5 with 0.1% of DDM. Then, a covalent binding between the 4-ATP SAM and the hydrogenase was facilitated by incubating in a solution of 11.6 mM EDC for 30 minutes. Both solutions were prepared in 10 mM MES buffer at pH 6 with 0.1% of DDM. Once the protein was covalently

bound, the cell was cleaned with 10 mM MES buffer at pH 6 with 0.1% of DDM several times. Then, the phospholipid bilayer was formed incubating the liposome solution mentioned above in presence of biobeads until changes were not observed in the infrared spectra.

3.6.2 Complex I from *Rhodotermus marinus*

Two different strategies were developed to immobilize Complex I. Two types of liposomes were used; 9 PC:1 PA in weight liposomes, with and without DMN.

3.6.2.1 Complex I inserted in liposomes:

10 µL of 6,2 mg/mL complex I were added to 500 µL of the liposome (with or without DMN) suspension at pH 5 and stirred softly with vortex at 4^{o}C during 15 min. After this, 15 mg of CALBIOSORB adsorbent biobeads (Calbiochem) were added to the suspension, which was stirred again for 1 hour. Then, this operation was repeated twice, stirring 30 minutes each time.

After this procedure, the proteoliposome suspension was deposited overnight over the gold surface functionalized with 4-ATP at 4ºC in presence of CALBIOSORB adsorbent biobeads.

3.6.2.2 Complex I inserted on the biomimetic bilayer formed over gold:

Firstly, the 4-ATP-modified gold was incubated in the liposome suspension for 3 hours at room temperature. Then, the suspension was removed and the surface was cleaned with pH 7.0, 0.1 M phosphate buffer several times. After this, 10 µL of 6,2 mg/mL complex I were added to the residual clean buffer in the SEIRAS cell and it was left overnight at 4ºC in presence of CALBIOSORB adsorbent biobeads.

3.7 Atomic Force Microscopy (AFM)

This technique was chosen for the surface characterization of modified gold due to its high resolution (≤1nm) and because of the possibility of studying biological samples in liquid that AFM offers. As shown in the scheme, in this technique a tip located at the end of a cantilever is used to scan a surface (the sample). The scanning is made by the expansion and contraction of a piezoceramic tube controlled by a computer system with subnanometer accuracy. An optical system is used to monitor the deflection of the cantilever, and a topographic image of the sample is obtained plotting this deflection versus the position on the sample.

There are three operation modes for the AFM: 1.-contact mode, 2.-dynamic mode and 3.-intermittent contact mode.

The second one, dynamic mode, operates in the non-contact region of the interaction potential. A second piezoelectric piece is needed to put the cantilever under resonance to keep the resonance amplitude constant or the resonance frequency constant. Any change in topography generates a change in the resonance amplitude or frequency. In this thesis, the samples were measured in the non-contact region maintaining the amplitude constant, known as the "tapping mode".

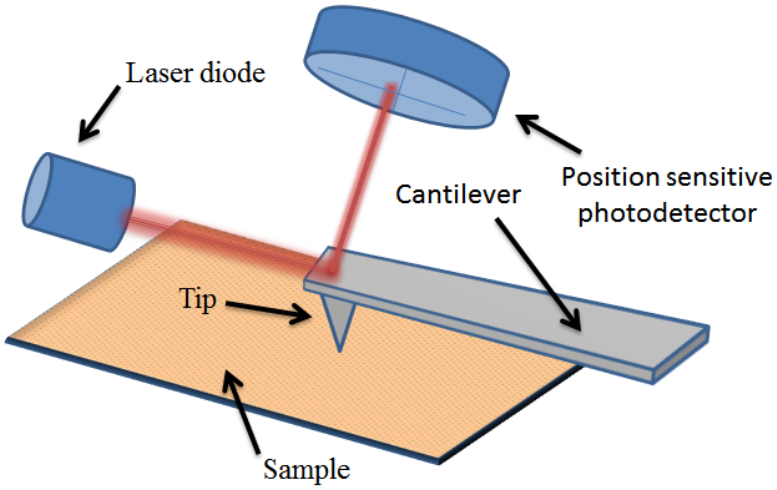

Figure 3.3: *Schematic representation of the main parts of an atomic force microscope.*

The microscope used for AFM imaging was an Agilent Technologies 5500 instrument. Measurements were always made under liquid conditions in pH 7.0, 0.1M phosphate buffer at room temperature. All samples were measured using Olympus rectangular silicon nitride cantilevers (RC800PSA, 200 × 20 μm^2) with a spring constant of 0.05 N/m, an estimated tip radius of 20 nm, and a resonance frequency in the liquid cell of approximately 27 kHz. Scanning rates were kept close to 1 Hz. All images contain 512 pixels x 512 pixels and were first-order flattened using Picoimage software from Agilent.

3.8 Surface Enhanced Infrared Spectroscopy (SEIRAS)

SEIRAS is a non-conventional infrared spectroscopy technique. It is based in the surface enhancement effect of infrared absorption in rough (at the nanoscale) metals. A ten-fold stronger electromagnetic (EM) field was calculated to contribute to the overall surface enhancement. Two features of SEIRAS are crucial for understanding the results obtained with this non-conventional infrared spectroscopy:

1. The local EM field intensity decays sharply with the distance from the surface (in the order of 10 nm).

2. The vibrational modes whose dipole moment changes parallel to the surface normal are strongly enhanced compared to those comprising a perpendicular component (surface selection rule).

The spectroelectrochemical measurements were performed using a trapezium-shaped silicon ATR-IR element (W × L × H: 20 × 25 × 10 mm^3) covered with a nanostructured SEIRA Au film formed by electroless deposition (described before). This prism was located in the SEIRA cell as shown in **Figure 3.4**.

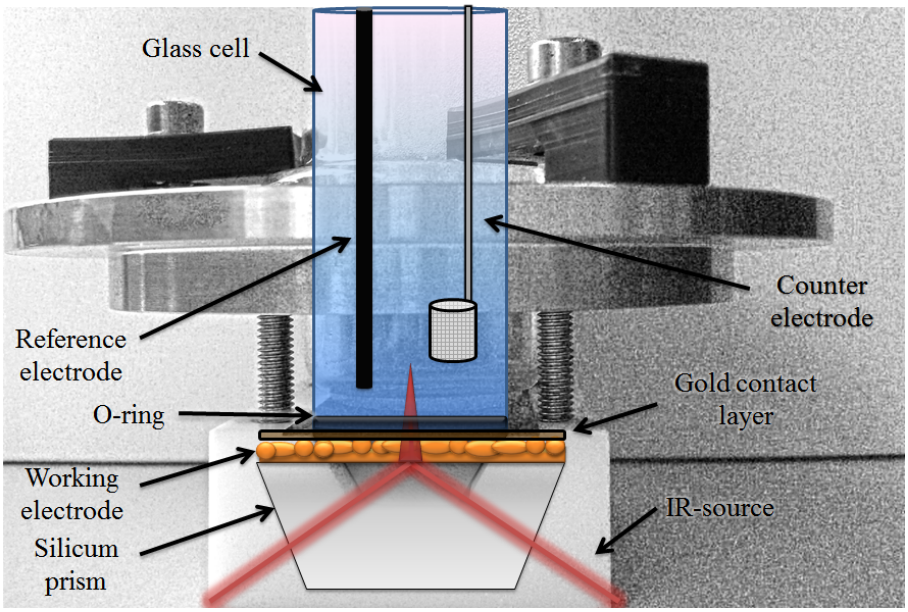

***Figure 3.4**: Schematic representation of the cell used to perform electrochemical-SEIRAS experiments.*

SEIRA was performed with a Kretschmann-ATR configuration under an angle of incidence of 60 ° (**Figure 3.5**). All spectra were recorded in a spectral window of 4000 to 1000 cm-1 and with a resolution of 4 cm-1 using a Bruker 27 or a Bruker IFS66v/s spectrometer with a photoconductive MCT detector. For each spectrum, 400 scans were accumulated.

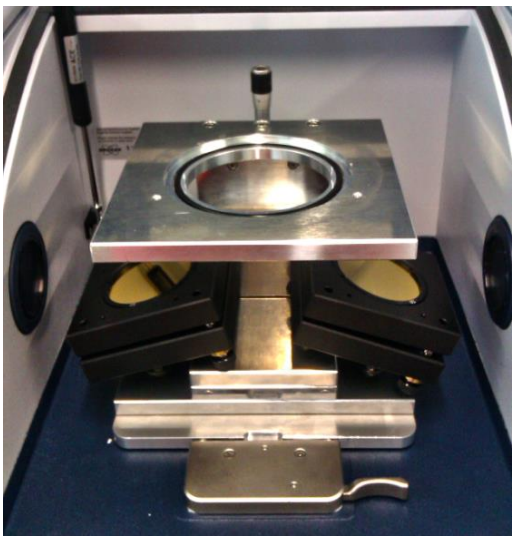

Figure 3.5: *Photograph of the ATR configuration in the BRUKER 27 FTIR-spectrometer used for SEIRAS measurements.*

4. H^+/D^+ Isotope exchange activity study of the NiFeSe Hase from *Desulfovibrio vulgaris*

4.1 Introduction

The use of hydrogen isotopes (deuterium, tritium) allows the detection of hydrogen molecule splitting by hydrogenases. The exchange reactions of deuterium gas in water (H^+/D_2), or hydrogen gas in deuterated water (D^+/H_2), evidence the reversible activity of hydrogenases, catalysing both dihydrogen oxidation and production, and provides an intrinsic measure of their catalytic activity, as it does not depend on the presence of a redox mediator or an electrode (Alvin 1979). This activity has been used to study the mechanism of the enzyme action (see below). It is well known that hydrogenases catalyse the heterolytic splitting of hydrogen with formation of an intermediate in which the hydride binds to the active site metals and the proton to one of the terminal cysteines of the Ni (De Lacey, Fernández et al. 2007):

$$\text{Cys-NiFe} + H_2 \leftrightarrow H^+\text{:Cys-NiFe:}H^-$$

Where NiFe is the bimetallic active site of hydrogenases. In the case of using D_2 instead of H_2 the reaction is the same but changing H by D. When no electron donor or acceptor is present the reaction shown becomes completely reversible. The presence of the isotope leads to protons and deuterons exchange and the formation of HD as detectable intermediate:

$$H+\text{:Cys-NiFe:}H^- + D^+ \leftrightarrow D^+\text{:Cys-NiFe:}H^- + H^+$$

$$D+\text{:Cys-NiFe:}H^- \leftrightarrow \text{Cys-NiFe} + HD$$

The HD intermediate may react again with the active site:

$$\text{Cys-NiFe} + HD \leftrightarrow H^+\text{:Cys-NiFe:}D^-$$

$$H^+\text{:Cys-NiFe:}D^- + D^+ \leftrightarrow D^+\text{:Cys-NiFe:}H^- + H^+$$

$$D^+\text{:Cys-NiFe:}D^- \leftrightarrow \text{Cys-NiFe} + D_2$$

Proton isotope exchange reaction can be followed by mass spectrometry (Jouanneau, Kelley et al. 1980).

This technique has been used in this thesis with the aim of elucidating the behavior of NiFeSe Hase isotope exchange activity from *D. vulgaris* and to compare it with other Hases isotope exchange activity described previously. This study allows determining the influence of the Se atom in the catalytic properties of this hydrogenase versus the changes in the protein structure surrounding the active site.

4.2 Results

A representative measurement done with the mass spectrometer of the D_2/H^+ exchange activity of *D. vulgaris* NiFeSe hydrogenase at pH 7.0 and 37ºC is shown in **Figure 4.1**. After hermetic closure of the reactor (time zero) the mass 4 signal starts to decrease indicating that the deuterium gas in the sample starts to be consumed by the mass spectrometer. Only after the hydrogenase had been added did the signals of masses 2 (H_2) and 3 (HD) start to increase due its isotope interchange activity. The previous addition of detergent to the reactor was necessary to retain the maximal catalytic activity of the membrane hydrogenase during the D_2/H^+ exchange activity assays (Valente, Oliveira et al. 2005, Valente, Pereira et al. 2007).

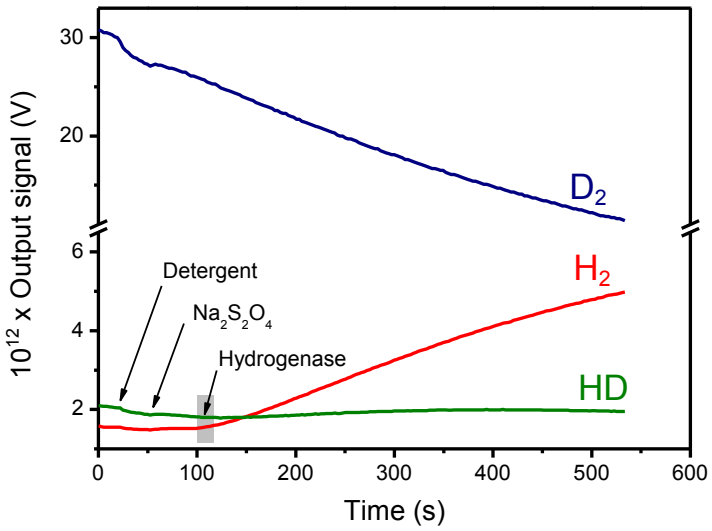

Figure 4.1: *Measurement of D_2/H^+ exchange activity of NiFeSe Hase. The reaction was performed in pH 7, 20 mM phosphate buffer at 37 ºC saturated with with 20 % D_2 in 80 % Ar gas. The enzymatic reaction was started by adding as indicated 100 µL of 1 % DDM, 1 µL of 1 M of sodium dithionite (to eliminate residual oxygen) and 25 µL of 0.1 µM hydrogenase solution.*

The addition of sodium dithionite as a chemical reducer was required in order to activate the hydrogenase. As shown in **Figure 4.1**, it is clear that the rate of formation of the double-exchange product (H_2) is much higher than that of the single-exchange product (HD), which is the typical kinetic functioning of the NiFeSe hydrogenases under similar conditions (Fauque, Berlier et al. 1987, Berlier, Lespinat et al. 1990, P 2002).

The D_2/H^+ isotope exchange activity of this hydrogenase was dependent on the pH as shown in **Figure 4.2**. This graph shows the trends of the specific activities of H_2 and HD formation at different pH values. The optimum of the overall isotope exchange activity is at pH 6, as also for the H_2 production activity. The single exchange activity does not depend so much on the pH as the double exchange activity, and predominated over H_2 production at high and low pH. Overall, the H_2/HD ratio of the isotope exchange activity is only high around the pH optimum, decreasing dramatically at lower and higher pH values. This means that the double-exchange reaction only occurs faster than the single-exchange reaction under the conditions in which the enzyme is working at higher turnover rates.

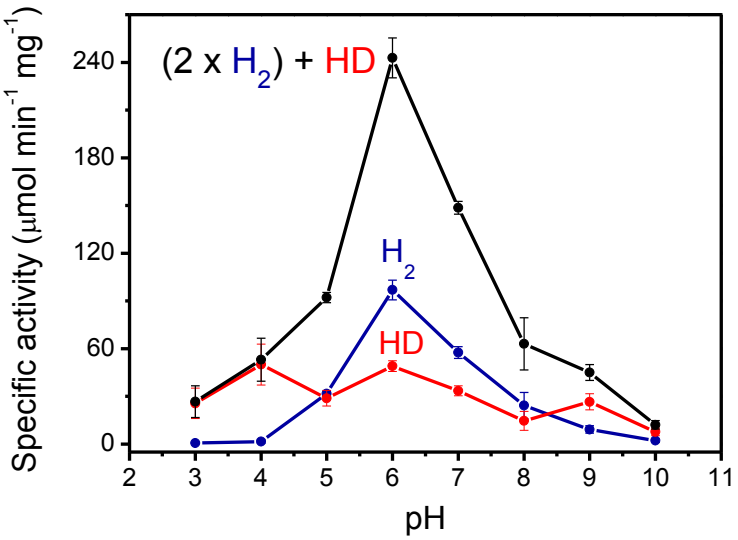

Figure 4.2: *Dependence of the D_2/H^+ isotope exchange activity of NiFeSe Hase on pH. Rates of double-exchange production (H2)(blue), of single-exchange production (HD)(red) and total proton exchange activity (2 x H2 + HD)(black). Measurements were done at 37ºC with the following mixture of buffers: sodium citrate, 2-morpholinoe-thanesulfonic acid, N-(2-hydroxyethyl)piperazine-N0-ethanesulfonicacid, tris (hydroxymethyl) aminomethane, and sodium carbonate, each one at 10 mM concentration.*

The influence of the substrate concentration on the D_2/H^+ exchange activity of the NiFeSe Hase was also measured. In order to avoid the effect of the continuous uptake of gases by the spectrometer, which is under high vacuum conditions, only the initial rates of HD and H2 production were measured at different initial D_2 concentrations. In this

way, the background uptake of HD and H_2 by the spectrometer is very small and can be easily eliminated by subtracting the slopes before addition of the enzyme from those after addition of the enzyme.

In order to analyse the results obtained from the study of the D_2/H^+ activity dependence on substrate concentration, the following equation based in the Michaelis-Mentel model (Baldwin 2000) was used:

$$E \underset{k_{-1}^{D_2}}{\overset{k_{+1}^{D_2}[D_2]}{\rightleftharpoons}} E\text{-}D_2 \xrightarrow{k_{cat}^{H_2O}} E + HD/H_2 \qquad (1)$$

Where k_{+1}^{D2} is the rate constant of substrate binding to the enzyme (E) and and k_{-1}^{D2} is the rate constant for its dissociation. Once the deuterium molecule is bound to the active site of the hydrogenase, the molecule suffers heterolytic cleavage followed by interchange of deuterium atoms with protons from water. This interchange can be single or double as indicated in the reaction *(1)*, leading to HD and H_2 production. The overall catalytic cycle is governed by an apparent first order rate constant (k_{cat}^{H2O}). According to Michaelis-Menten kinetics, we can describe the specific activity of D_2/H^+ (*V*) as follows (Baldwin 2000):

$$V = \frac{[D_2]\, V_{max}^{H2O}}{[D_2] + k_M^{D_2}} \qquad (2)$$

Where V_{max}^{H2O} is the specific activity of D_2/H^+ and k_M^{D2} is the Michaelis constant for the substrate, which it can be described as:

$$k_M^{D_2} = \frac{k_{cat}^{H_2O} + k_{-1}^{D_2}}{k_{+1}^{D_2}} \qquad (3)$$

Multiple measurements at different initial substrate concentrations were done. To study the dependence of the specific activity on substrate concentration we represented the $HD+H_2$ production by the enzyme, which is equivalent to D_2 uptake, versus the initial D_2 concentration. The experimental data were fitted to the Michaelis-Menten equation

(**Figure 4.3**) in order to determine the Michaelis constant for D_2 (k_M^{D2} **= 6 ± 1 µM**) and the maximal D_2/H^+ specific activity (V_{max}^{H2O}**= 154 ± 7 µmol min^{-1} mg^{-1}**).

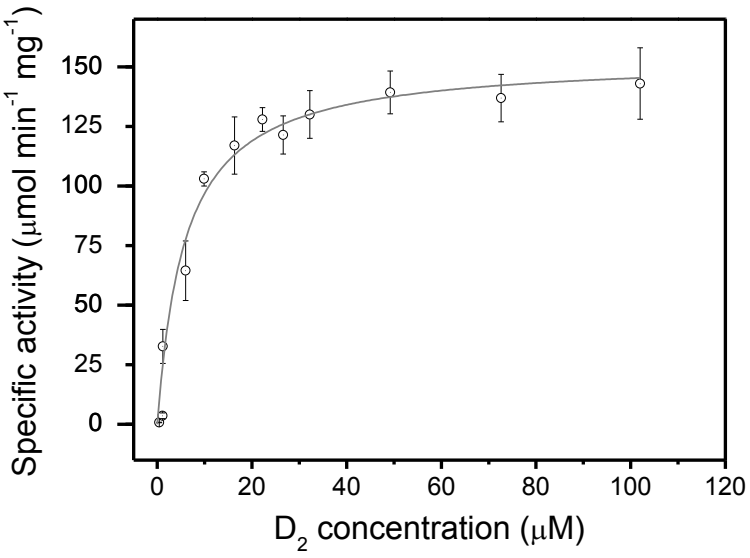

Figure 4.3: *Dependence of the specific D_2/H^+ activity ($HD+H_2$ production) on substrate concentration of NiFeSe Hase. The grey line corresponds to the best fit to equation (2).*

Buffered deuterated water saturated in H_2 was also used to measure the isotope exchange activity of the hydrogenase. The first observable change versus measurements in D_2/H_2O was that in the H_2/D^+ assay the rate of single-exchange production is higher than double-exchange production (**Figure 4.4**).

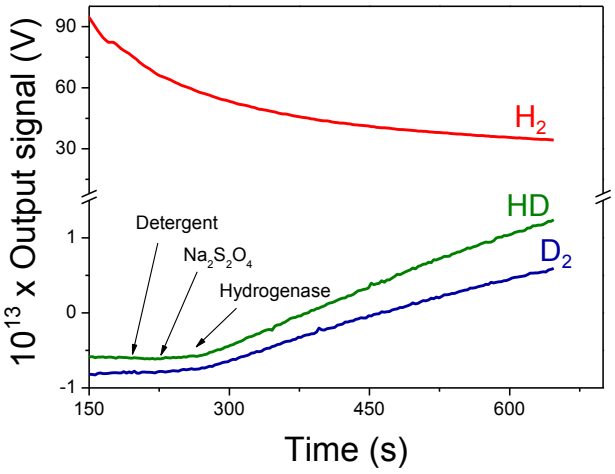

Figure 4.4: *Measurement of H_2/D^+ exchange activity of the NiFeSe Hase. The reaction was performed in 20 mM phosphate buffer in D_2O at 37 ºC, pD 7.0, saturated with 99.9% H_2 gas*

(450 µM of H_2 at the beginning of the reaction). The enzymatic reaction was started by adding as indicated 100 µL of 1 % DDM, 1 µL of 1 M of sodium dithionite (to eliminate residual oxygen) and 25 µL of 0.1 µM hydrogenase solution.

As for the D_2/H^+ activity, the dependence of the H_2/D^+ exchange activity on the substrate concentration was studied (**Figure 4.5**). By fitting the experimental data to theoretical Michaelis–Menten kinetics, the Michaelis constant for H_2 ($\boldsymbol{k_M^{H2}}$ **= 34 ± 3 µM**) and the maximal specific activity max in D_2O (V_{max}^{D2O} **= 142 ± 7 µmol min^{-1} mg^{-1}**) were determined. As it can be seen in the **Table 4.1**, there is a significant isotope effect in the Michaelis constant for the substrate but not in the maximal specific exchange activity. The K_M for H_2 is around five times higher than the K_M for D_2. This means that there is a significant isotope effect in the affinity of this hydrogenase for the substrate.

	D_2/H_2O	H_2/D_2O
V_{max} (µmol min^{-1} mg^{-1})	154 ± 7	142 ± 7
K_m (µM)	6 ± 1	34 ± 3

Table 4.1: Maximal specific exchange activity and Michaelis constant for D_2 and H_2 of NiFeSe hydrogenase from *D.vulgaris.*

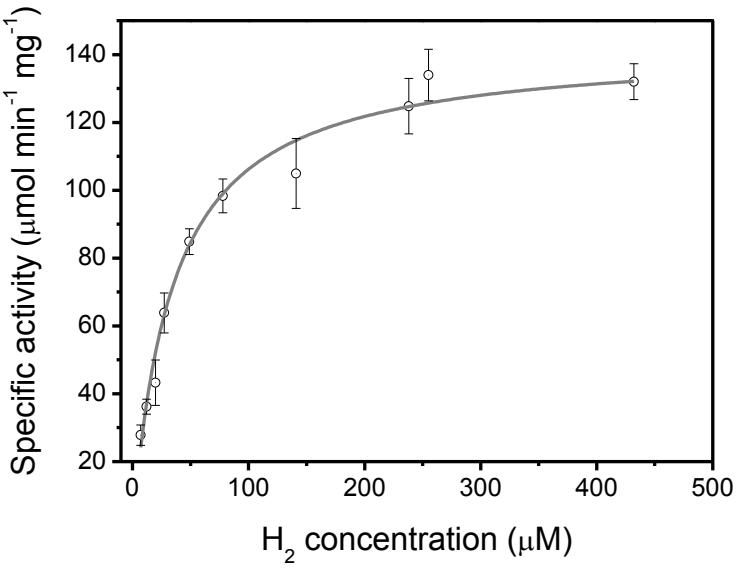

Figure 4.5: *Dependence of the specific H_2/D^+ activity ($HD+D_2$ production) on substrate concentration of NiFeSe Hase. The grey line corresponds to the best fit to equation (2).*

	NiFeSe *D. vulgaris*[a]	*D. gigas*[b]	*Ralstonia eutropha* H_2 *sensor*[c]	*Thiocapsa roseopersicina*[d]	*Rhodobacter capsulatus*[e]	*Pseudomonas denitrificans*[f]
HD/H_2 (H_2O)	0.4	2.5	0	2.5	0.4	0.4
HD/D_2 (D_2O)	2.0	5.0	0.8	2.5	1.4	0.6

[a] Determined in this thesis
[b] From A.L De Lacey and V.M Fernández (unpublished data)
[c] From (Bernhard, Buhrke et al. 2001)
[d] From (Zorin, Dimon et al. 1996, Bertrand, Dole et al. 2000)
[e] From (Jouanneau, Kelley et al. 1980)
[f] From (Paulette, Michele-France et al. 1982)

Table 4.2: *Ratios of single/double exchange of D_2 in H_2O and H_2 in D_2O for different hydrogenases at their optimum pH.*

Table 4.2 indicates that for the NiFeSe hydrogenase and the aerobic hydrogenase from *R. eutropha* the isotope effect is important. In contrast, for anaerobic NiFe hydrogenases (such as those from *Thiocapsa roseopersicina* and *Desulfovibrio gigas*) there is a small or no isotope effect.

The isotope exchange activity has been measured also for a mutant of NiFeSe Hase prepared by de group of Dr. Inês Pereira, in which the SeCys of the active site was replaced by a Cys (U489C). Mass spectrometry measurements in D_2/H_2O gave optimal rates of single exchange of 16 ± 5 µmol min^{-1} mg^{-1} and a double exchange of 29 ± 3 µmol min^{-1} mg^{-1}. Therefore, the mutation at the active site seldom affects the single/double exchange ratio (**Figure 4.6**).

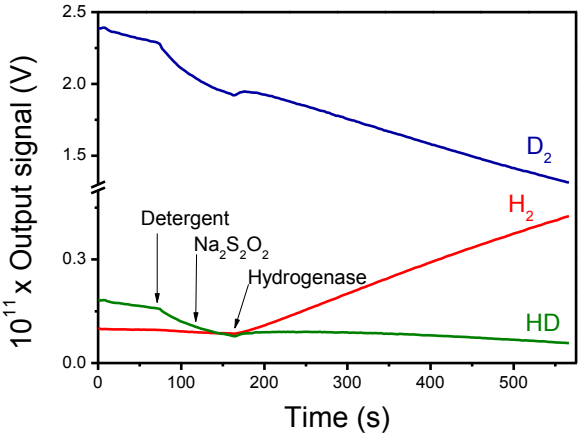

Figure 4.6: *Measurement of D_2/H^+ exchange activity of the U489C mutant of NiFeSe Hase. The reaction was performed in pH 7, 20 mM phosphate buffer at 37 ºC saturated with with 20 % D_2 in 80 % Ar gas. The enzymatic reaction was started by adding as indicated 100 µL of 1 % DDM, 1 µL of 1 M of sodium dithionite (to eliminate residual oxygen) and 25 µL of 0.1 µM hydrogenase solution.*

4.3 Discussion

Figure 4.1 shows that the D_2/H^+ activity of the NiFeSe Hase is dependent on pH and that the optimum of activity is at pH 6. This fact suggests that proton exchange at the active site is rate-limited by a protonable group with a pKa near the optimum pH of D_2/H^+ activity. If we assume that the exchange mechanism involves deprotonation and reprotonation of a dihydrogen complex intermediate, we would expect a maximum exchange rate near the pKa of this intermediate as well a decrease in exchange rate at higher and lower pH values (Jennifer, Paul et al. 2007). This optimum pH value changes for different hydrogenases. The reported pH optimum for the NiFe hydrogenase from *D. gigas* in the same assay was 7.8, whereas for another NiFeSe hydrogenase (from *D. baculatum*) it was 4.5 (Fauque, Peck et al. 1988). These results indicate that the optimum pH of NiFeSe hydrogenases is lower than for NiFe hydrogenases due to the existence of a protonable group with different pKa. The change of the terminal cysteine of the active site by a selenocysteine, as the latter amino acid has a lower pKa, can be the explication for this shift (Baltazar, Marques et al. 2011). Nevertheless, we cannot rule out that several other basic sites of the enzyme may also limit the rate of the catalytic process.

It has been described that in the D_2/H^+ activity measurements for NiFe hydrogenases the single exchange is faster than the double exchange, whereas for NiFeSe hydrogenases the single exchange is slower than the double exchange, as shown in **Table 4.2** (Jouanneau, Kelley et al. 1980, Paulette, Michele-France et al. 1982, Zorin, Dimon et al. 1996, Bertrand, Dole et al. 2000, Bernhard, Buhrke et al. 2001). In order to explain this catalytic property of NiFeSe hydrogenases two different hypothesis have been proposed in the literature. The first one considers that a less electronegative atom than sulphur (selenium) coordinated to the active site nickel destabilizes the hydride intermediate of the catalytic cycle (Alvin 1979, Paulette, Michele-France et al. 1982, Teixeira, Fauque et al. 1987, Zorin, Dimon et al. 1996). The second hypothesis assumes a ‘‘cage effect’’ of the protein structure favouring successive reactions of formed HD intermediates (Tamiya and Miller 1963, Alvin 1979, Bernhard, Buhrke et al. 2001).

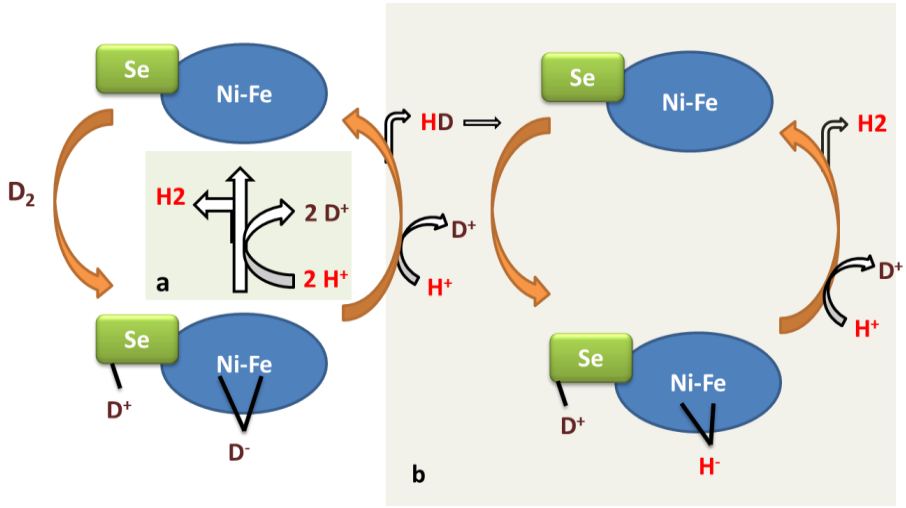

Figure 4.7: *Catalytic mechanism of D_2/H^+ exchange by NiFeSe hydrogenases. The high initial rate of the double-exchange reaction can be explained by fast exchange at the protic and hydride sites before release of dihydrogen (a) or by successive reactions of the HD intermediate formed before it is released from the enzyme (b).*

In **Figure 4.7** we can observe a scheme of the two proposed catalytic cycles for H^+/D_2 activity in NiFeSe hydrogenases. The first one (a) suggests that the lower electronegativity of selenium, compared with sulphur, increases the electron donation to the bimetallic active site, thus favouring the isotope exchange of D^- after heterolytic cleavage of D_2 and before the formation of HD at the active site (Paulette, Michele-France et al. 1982, Teixeira, Fauque et al. 1987, Zorin, Dimon et al. 1996). This hypothesis is supported by the lower vibrational frequencies measured by FTIR spectroscopy for the active site's CO ligand (De Lacey, Gutiérrez-Sánchez et al. 2008), confirming higher electron donation from the selenium to the bimetallic active site. The second proposal explains the formation of H_2 as a consequence of successive exchange reactions of the intermediate HD owing to its accumulation near the active site, as shown in **Figure 4.7** (step b). This effect would be caused by slow release of the intermediate to the solution owing to a steric effect of the protein structure surrounding the active site, the named ''cage effect'' (Tamiya and Miller 1963, Alvin 1979, Bernhard, Buhrke et al. 2001).

Our results clearly show that the double exchange (D_2) is only faster than the single exchange (HD formation) at pH values around the activity optimum. At lower and higher values of pH the single exchange prevails over the double exchange. If the double exchange (H_2 formation) is produced in a cycle that involves the exchange of

two protons, a higher activity would be expected at high proton concentrations. This is the case described for D_2/H^+ exchange activity of rhodium complexes, for which a catalytic mechanism was proposed where two successive protonation steps occur in the same cycle at higher proton concentration. In contrast, if the double-exchange formation requires the formation of an intermediate (HD) followed by re-coordination, then the double exchange/single exchange ratio would increase at pH values where the catalyst turnover is higher (Jennifer, Paul et al. 2007). Taking into account this behaviour, we can postulate that what we observe for *D. vulgaris* hydrogenase in **Figure 4.7** corresponds to a "cage effect". This difference between the organometallic catalyst and the biocatalyst is in consonance with the bimetallic active site of the hydrogenase being buried inside the protein structure (Marques, Coelho et al. 2010).

The "cage effect" can explain the considerable isotope effect measured in the H^+/D^+ exchange activity of the NiFeSe hydrogenase. The existence of this effect would favour the diffusion of lighter compounds outside the protein versus heavier compounds. In this sense, the heavier products (D_2 in the H_2/D_2O experiment and HD in the D_2/H_2O experiment) will diffuse slower to the solution and have more probabilities of a second exchange reaction. Also, the higher double exchange rate than the single one found in the U489C mutant is in agreement with a catalytic mechanism controlled by the cage effect. If the presence of selenium in the active site would be the responsible of the predominance of double exchange versus single exchange, then the mutation of a SeCys for a Cys should modify considerably the rate ratio, which is not the experimental result. A scheme of the the "cage effect" on the isotope exchange activity is shown in **Figure 4.8**.

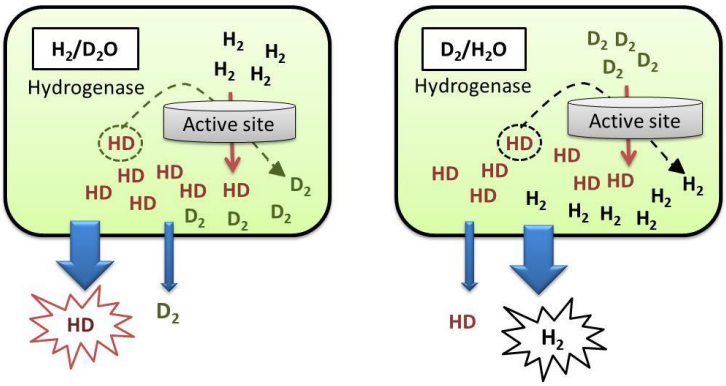

Figure 4.8: *Scheme of the cage effect in H_2/D_2O and D_2/H_2O experiments. In H_2/D_2O experiment (left), the H_2 is split at the active site producing HD, which is able to be split again*

forming D_2. HD, lighter than D_2, diffuses faster than D_2 to the solution. In D_2/H_2O experiment (right) D_2 is split at the active site giving HD which can again be split forming H_2. Dihydrogen, lighter than HD, diffuses faster than HD to the solution.

The isotope effect is dramatically different depending on the types of hydrogenases studied, as shown in **Table 4.2**. The remarkable isotope effect for the H_2 sensor hydrogenase from *Ralstonia eutropha* hydrogenase was attributed also to a ‘‘cage effect’’ caused by the presence of bulky amino acid residues surrounding the access of the H2 channel to the active site (Bernhard, Buhrke et al. 2001). In contrast, small or insignificant isotope effect is found in other hydrogenases. This variety of results suggests that the protein structure surrounding the active site of each hydrogenase modulates the rates of transport of dihydrogen molecules to/from the active site. In this line, the analysis by computational study of H_2 transport inside the NiFe hydrogenase from *D. gigas* and in the NiFeSe hydrogenase from *D. baculatum* evidenced the changes in H_2 access routes to the active site due to the amino acid composition of the active site surroundings (Baltazar, Teixeira et al. 2012)

Molecular Dynamics (MD) simulations of the diffusion of H_2 and D_2 in the NiFeSe Hase have been performed by Carla Baltazar and Claudio Soares (Oscar, Marta et al. 2013). This study concluded that H_2 and D_2 molecules use an alternative channel to access the active site in this enzyme, similarly to what was found in the *D. baculatum* enzyme for H_2 (Baltazar, Teixeira et al. 2012). The MD simulations revealed higher accumulation of D_2 in comparison with H_2 in the previously mentioned channel of the *D. vulgaris* hydrogenase. This difference is related to the different masses of the two species, since mass was the only parameter changed. Despite not having simulated HD, it was assumed that it would behave between these two extreme situations, accumulating more than H_2 but less than D_2.

The results obtained of the MD simulations are in agreement with the experimental H/D exchange activity results. The differences in the exchange activity of different hydrogenases showed in **Table 4.2** may due to their structural differences in the surroundings of the active site cavity. In this line, the larger the gas cavity next to the active site means more product molecules accumulated near to the active site (Baltazar, Teixeira et al. 2012), so the ‘‘cage effect’’ in the catalytic activity will be increased.

The strong isotope effect in the K_M for the substrate is also in agreement with the ‘‘cage effect’’ on the exchange activity. MD simulations support the experimental results, suggesting higher affinity of D_2 for the protein when compared with H_2. This is deduced from the higher accumulation of D_2 near the active site, which can be interpreted as a higher affinity and, consequently, a lower K_M.

Furthermore, as indicated above (equation 3), K_M depends on k_{cat} and on the dissociation constant of the substrate. Therefore, the large increase of the K_M for H_2 is due to an increase of its dissociation constant from the active site compared with D_2, because V_{max} is not affected by the isotope effect. In such way, it has been reported that the measured $K_M^{H_2}$ of another NiFe Hase is very sensitive to mutations of amino acid residues lining the H_2-transport channel, increasing by up to two orders of magnitude when the putative H_2 channel was made narrower by introducing bulkier amino acids (Leroux, Dementin et al. 2008, Liebgott, Leroux et al. 2010). Thus, the high isotope effect in K_M for the substrate measured for the NiFeSe Hase can also be correlated with the structural differences of the H_2-transport channels to/from the active site in NiFeSe hydrogenases (Baltazar, Teixeira et al. 2012).

5. Orientation and Function of a Membrane-Bound Hydrogenase monitored by Electrochemical Surface-Enhanced Infrared Absorption Spectroscopy (SEIRAS)

5.1 Introduction

The work presented in this chapter was done during the short stay of the PhD applicant in the group of Prof. Wolfgang Lubitz, from the Max Planck Institute for Chemical Energy Conversion, Muelheim, Germany.

The purpose of the work was to characterize by Surface Enhanced Infrared Spectroscopy (SEIRAS) combined with electrochemistry the two immobilization strategies described previously by Cristina Gutiérrez-Sánchez *et al.* (Gutiérrez-Sánchez, Olea et al., 2011) for the membrane-bound NiFeSe hydrogenase from *Desulfovibrio vulgaris* Hildenborough.

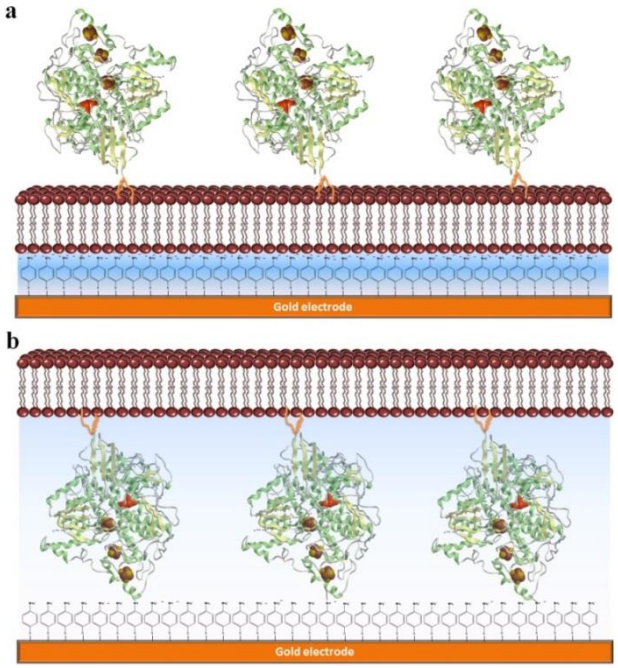

Figure 5.1: *Schematic representation of both studied constructions: (a) Electrode-Bilayer-Hase construction (E-B-H) and (b) Electrode-Hase-Bilayer construction (E-H-B).*

Cristina Gutiérrez-Sánchez *et al.* developed a strategy to reconstitute the NiFeSe Hase on gold electrodes in an orientated way. In this work, they took in advance the structural properties of this membrane-bound enzyme (Marques, Coelho et al. 2010): its lipid tail, which is the anchor in the periplasmic membrane, is in the opposite site from the distal Fe_4-S_4 cluster, which is the centre for exchanging electrons with its redox partner (a cytochrome, a redox dye or an electrode). In addition, the region surrounding the distal Fe_4-S_4 cluster is majorly composed by negative charged residues. In this way, thanks to these characteristics they were able to immobilize the hydrogenase over 4-ATP-modified Au electrodes in both configurations represented in **Figure 5.1**.

In this chapter data are presented of the chemical structure of the membrane-bound hydrogenase immobilized on a gold electrode surface in the two different orientations, and these are compared with its *in situ* electrocatalytic activity for H_2-oxidation.

SEIRA spectroscopy was used to monitor the whole modification steps of the two different strategies (**Figure 5.1**) for immobilizing NiFeSe Hase on a gold surface.

5.2 Results:

5.2.1 Electrode- Bilayer-Hase construction

To achieve the configuration shown in **Figure 5.1 (a)** a SAM of 4-ATP was formed on the gold surface. SEIRA spectra were begun to be recorded until the stabilization of the system on phosphate buffer 0.1 M at pH 5.5. After the system was stabilized, a phospholipid vesicles suspension was added to the measurement cell. Spectra were recorded at different times after the deposition (**Figure 5.2**). We observed the appearance of vibrational bands at 2926, 2873, 2854 and 1742 cm^{-1} during the 10 hours of incubation.

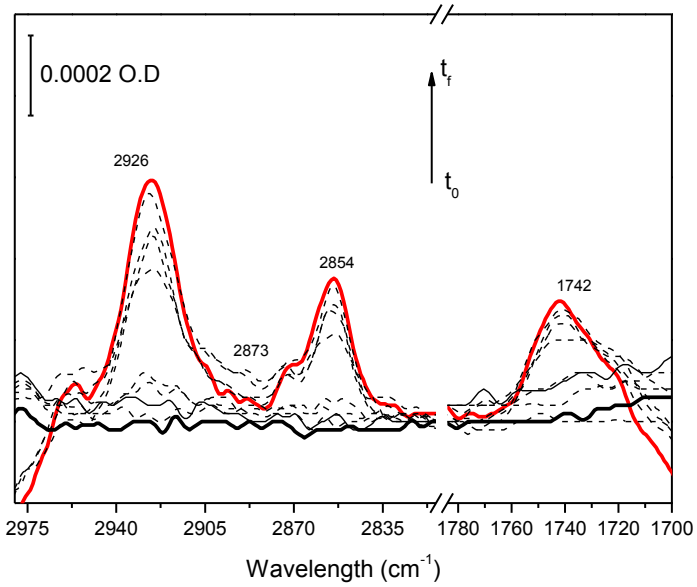

Figure 5.2: *Difference spectra obtained during the incubation of phospholipids vesicles from E.coli Polar extract of 0.2 µm diameter. Time zero (t_0) (solid black line) corresponds to the first spectrum obtained. Red line corresponds to the spectrum obtained at the end of the incubation (final time (t_f)). Spectra obtained between t_0 and t_f are represented with dashed lines. The reference spectrum is that of the 4-ATP-modified gold.*

The growth of peaks 2926, 2873, 2854 and 1742 was always associated to the disappearance of a broad band in the region comprised between 3650 cm^{-1} and 3000 cm^{-1}. In addition, the growth of peaks mentioned above was related with the growth of a broad peak at 3700 cm^{-1}, as shown in **Figure 5.3**.

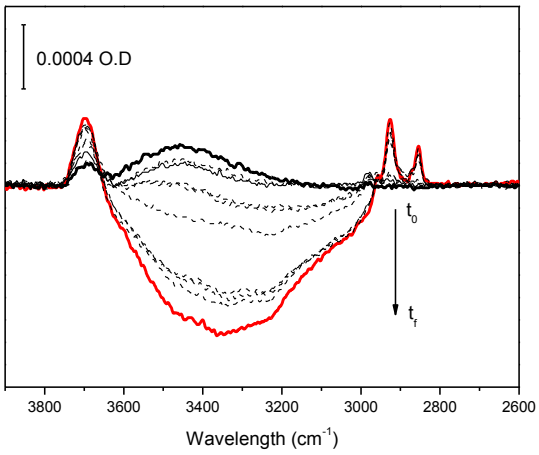

Figure 5.3: *Difference spectra obtained during the incubation of phospholipids vesicles from E.coli Polar extract of 0.2 µm diameter. Time zero (t_0) (solid black line) corresponds to the first spectrum obtained. Red line corresponds to the spectrum obtained at the end of the incubation (final time (t_f)). Spectra obtained between t_0 and t_f are represented with dashed lines.*

After the bilayer formation over the modified gold we proceeded to add the enzyme in presence of biobeads. The addition of these microspheres is indispensable in order to remove the detergent from the buffer forcing the hydrophobic tail of the hydrogenase to incorporate into the bilayer formed in the previous step. The adsorption of the enzyme to the surface is observed by SEIRA due to the growth of typical amide bands I and II (Siebert and Hildebrandt 2008) (**Figure 5.4**).

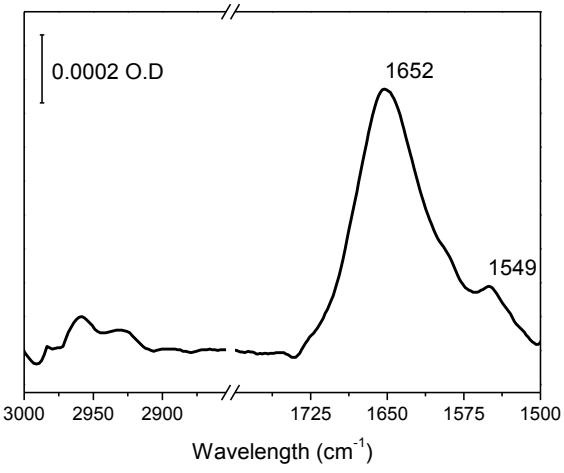

Figure 5.4: *Difference SEIRA spectrum after NiFeSe Hase immobilization. The position of amide I (1652 cm^{-1}) and II (1549 cm^{-1}) bands are indicated. The reference spectrum is the corresponding to the phospholipid-modified electrode.*

After protein immobilization the cell was cleaned several times with new buffer solution in order to remove the non-attached hydrogenase molecules and electrochemical measurements were performed in the SEIRAS cell. These experiments showed that the hydrogenase inserted into the supported biomimetic membrane is catalytically active for H_2-oxidation as shown in **Figure 5.5**. In this figure it is observed that when the enzyme is under N_2 atmosphere there is no catalytic wave in the CV (black line), only the background current of the electrode is measured. The same behaviour is observed when the enzyme is reduced under H_2 atmosphere during 30´ (red solid line). The addition of a redox mediator, in this case methyl viologen (MV), when the enzyme has been reduced produces an increase in the oxidation current that reaches a plateau at -0.2 V, which indicated a redox-mediated electrocatalytic process (red dashed line). This behaviour indicates that the enzyme is active but the distal Fe_4-S_4 cluster is too far away from the electrode to transfer the electrons directly to the electrode, as schematized in **Figure 5.5 (b)**. In this sense, the addition of a redox mediator allows the transfer of the electrons produced by the H_2 oxidation activity of the NiFeSe Hase from the distal Fe-S cluster to the electrode through diffusion of the redox mediator.

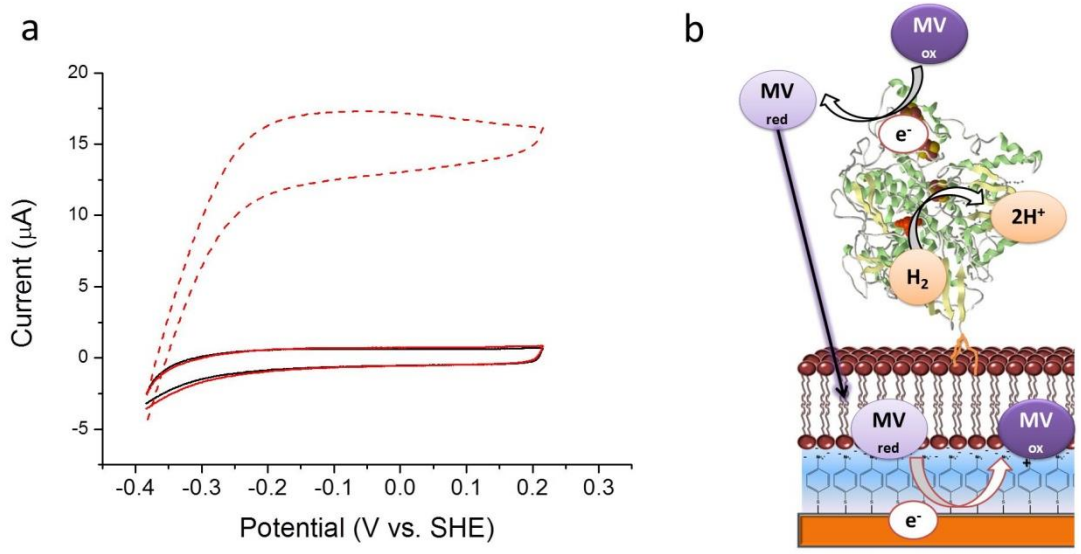

Figure 5.5: *(a) Cyclic voltammogram recorded at 10 mV/s after activation with H_2 without redox mediators in a N_2 (black line) or H_2 (black dot line) atmosphere and after the addition of methyl viologen (MV) as a mediator (red dashed line). (b) Schematic representation of the redox mediator action in the system.*

5.2.2 Electrode-Hase-Bilayer construction

In this configuration (**Figure 5.1(b)**) the hydrogenase is covalently attached to the 4-ATP modified gold surface through amide bonds and with its lipid tail inserted into the phospholipid bilayer formed on top. We have monitored by SEIRAS the step-by-step formation of this construction.

Firstly, the hydrogenase was incubated on the gold surface modified with 4-ATP in presence of detergent (DDM). The incubation time was determined by the changes observed in the difference spectra obtained between consecutive spectra. When changes were insignificant the incubation was stopped. After the protein adsorption, EDC and NHS were added to the solution in order to bind covalently the hydrogenase to the surface by amide bonds between carboxylic residues of the enzyme and the amino phenyl groups of the SAM. Then, the SEIRAS cell was cleaned carefully and the spectrum shown in **Figure 5.6** was recorded. This time, in addition to the amide bands the typical bands of the active site of the hydrogenase are observable: one CO band (1906 cm^{-1}) and the CN^-bands (2072 and 2085 cm^{-1}) (inset **Figure 5.6**).

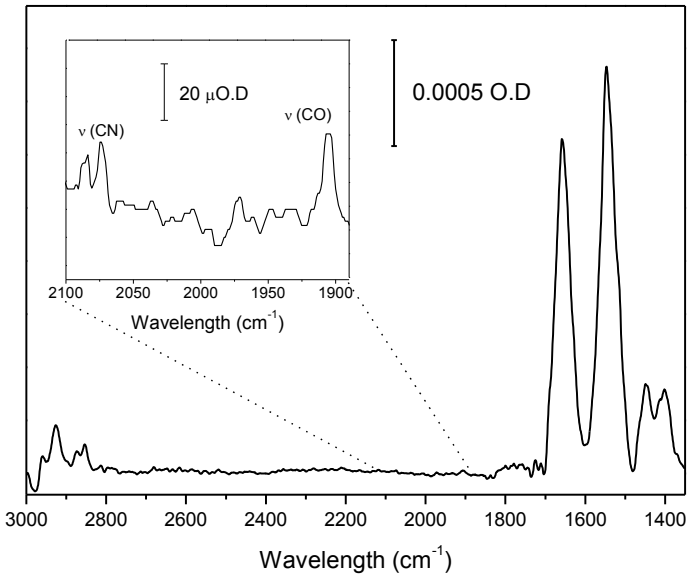

Figure 5.6: *Difference SEIRA spectrum after protein immobilization on a 4-ATP SAM using as reference spectrum the Au/4-ATP/Bil electrode, showing the amide I and II bands. The inset shows an approach to the active site region of the spectrum.*

In contrast with the previous case, this intensity ratio between the amide I and amide II bands was reproducible in different experiments. Once the enzyme was attached covalently on the surface, it was incubated in a liposomes suspension in presence of biobeads in order to facilitate the incorporation of the lipidic tail of the NiFeSe Hase into the bilayer. The growth of the bilayer was monitored by SEIRAS. After the liposomes deposition on the modified gold surface, the vibrational bands of the C−H modes of the phospholipids alkyl chains gradually increased during the incubation time as shown in **Figure 5.7**.

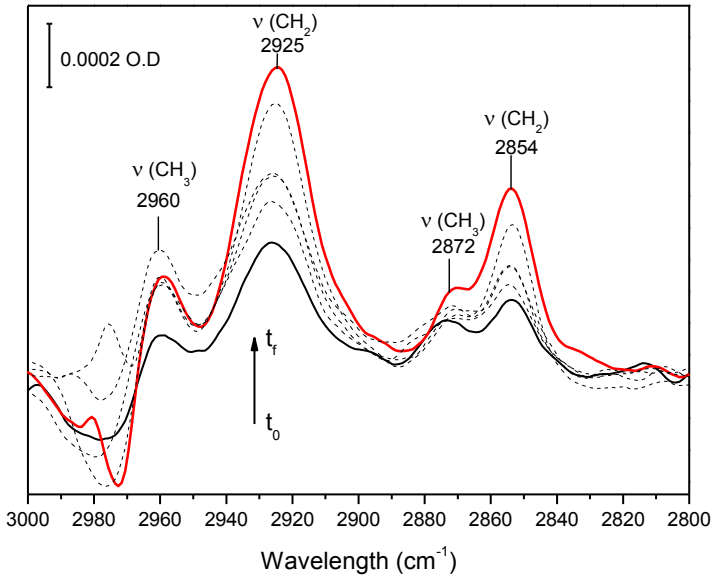

Figure 5.7: *SEIRA spectra recorded during phospholipid bilayer formation on top of the hydrogenase in 10 mM MES buffer at pH 5.0 over 10 h (black line is the first spectrum, red line is the final one).*

When the growth of the mentioned peaks stopped, the cell was cleaned to remove the excess of phospholipids present in the cell. Then, electrochemical experiments were performed. In **Figure 5.8** is shown that under N_2 atmosphere there was not an increase in the current of the CV from the background level. In contrast, when the atmosphere is changed to H_2, an electrocatalytic current is monitored (red dashed line) due to the direct electron transfer from H_2 oxidation to the electrode by the hydrogenase (**Figure 5.8**). In this modified electrode configuration, a direct electron transport from the NiFeSe Hase is possible thanks to the orientation of the distal Fe_4-S_4 cluster, which is facing the electrode (**Figure 5.1 (b)**).

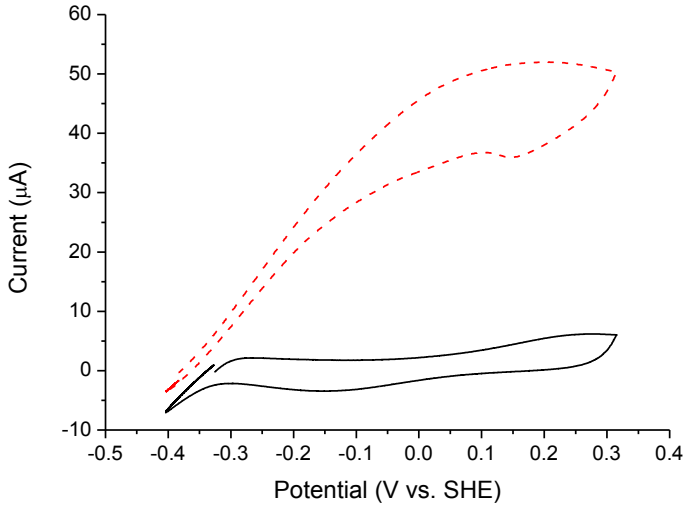

Figure 5.8: *CVs recorded at 10 mV/s after activation with H_2 (black) and in a N_2 atmosphere (red) in the absence of redox mediators. All measurements were performed at 25 °C.*

5.3 Discussion

5.3.1 Electrode-Bilayer-Protein construction

The first step to get the configuration shown in **Figure 5.1(a)** is the formation of a bilayer over the gold modified with 4-ATP. The appearance of vibrational bands at 2926, 2873, 2854, and 1742 cm^{-1} is in agreement with the formation of a phospholipid bilayer (Ataka, Giess et al. 2004, Kozuch, Steinem et al. 2012), as observed by AFM in a previous work realized in our laboratory (Gutierrez Sanchez, Fernandez et al. 2011). The band at 1742 cm^{-1} is assigned without doubt to the ester groups of the phospholipids from the bilayer, as previously observed (Ataka, Giess et al. 2004, Kozuch, Steinem et al. 2012). The broad band at 2926 cm^{-1} is due to the asymmetrical stretching C−H modes of the phospholipids alkyl chains, whereas the 2873 and 2854 cm^{-1} bands are assigned to the symmetrical modes of the methyl and methylene groups, respectively (Kozuch, Steinem et al. 2012). The formation of the bilayer is also detected due to the replacement of water at the gold surface by the phospholipids. In SEIRAS, the absorbance intensity decreases proportionally to the distance from the surface. In this sense, the absorbance of water adsorbed on the electrode decreases dramatically (*ν*(chelate OH) 3200-3000 and *ν*(OH bridge) 3600-3200) as shown in **Figure 5.3,** which is associated to the increase of the phospholipids bands (Kozuch, Steinem et al. 2012).

After the bilayer formation, the hydrogenase was immobilized. The difference spectra of **Figure 5.4**, using now as reference spectrum the phospholipid-modified electrode one, shows the appearance of the typical amide I (at 1652 cm−1) and amide II (at 1549 cm−1) vibrational bands of proteins (Wharton 1986). The thickness of the bilayer formed on the gold electrode is approximately 4-5 nm, as known from AFM experiments of a previous work (Gutierrez Sanchez, Fernandez et al. 2011), and thus the SEIRA spectrum shows the hydrogenase adsorption into the supported biomimetic membrane. In these sense, these bands can only be assigned to immobilized enzyme since SEIRA spectroscopy is not sensitive to distances beyond 10 nm from the metal surface (Wang, Jiang Xiu et al. 2012). The frequencies of these amide bands suggest that α-helixes are predominant in the secondary structure of the hydrogenase (Wharton 1986), in agreement with its published crystal structure (Marques, Coelho et al. 2010). In this case, the ratio of Amide I/Amide II intensities changed greatly between different

experiments performed under similar conditions. Changes in this ratio that were attributed to enzyme reorientation have also been reported for a hydrogenase adsorbed on a SAM-modified gold surface (Olejnik, Palys et al. 2012, Utesch, Millo et al. 2013). In this sense, our results suggests the existence of a significant degree of freedom in the orientation of the hydrogenase molecules relative to the surface normal when they are immobilized through insertion of their lipid tail into the supported phospholipid bilayer.

Electrochemical experiments performed in the SEIRAS cell showed that the hydrogenase inserted into the bilayer is catalytically active for H_2-oxidation. This activity only was able to be measured by mediated electron transfer using MV for transferring electrons from the enzyme to the electrode (**Figure 5.5**). This behaviour is expected for the hydrogenase immobilized as indicated in **Figure 5.1(a)** due to the large distance between the electrode surface and its most exposed redox site (distal Fe-S cluster) to the solution, avoiding the possibility to establish a direct electron transfer between both (Gutierrez Sanchez, Fernandez et al. 2011). In order to solve this handicap MV added in solution is able to receive electrons from the hydrogenase and to donate them to the electrode by diffusing through defects in the phospholipid bilayer (Gutierrez Sanchez, Fernandez et al. 2011).

5.3.2 Electrode-Hase-Bilayer construction

In this configuration the hydrogenase has its lipid tail inserted into the phospholipid bilayer formed on top (Gutierrez Sanchez, Fernandez et al. 2011).

The first goal for achieving the configuration shown in **Figure 5.1(b)** is to covalently immobilize in an oriented way the hydrogenase to the modified gold surface. The spectrum of the complete immobilization process is shown in **Figure 5.6**. The most visible vibrational bands in this spectrum are those corresponding to amide I and amide II of the immobilized hydrogenase, which are at similar frequencies as in the previous configuration. The intensity ratio for this construction between these two bands is closer to 1. This result indicates that the α-helixes of the enzyme deviate now more from the gold surface normal on average (Jiang, Zaitseva et al. 2008), which is in agreement with a different orientation of the immobilized hydrogenase in this configuration compared with the previous one. The ratio of intensities of amide bands for this configuration is

reproducible. This behaviour suggests a rigid immobilization of the hydrogenase molecules due to the covalent bonds with the electrode surface, and is in agreement with their homogenous orientation controlled by electrostatic interactions between the protonated aminophenyl groups of the gold surface and the negatively charged region surrounding the distal cluster (Ruediger, Gutierrez Sanchez et al. 2010). In a more detailed view, in contrast to the results obtained with the previous configuration, vibrational bands due to the CO and CN^- ligands of the hydrogenase active site can be now detected (inset of **Figure 5.6**). This can be explained by the shorter distance between the electrode and the hydrogenase active site when it is attached directly to the gold surface than when it is immobilized over the bilayer. This increases the SEIRA effect and thus the spectral sensitivity. The frequencies of the CO band (1906 cm^{-1}) and the CN-bands (2072 and 2085 cm^{-1}) are similar to those measured by transmission infrared spectroscopy for a solution of the same hydrogenase in the oxidized state (1904, 2076, and 2085 cm^{-1}) (De Lacey, Gutiérrez-Sánchez et al. 2008).

Once the enzyme was attached to the surface, the formation of the bilayer over it was carried on. In **Figure 5.7** are shown when the SEIRA spectra recorded at different times after the deposition of phospholipid vesicles on the electrode previously modified with the oriented hydrogenase. The vibrational bands from the C−H modes of the phospholipids alkyl chains (ν (CH_3) at 2960 and 2872 cm^{-1}; ν (CH_2) at 2925 and 2854 cm^{-1}) gradually increased during the incubation time after the addition of the liposomes suspension. This confirms that the topology change observed in the same system by AFM (Gutierrez Sanchez, Fernandez et al. 2011) corresponds to the formation of a phospholipid bilayer on top of the immobilized hydrogenase.

In order to probe the functionality of this configuration, electrochemical measurements were performed in the SEIRAS cell. In **Figure 5.8** is shown an electrocatalytic current due to the H_2 oxidation catalyzed by the hydrogenase in absence of any electron transfer mediator. This result clearly indicates that in this configuration the hydrogenase can directly transfer electrons to the gold electrode, again in agreement with the covalently bound hydrogenase having the orientation shown in **Figure 5.1(b)**, in which the distal Fe-S cluster is facing the electrode and the opposite lipid tail is inserted into the phospholipid bilayer.

6. Electrochemical study of the functional properties of NiFeSe hydrogenase from *D. vulgaris* reconstituted on biomimetic membrane supported on gold electrodes

6.1 Introduction

The aim of the work presented in this chapter was to study the electrocatalytical properties of the NiFeSe Hase immobilized with the Electrode-Hase-Bilayer configuration for H_2 oxidation and production in a standard electrochemical setup. Moreover, the final goal was to achieve an electric membrane potential by accumulating protons in the interface between electrode and bilayer due to the NiFeSe Hase electroenzymatic activity, as indicated in the **Figure 6.1.**

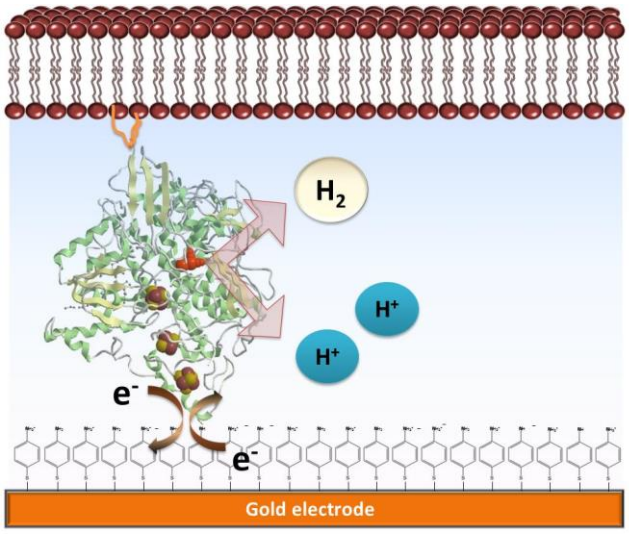

Figure 6.1: *Schematic representation of the electroenzymatic activity of reconstituted NiFeSe Hase for oxidizing H_2 and producing it. As indicated, the H_2 oxidation and its production involve a direct electron transfer between the distal Fe_4-S_4 cluster and the electrode.*

6.2 Results

6.2.1 Internal pH probe:

In order to be able of probing the local proton concentration of the electrode/bilayer interface, an original method was setup based on the generation of a pH-dependent redox couple attached to the electrode surface. The internal pH probe was formed by oxidizing the 4-ATP SAM on gold wires by recording 15 CVs between 0.225 and 0.725 V, as shown in **Figure 6.2** (Lukkari, Kleemola et al. 1998). In this figure, the first voltammogram (black solid line) and the 15th (red dashed line) are shown. In the first voltammogram an oxidative current is observed up to 0.5 V, which has disappeared in the 15th, indicating the complete oxidation of the aminophenyl rings to aniline dimers. Instead of the irreversible oxidative current, in the 15th CV a reversible redox wave is observed at 0.42 V, which corresponds to a 2 e^-/2 H^+ process of the formed aniline dimers (**Figure 6.2** (a)).

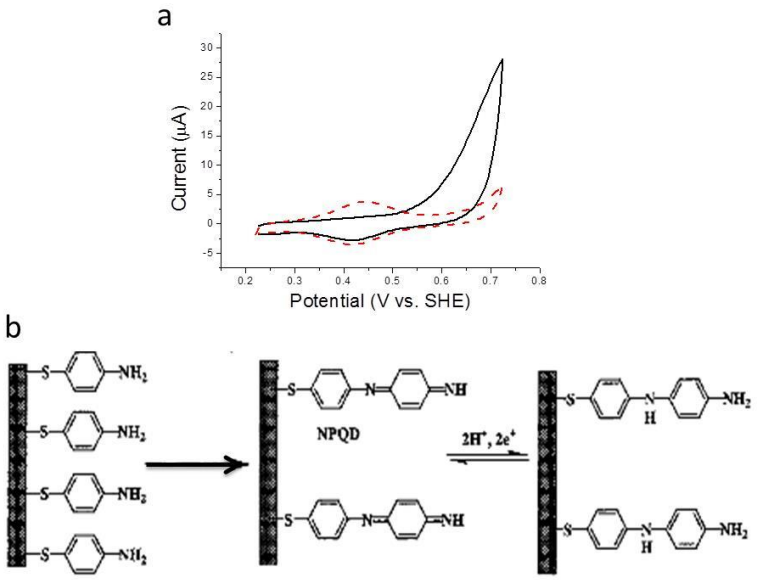

Figure 6.2: (a) *First (black line) and* 15th *(red dashed line) CVs at 100 mV/s for the oxidation of a 4-ATP SAM on Au wires. The supporting electrolyte was pH 7 0.1 M phosphate buffer. (b) Scheme of the 4-ATP SAM oxidation process proposed by Raj et al. (Raj, Fusao et al. 2001).*

In order to supress the capacitive current, Differential Pulse Voltammetry (DPV) measurements were carried on, thus allowing a more sensitive detection of the shifts of peak potentials. A calibration curve of the pH dependence of the peak potential of the

oxidation wave of the probe on phosphate buffer was performed (**Figure 6.3**). At 30ºC in 0.1 M phosphate buffer 0.1 M a shift of 64 ± 4 mV per pH unit was measured (**Figure 6.3** (b)), which is near to the theoretical value for a $2e^-/2H^+$ process at 30ºC (60 mV) (Linnett 1970).

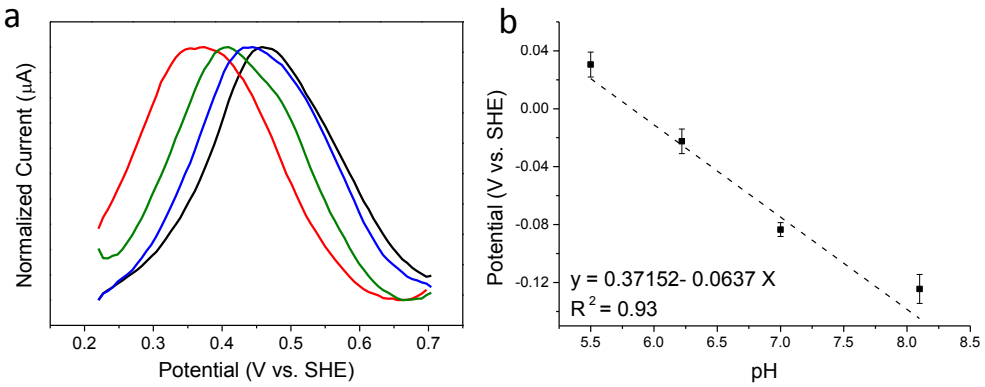

Figure 6.3: *(a) DPV measurements in 0.1M phosphate buffer at 30ºC of a gold wire modified with 4-ATP after oxidative treatment at pH 8.1, 7.0, 6.2 and 5.5 from left to right.(b) Calibration line obtained from DPV measurements.*

6.2.2 Hydrogenase inhibition by O_2 and CO during its H_2 production activity:

The functional properties of the membrane-bound hydrogenase immobilized on gold electrodes with the orientation shown in **Figure 6.1** were studied electrochemically. In order to activate the enzyme it was incubated in H_2 atmosphere for 30 minutes. After this incubation time CVs were measured (**Figure 6.4**) under H_2 (red line) and N_2 atmosphere (black line). It was observed that under H_2 atmosphere the current increased respect to the CV recorded under N_2 conditions, which indicated that the hydrogenase was activated.

In order to study the inhibition of this hydrogenase by carbon monoxide and di-oxygen, a choronoamperommetry was measured under H_2 production conditions (at an applied potential of -340 mV under N_2) as shown in **Figure 6.5**. Once a stable basal catalytic current of H_2-production by the Hase was reached, 20 µM of oxygen was added. Immediately, a great increase of the reduction current was observed due to the direct reduction of O_2 on the electrode.

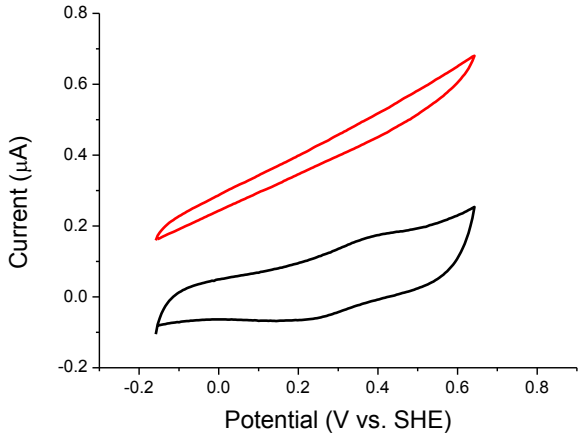

Figure 6.4: *CVs recorded at 10 mV/s and 30ºC of NiFeSe Hase immobilized on a gold wire electrode as shown in the scheme of Figure 6.1. The supporting electrolyte was in pH 8.0, 0.1 M phosphate buffer.*

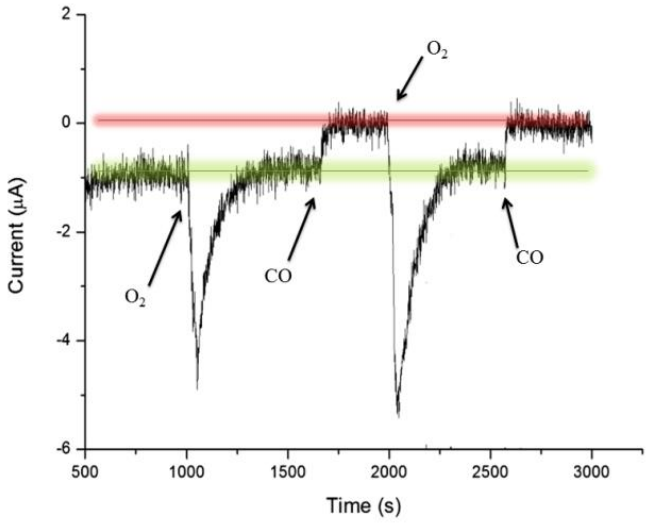

Figure 6.5: *Chronoamperogramm at -0.340 V and t 30ºC under H_2 production conditions of the NiFeSe Hase. The green line marks the basal current of electroenzymatic H_2 production and the red line the background current with inhibited enzyme.*

After 4-5 minutes of oxygen reduction at the electrode, the basal current due to the H_2 production activity of the enzyme was completely recovered (green line in **Figure 6.5**), Therefore, no inhibition of the enzyme was observed with the addition of 20 µM of oxygen. However, after adding 22 µM carbon monoxide, the hydrogen production was completely inhibited as the measured current was negligible (red line in **Figure 6.5**).

This inhibition effect disappeared when 26 µM O_2 was added. After the complete reduction of the added O_2 on the electrode, the activity of the enzyme came back to the same level (green line). After, 20 µM of monoxide carbon was added again into the cell and the same result was obtained: the complete inhibition of the hydrogen production by the NiFeSe Hase. Thus, the effects of O_2 and CO on the H_2-production activity of the immobilized hydrogenase were completely reversible and the electroenzymatic system is very stable.

6.2.3 Control and monitoring of the proton concentration in the phospholipid bilayer-electrode interface:

As shown in the **Figure 6.6**, when the enzyme was inactivated, the DPV wave peak was at 380 mV (black line). Afterwards, the enzyme was incubated during 30 minutes under H_2 atmosphere in order to activate it. A DPV measurement was carried on with a pretreatment of 90 seconds oxidizing H_2 at 180 mV followed by a resting time of 60 seconds in which 25 µM CO was added to the solution. The addition of CO was needed to supress the electrocatalytic current and to allow a clear visibility of the oxidative peak of the probe. The peak was detected at 493 mV (red dashed line, Figure 6.6). The peak potential shift after the period of H_2-oxidation activity corresponds to a change of nearly 2 pH units at the electrode boundary, which means that the hydrogenase was accumulating protons in the electrode/bilayer interface. After, O_2 was added to the solution to reactivate the enzyme by removing the extrinsic CO, as shown in section **6.2.2**. A reduction potential of –340 mV under N_2 atmosphere was applied until a catalytic current of H_2 production was established during 15 minutes. Then, a DPV measurement was performed (blue dot line, **Figure 6.6**). Due to proton reduction catalysed by the hydrogenase the pH of the interface went back to a basic value, as the peak potential was at 420 mV. Therefore, the proton gradient established across the biomimetic membrane was reversible, H_2 oxidation activity of the immobilized NiFeSe Hase shifted the pH at the electrode/bilayer interface to more acidic values and H_2 production activity shifted it to more alkaline values.

A control experiment without the presence of a supported bilayer on the electrode was performed to demonstrate that the change of the proton concentration monitored was caused by the presence a supported phospholipid bilayer that confined the electroenzymatic system (**Figure 6.7**).

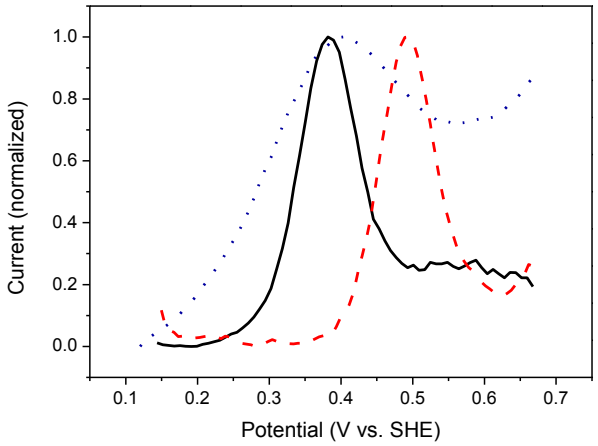

Figure 6.6: *DPV measurements of the Electrode/Hase/bilayer system in pH 8.0, 0.1M phosphate buffer at 30ºC under N_2 atmosphere before hydrogenase activation (black line), after electro-enzymatic H_2-oxidation (red line) and after electro-enzymatic H_2-production under N_2 atmosphere (blue dashed line).*

The DPV experiments were carried out after applying different periods of hydrogen oxidation by the immobilized hydrogenase and the result was always the same. No shift of pH at the electrode boundary was observed after doing DPV measurements under N_2 or H_2 atmosphere (Fig, 5.7,b), even if the immobilized hydrogenase was catalytically active (Fig 5.7, a).

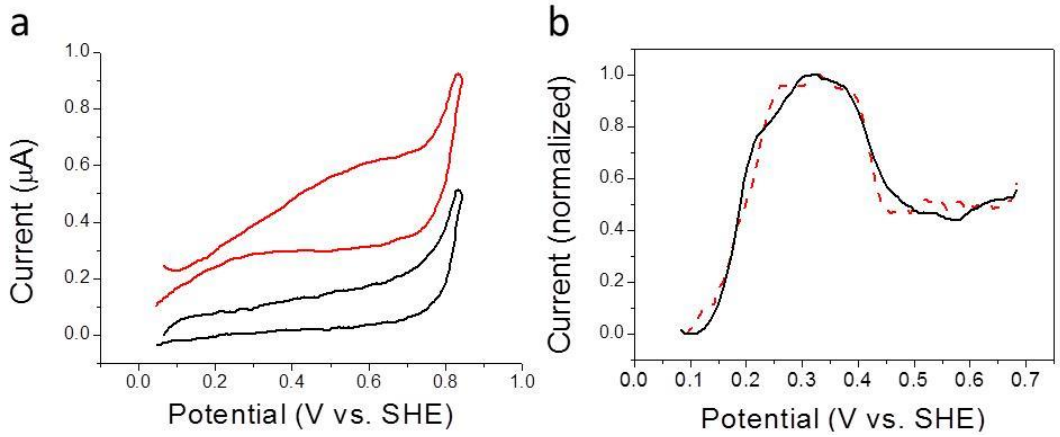

Figure 6.7: *CVs (a) and DPVs (b) measurements of an electrode modified with NiFeSe Hase without bilayer on top. (a) After activation, under N_2 atmosphere (black line) and under H_2 atmosphere (red line). (b) Before hydrogenase activation (black line) and after activation and H_2 oxidation activity (red dashed line).*

6.3 Discussion

6.3.1 Hydrogenase inhibition by O_2 and CO during H_2 production:

Oxygen and carbon monoxide are common inhibitors of hydrogenases (Gutiérrez-Sánchez, Rüdiger et al. 2010). Inhibition of hydrogenases by O_2 and CO is a handicap for their application in biofuel cells or in big scale H_2 production because CO is a typical contaminant of H_2 obtained from steam reforming, and because to perform industrial processes at anaerobic conditions is expensive (Lubitz, Ogata et al. 2014). NiFeSe Hase from *D. vulgaris* inhibition was studied previously by mass spectrometry, electrochemistry and FTIR (Gutiérrez-Sánchez, Rüdiger et al. 2010). This study concluded that the NiFeSe Hase is quite sensitive to oxygen and carbon monoxide under H/D isotope exchange activity and H_2 oxidation activity conditions. Our results complement Gutiérrez-Sánchez *et al.* results and determine that the electrochemical H_2 production activity of this enzyme is only inhibited by CO, not by O_2.

Similar results were obtained for the NiFeSe Hase from *D. baculatum*, for which lower inhibition by oxygen in H_2 production activity than in H_2 oxidation activity was described (Parkin, Goldet et al. 2008). Our results show a complete reversion of the enzyme activity after O_2 addition. This behaviour may be explained by the negative potential applied at the electrode and/or to the presence of Se instead of S in the active site. The negative potential facilitates the decrease of oxygen concentration around the immobilized enzyme due to its reduction at the electrode. In addition, selenium reacts faster with O_2 than sulphur to form a selenoate, which is also quickly reduced back to the selenide at low potentials , avoiding the inhibition of the H_2 production activity (Snider, Ruggles et al. 2013). This behaviour is explained by the absence in NiFeSe hydrogenases of the typical "unready" Ni-A state of NiFe hydrogenases (Baltazar, Marques et al. 2011). Thus, in electroenzymatic H_2 production we can consider NiFeSe hydrogenases as oxygen tolerant enzymes.

The effect of CO inhibition has been shown to be the same as described for the anaerobic NiFe hydrogenases. Anyway, the fast reactivation of the enzyme from CO inhibition thanks to oxygen addition is interesting for possible technological

applications. The replacement of CO by oxygen in this enzyme was previously observed by FTIR due to the disappearance of the extrinsic CO vibrational band when the CO-inhibited hydrogenase was exposed to air (Gutiérrez-Sánchez, Rüdiger et al. 2010). Our results show this replacement, under H_2 production conditions, is instantaneous and it does not affect the catalytic activity of the enzyme.

6.3.2 Control and monitoring the proton concentration in the interface bilayer-electrode:

Membrane potential is essential for life. Thanks to the capability of cells to establish a membrane potential and to regulate it, many functions in cells, such us ATP synthesis, motility, electrical signal transmission are possible (Mitchell and Moyle 1967). Our results show we are able to control and monitor electrochemically the proton concentration at the interface between the electrode and a supported phospholipid bilayer.

Up to date, proton concentration in surface/bilayer interfaces was measured commonly by fluorescence techniques (Demchenko, Mély et al. 2009). This supposes the addition of a compound sensitive to pH that may interact with the system. In this work we demonstrate the possibility to use one element of the biomimetic construction to report the proton concentration. The use of an internal probe supposes a clear advantage. In our case, we have used the oxidation of the 4-ATP SAM in order to obtain a couple redox which is pH-dependent according to theory (Lukkari, Kleemola et al. 1998), and whose oxidative peak potential can be measured sensitively by DPV.

In summary, the results showed in this chapter represent an original method for monitoring and controlling the membrane potential in bioelectronic devices. These results open the door to different applications, such as drug testing in biomimetic environment (Preissl, Bick et al. 2011), development of new biosensors, artificial ATP production from H_2 in a biomimetic environment, as well as for fundamental studies of cell metabolism.

7. Reconstitution of Respiratory Complex I on a Biomimetic membrane supported on Gold Electrodes

7.1 Introduction

In this chapter are presented the results obtained for the immobilization of Respiratory Complex I on gold electrodes modified with a phospholipid bilayer. Firstly, the Atomic Force Microscopy structural characterization of the biomimetic construction on gold substrate plates is presented, which is followed by an Impedance Spectroscopy characterization of the step-by-step modification on gold wires, and finished by an electrochemical study of the activity of this immobilized enzyme. The enzyme was provided by the laboratory of Dr. Manuela Pereira, ITQB, Lisbon (Portugal).

Figure 7.1 shows the scheme of the configuration aimed for the reconstitution of this enzyme by the methodology described in the Materials and Methods section.

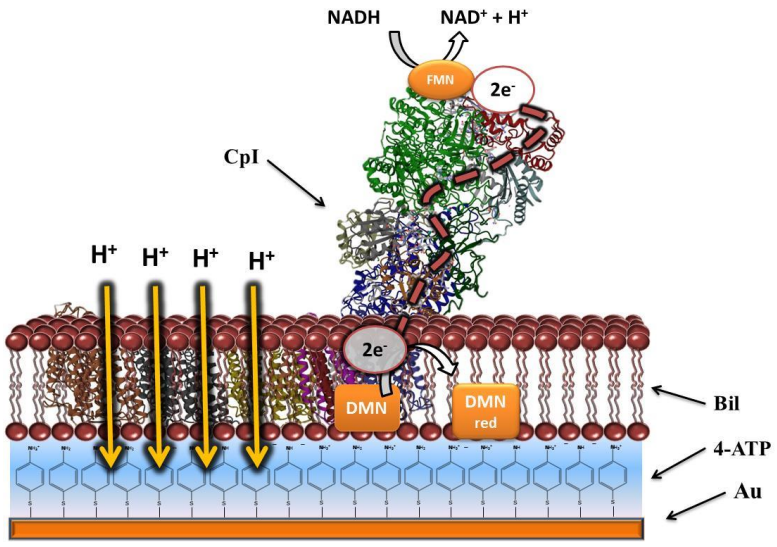

Figure 7.1: *Scheme of Respiratory Complex I (CpI) immobilized on a gold electrode modified with 4-ATP on a biomimetic bilayer (Bil). The blue space between electrode and phospholipids represents the electrode/bilayer interface.*

7.2 Results:

Two types of surfaces were used in the experiments; Au (111) plates and wires. Both surfaces were treated always with the same protocol (**Figure 7.2**).

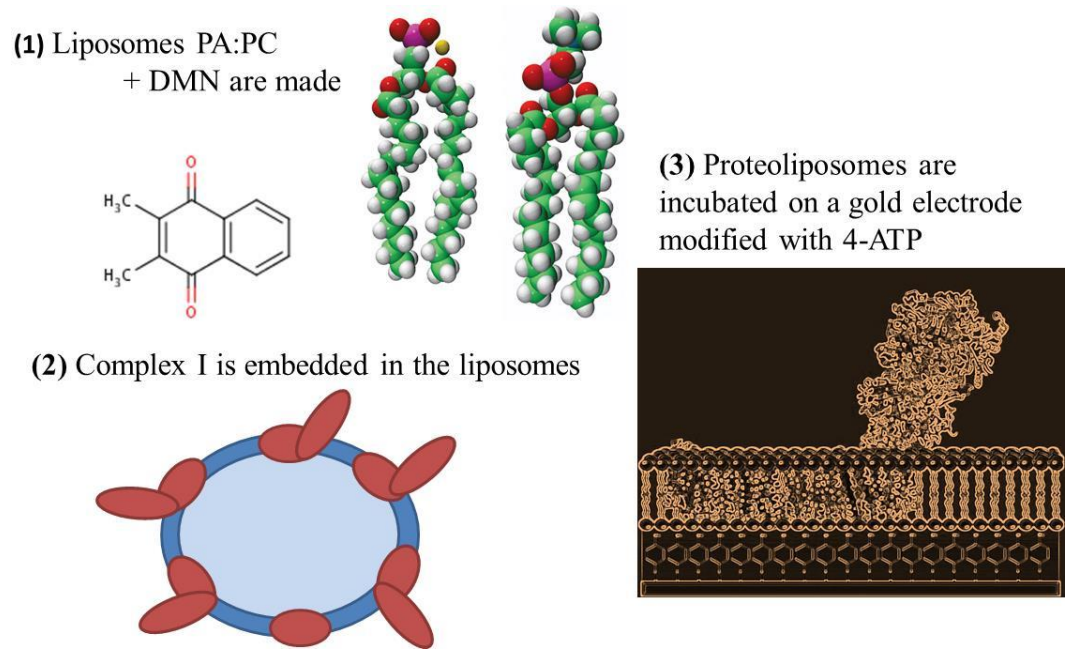

Figure 7.2: *Scheme of the protocol followed to reconstitute CpI on the Au surface. See a detailed description in materials and methods section.*

7.2.1 AFM study

Figure 7.3 (a,b) shows images of the gold surface modified with a 4-ATP SAM after overnight incubation in a CpI proteoliposomes suspension at 4ºC. **Figure 7.3** (c) shows an indentation curve that indicates that the AFM tip, upon approach to the surface, penetrated through a soft material, approximately 5 nm in depth, before reaching the hard underlying gold substrate. This result is similar to the one obtained for a *E. coli* polar fraction phospholipid bilayer lying on top of the 4-ATP SAM-modified surface (Gutierrez Sanchez, Fernandez et al. 2011). The observed density of protrusions on the flat regions of the gold terraces (**Figure 7.3** (a,b)) coincide within the expected 4-10% surface area covered by protein, taking into account that the lipid:protein molar ratio used to prepare the samples was 7000:1. The height of these protusions is around 6-8 nm as observable in Figure 7.3 (d). This height correlates with the expected values for

the hydrophilic arm of CpI extending outside the membrane. The lateral dimensions observed are ultimately determined by the tip diameter; therefore we can only reliably estimate that the height of the proteins is indeed within the range expected for the soluble part sticking out of the membrane.

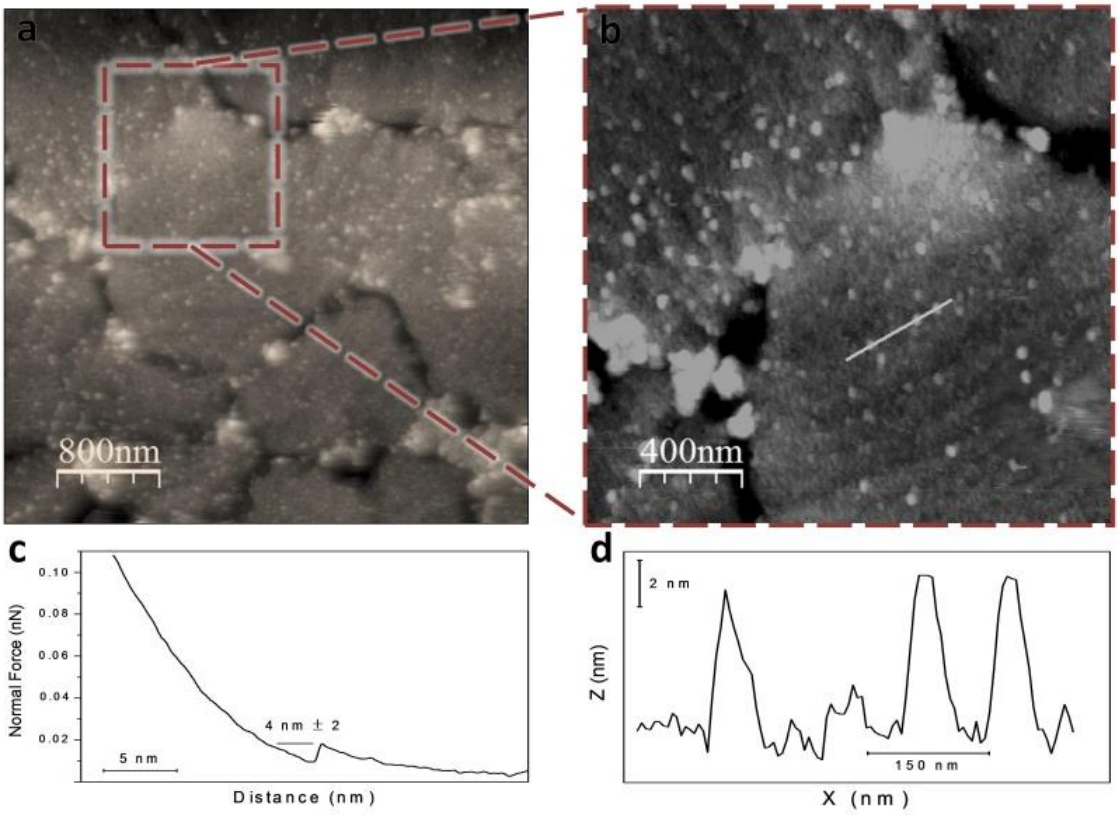

Figure 7.3: *AFM images of reconstituted CpI: (a) and (b) tapping-mode AFM topography of a 4-ATP-modied gold plate to which CpI has been immobilized in presence of phospholipids and CALBIOSORB adsorbent; (c) force-distance (z axis) curve acquired over a flat gold area; (d) z-axis profile across the line drawn in (b).*

Control measurements were carried on in order to demonstrate the existence of a bilayer on the gold surface. In **Figure 7.4** (a) the image obtained from a gold flat only modified with 4-ATP can be observed, and in **Figure 7.4** (b) the z-axis profile across the line drawn in (a) is shown. **Figure 7.4** (c) shows the image obtained from a measurement of a modified surface in which a region of the biomimetic membrane was removed by scratching it with the AFM tip. In (d) it can be observed that the bilayer/CpI layer has an average expected height of about 8 nm on top of the bare gold**.**

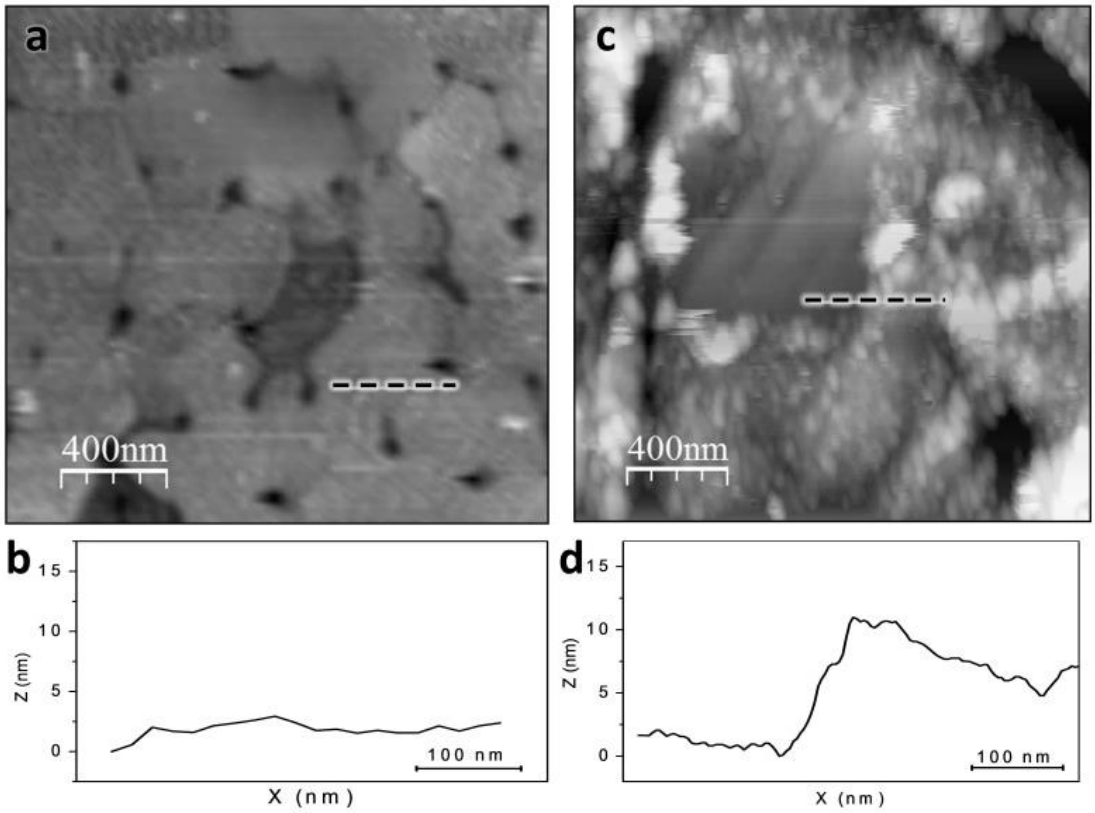

Figure 7.4: *Topographic image of a clean annealed gold surface. b) Height profile of the line indicated in a). c) Gold surface after modification with the self-assembled monolayer, and the lipid bilayer with reconstituted protein. A small square area was scratched with the tip scanning at high force. d) Height profile of the line indicated in (c).*

7.2.2 Impedance study

Once the biomimetic construction was characterized by AFM on the plate surfaces, all the steps of the CpI reconstitution were studied on Au wire electrodes using faradaic impedance spectroscopy. The impedance spectra were recorded for each of the following levels of gold wire electrode modification: bare Au, Au modified with 4-ATP (Au/4-ATP), Au modified with the bilayer (Au/4-ATP/Bil) and the complete construction (Au/4-ATP/Bil/CpI). The impedance spectrum measured on the bare Au electrode (**Figure 7.5**) showed a typical response dominated by a Warburg process of mass transfer kinetic limitation (Zoski 2006). However, from the highest frequency data a charge resistance of 50 Ω can be estimated (inset **Figure 7.5**). The impedance spectrum measured for the Au/4-ATP electrode also showed an electrical resistance (R_{et}) lower than 100 Ω, indicating that the assembled monolayer is not insulating the

electrode surface. The effect of the bilayer on Au/4-ATP electrodes was studied by incubation of the electrode in the liposomes suspension under two different conditions: (1) at room temperature during 3 hours and (2) overnight at 4ºC. The impedance spectrum measured for the Au/4-ATP/Bil (1) electrode showed a R_{et} of ca. 500 Ω, which is 7 times higher than the R_{et} measured for the Au/4-ATP electrode (**Figure 7**.5). The impedance spectrum measured for the overnight Au/4-ATP/Bil electrode showed a R_{et} of ca. 1100 Ω, which is an 11-fold increase on the previous step. These results evidence the presence of an additional charge-transfer barrier on the Au/4-ATP/Bil electrode, expected for the formation of a supported phospholipid bilayer. Furthermore, the lower R_{et} measured for the fast-formed bilayer than for the slow-formed one indicates that in the last case, the bilayer obtained is a more densely packed and less susceptible to defects bilayer. Thus, the overnight bilayer formation method was chosen in the further experiments. The complete construction, Au/4-ATP/Bil/CpI, was also measured. The impedance spectrum of Au/4-ATP/Bil/CpI gave a dramatically higher R_{et} of ca. 5.5 kΩ, which is a 6-fold increase over the R_{et} measured for the overnight Au/4-ATP/Bil (**Figure 7.5**). Taking into account the geometrical area of the Au wire electrode (0.065 cm^2) the normalized charge transfer resistance at the completely modified electrode was 0.36 kΩ × cm^2.

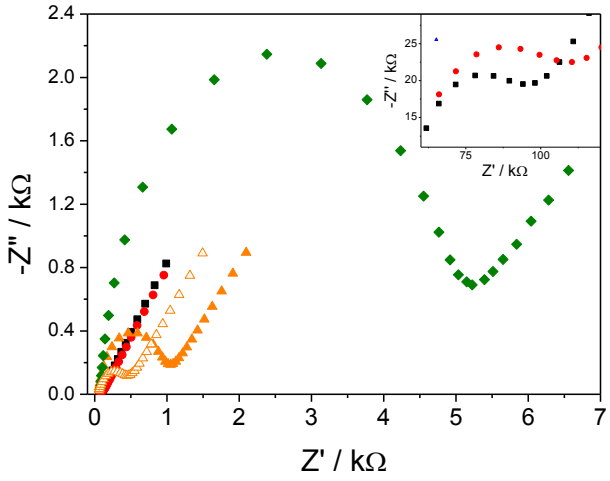

Figure 7.5: *Faradaic impedance spectra obtained in the presence of 2.5 mM $K_3Fe(CN)_6$ and 2.5 mM $K_4Fe(CN)_6$ in pH 7.0, 0.1 M phosphate buffer represented* as *Nyquist plots. Bare Au electrode (black squares), Au/4-ATP electrode (red circles), Au/4-ATP/Bil electrode formed by 3 h room temperature incubation (orange void triangles), Au/4-ATP/Bil electrode formed by overnight incubation at 4ºC (orange solid triangles) and Au/4-ATP/Bil/CpI electrode (green*

diamonds). It is important to note that the surface of the electrode is the same for all measurements.

7.2.3 Cyclic Voltammetry

The functionality of the reconstituted CpI for NADH reduction was studied by cyclic voltammetry. The quinone, DMN, was incorporated in the phospholipid bilayer as electron acceptor of the enzyme and redox mediator with the electrode. Various control experiments were done with modified electrodes at different complexity levels of the biomimetic construction.

Firstly, an Au/4-ATP electrode was measured in the presence or absence of NADH (**Figure 7.6**(a)). Direct oxidation of NADH on the Au/4-ATP electrode is observable by an anodic wave that starts at E= +300 mV. The direct oxidation of NADH at gold electrodes is an irreversible process (Blaedel and Jenkins 1975), which is confirmed by the absence of an electrochemical reduction process for NAD^+ in the cathodic scan (**Figure 7.6**(a) The reduction current observed at negative potentials is present in the CV recorded in absence of NADH, and may be attributed to non-scavenged oxygen at the electrode boundary. The presence of the bilayer on the electrode Au/4-ATP blocked the access of NADH to the Au/4-ATP, impeding the electrochemical oxidation of NADH (**Figure 7.6**(b)).

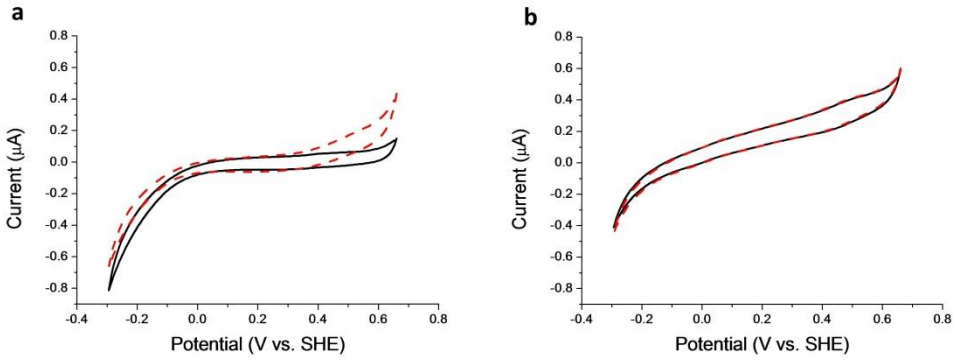

Figure 7.6: *CVs of control electrodes performed at 50 mV/s in 0.1 M phosphate buffer, pH 7.0 in the absence (red solid line) or in the presence of 60 µM NADH (black dashed line): (a) Au/4-ATP electrode; (b) Au/4-ATP/Bil electrode.*

Results obtained with the Au/4-ATP/Bil-DMN electrode are shown in **Figure 7.7** (a). The electrochemistry response of the embedded naphthoquinone is a quite complex process that provides the CVs with several reduction and oxidation peaks. This

electrochemical behavior is typical for quinone derivatives at pH 7 (McMillan, Marritt et al. 2012). The inset of **Figure 7.7** shows a CV measured at 100 mV/s scan rate, in which a better resolution of the DMN redox waves was achieved. The redox couple at +450 mV is not assigned to the naphthoquinone derivative, as it is also present in the CV recorded for an Au/4-ATP/Bil electrode in the absence of DMN (**Figure 7.7**). In fact, this redox couple is due to the oxidation of the 4-ATP SAM as indicated in the previous Chapter. Therefore, this quasi-reversible redox process is attributed to surface-confined aniline dimers formed by oxidation of part of the 4-ATP monolayer molecules, as reported by Raj *et al. (Raj, Fusao et al. 2001).*

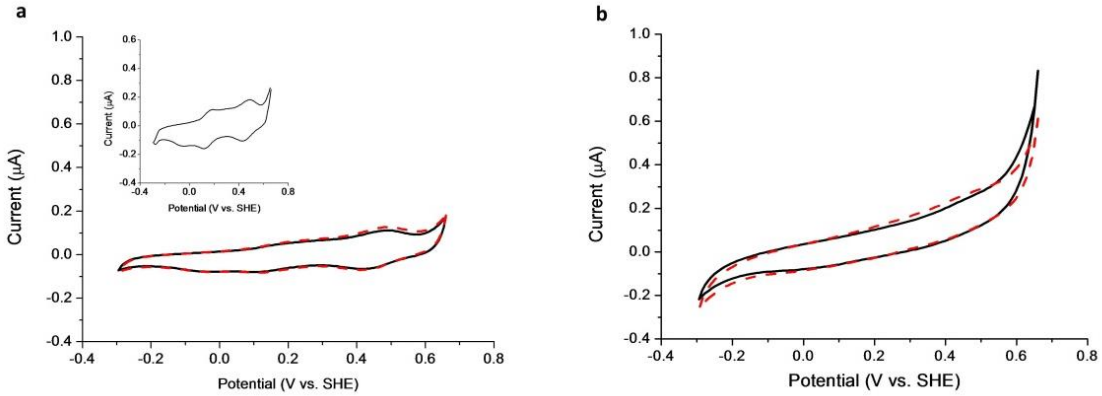

Figure 7.7: *CVs of control electrodes performed at 50 mV/s in 0.1 M phosphate buffer, pH 7.0 in the absence (black solid line) or in the presence of 60 µM NADH (red dashed line): (a) Au/4-ATP/Bil-DMN electrode, inset graph shows the same experiment at 100 mV/s of scan rate; (b) Au/4-ATP/Bil/CpI electrode.*

The redox signals attributed to DMN (reduction peaks at +120 mV and -65 mV, oxidation peak at +180mV) decreased with the number of cycles recorded as shown in **Figure 7.8**. This suggests that the reduced naphthoquinone may diffuse out of the bilayer due to its higher hydrophilicity. As shown in **Figure 7.8** (a), the addition of NADH to the solution did not generate a significant increase of the oxidative current. Thus, the presence of the quinone in the bilayer did not facilitate the direct or mediated (by DMN) oxidation of NADH on the electrode. An additional control experiment was done with an Au/4-ATP/Bil/CpI electrode, excluding DMN from the experiment (**Figure 7.8** (b)). The CVs of this experiment show that when the Complex I is

reconstituted in absence of the DMN, the increase of the oxidation current is insignificant when NADH was added to the solution.

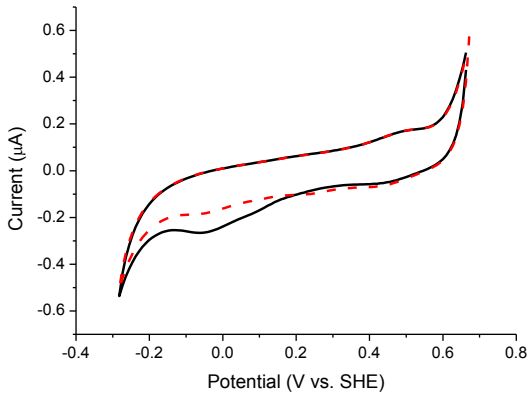

Figure 7.8: *CVs performed in 0.1 M phosphate buffer, pH 7 at 50 mV/s scan rate and at room temperature. (b) 1st (solid line) and 2nd (dashed line) scans of a Au/4-ATP/BIL-DMN electrode.*

The results obtained with the complete construction (Au/4-ATP/BIL-DMN/CpI) are shown in **Figure 7.9**. A clear oxidative electrocatalytic process that starts approximately at -0.1 V is observed when NADH was added to the solution. This electrocatalytic behavior due to the NADH oxidation by the reconstituted complex I was greater when the CV was recorded at 5 mV/s (**Figure 7.9** (b)). The lower ratio of the catalytic current relative to the non-catalytic current at higher scan rates indicates that the overall electrocatalytic process is slow.

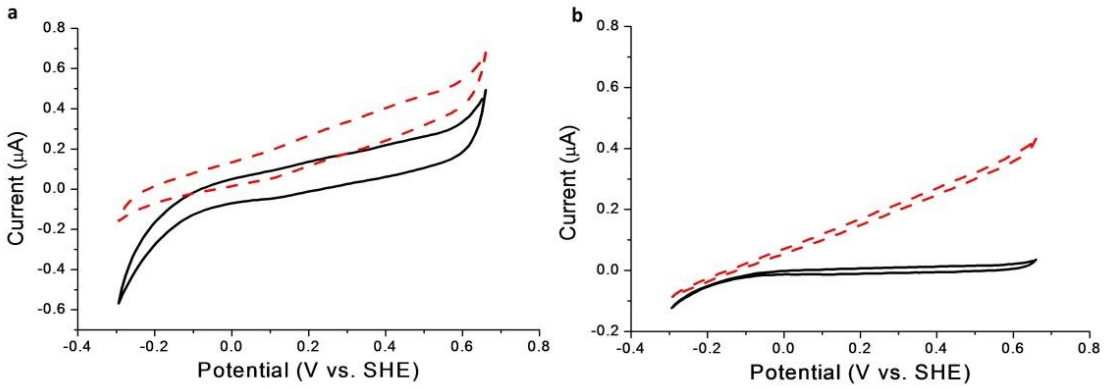

Figure 7.9: *CVs performed in 0.1 M phosphate buffer, pH 7 at 50 mV/s (a) and at 5 mV/s (b) scan rate and at room temperature. (b) Before (solid black line) and after the addition of 60 μM NADH (red dashed line) scans of a Au/4-ATP/PhL+DMN/CpI electrode.*

7.2.4 Chronoamperometry study

These experiments were performed with an Au/4-ATP/Bil-DMN/CpI electrode poised at +510 mV (**Figure 7.10**). NADH was added to achieve 60 µM concentration in the mesurement solution. As shown in **Figure 7.10**, the repeated addition of NADH produced increases of the oxidation current. It was observed that in the long term the steady-state current decreased, even if the bulk NADH concentration was higher. This behaviour could be due to the diffusion of DMN, which is the redox mediator in the electrocatalytic process, out of the biomimetic membrane towards the solution as shown in **Figure 7.8**. The same experiment did without the enzyme (Au/4-ATP/Bil-DMN) showed insignificant changes of the measured current upon NADH addition.Therefore, the increase of the current of NADH oxidation detected with the reconstituted CpI on membrane-modified electrodes is a consequence of its enzymatic activity.

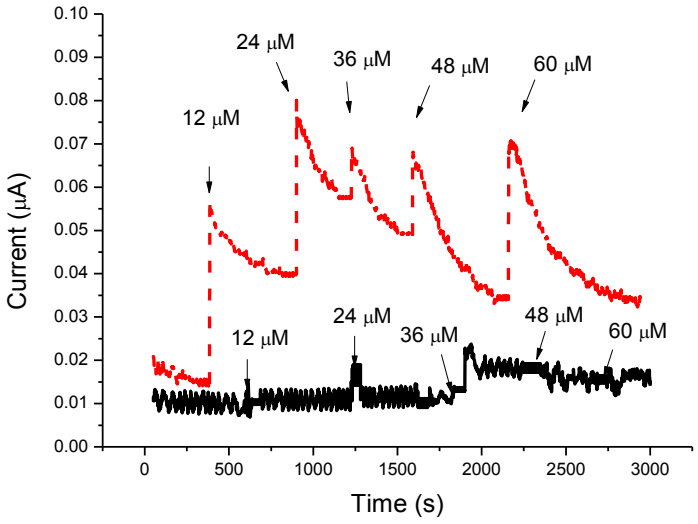

Figure 7.10. *Chronoamperommetry recorded in 0.1 M phosphate buffer, pH 7.0 with sequential additions of NADH (the concentration indicated in the graph is the final one in the solution) with Au/4-ATP/Bil-DMN/CpI (red dashed line) and Au/4-ATP/Bil-DMN (black solid line) electrodes.*

7.2.5 Differential Pulse Voltammetry (DPV) study

In natural conditions, CpI transports proton across a membrane coupled with its NADH oxidation activity. Once shown that the reconstituted CpI was catalytically active for NADH oxidation, we used the redox couple formed from the oxidation of 4-ATP

(**Figure 6.2**) in order to detect the proton transport activity of this enzyme. This 4'-mercapto-N-phenylquinone diimine/4'-mercapto-4-aminodiphenylamine conversion involves $2e^-/2H^+$, thus its formal redox potential should shift theoretically -56 mV/pH unit at 25ºC (Raj, Fusao et al. 2001). We have used DPV for measuring the oxidation peak potential of this process because it is a more sensitive electrochemical technique for measuring peak shifts than cyclic voltammetry.

As shown in **Figure 7.11** we made a calibration of the detection method with an Au/4-ATP electrode, which was firstly scanned 15 times between -0.1 and +0.7 V vs. Ag/AgCl. The peak shifts of the DPV wave were measured in buffer solutions of different pH values. The calibration shows that the peak potential shifted -56 mV per pH unit (**Figure 7.11**), in agreement with theory (Linnett 1970).

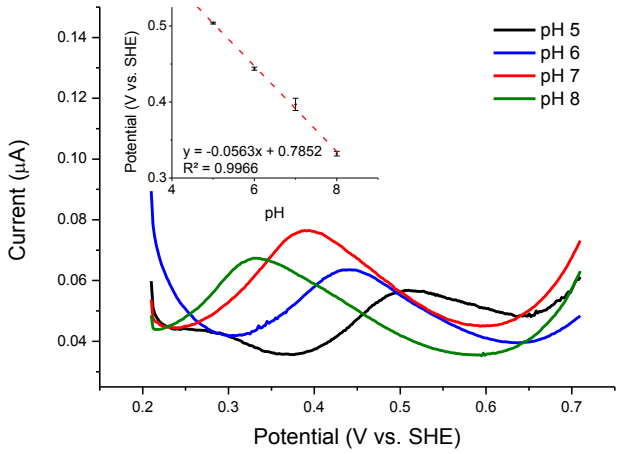

Figure 7.11: *DPVs of a gold wire modified with partially oxidized 4-ATP monolayer in 0.1 M phosphate buffer at different pH values. The inset shows the peak potential dependence on pH plot and the linear regression equation.*

The results obtained with the complete construction (Au/4-ATP/Bil-DMN/CpI) in 1 mM buffer concentration conditions are shown in **Figure 7.12**. The buffer concentration was chosen in order to reach a more sensitive measure of the proton concentration shift at the electrode/Bil interface. The addition of 60 µM NADH shifted the peak potential 46 mV to higher potentials compared to the system before the addition, which indicates that the local pH at the interface decreased almost one unit. The pH in the bulk solution was measured with a pH-meter and the pH value did not change, as expected taking into account its large volume (35 mL). To be sure that the increase of the proton

concentration in the interface was due to proton translocation across the biomimetic membrane, an ionophore (2,4-dinitrophenol, DNP) was added to the solution in order to homogenize the proton concentration of both compartments (interface and bulk). As expected, the peak potential shifted to lower potentials (66 mV), indicating an increase of the pH value in the interface. The shifts of the peak potential measurements were reproducible using several modified electrodes. The average shift was +50 ±10 mV (6 different electrodes) upon 60 µM NADH addition. A control measurement performed with an Au/4-ATP/Bil-DMN electrode (the enzyme was not present) is shown in the **Figure 7.12**. In this case, no changes were observed in the peak potential when NADH was added to the solution, which confirms that the pH changes at the membrane/electrode interface described above were due to the presence of Complex I.

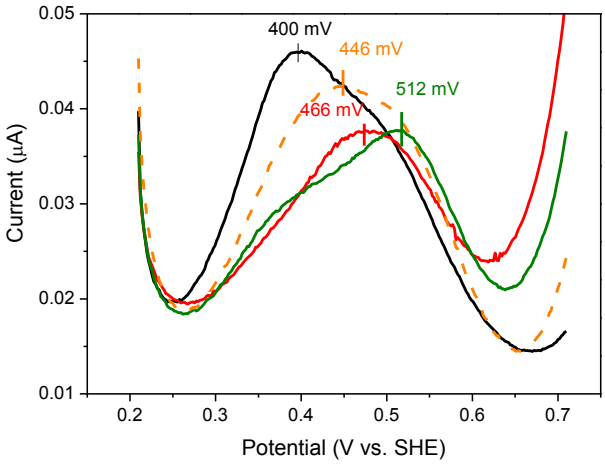

Figure 7.12: *DPVs of an Au/4-ATP/Bil-DMN/CpI electrode in 1 mM phosphate buffer, pH 7.0, 20 mM Na_2S (red line); after addition of 60 µM NADH (green line); after addition of 60 µM NADH and 2,4-DNP 70 µM (orange dashed line). The black line is a DPV measurement of an Au/4-ATP/Bil-DMN in presence of 60 µM NADH.*

7.3 Discussion

The results presented in this chapter present the first functional reconstitution of a respiratory Complex I on a biomimetic bilayer on a gold electrode. Up to the publication of these results (Gutierrez-Sanz, Olea et al. 2014) the studies of this enzyme were done with the two different domains (peripheral and membrane) separated and not in similar conditions to the natural ones (Hellwig, Scheide et al. 2000, Sazanov and Hinchliffe 2006, Barker, Reda et al. 2007).

The AFM study demonstrates that after an overnight incubation of the proteoliposomes suspension over modified gold with 4-ATP at 4ºC a phospholipid bilayer is created and that the CpI hydrophilic domains stand out of the biomimetic membrane towards the solution. The measurement of the height of these protrusions (6-8 nm) is correlated to the X-ray crystallography data, which indicate that the peripheral hydrophilic arm of the L-shaped Complex I extends about 13 nm over the phospholipid bilayer (Baradaran, Berrisford et al. 2013). The difference between the AFM measurements and X-ray data could be due to the fact that the peripheral domain is not orientated at a 90º angle with respect to the membrane surface, as was determined from the X-ray data. Also, this difference could be due to a possible deformation of the peripheral arm upon contact with the AFM tapping tip during the measurement. We cannot assure that whole population of CpI molecules are in the same orientation, but we can say that there is a population that occupies 4-10% of the membrane surface whose configuration is the shown in **Figure 7.1**.

Thanks to the impedance study we have confirmed the formation of the phospholipid bilayer over the gold wires used for the electrochemical measurements (Jeuken, Connell et al. 2005). The dramatically increase of the charge resistance at the electrode surface measured upon overnight incubation in the liposomes suspension is not compatible with only an adsorption of liposome vesicles (Jeuken, Connell et al. 2005). This increase of 7 times in the charge resistance indicates the formation of a phospholipid bilayer, as observed in flat gold surfaces by AFM. The presence of the CpI in the construction increases the charge resistance, indicating that the bilayer is more impermeable than in the absence of the enzyme. This result is quite interesting because suggests that the insertion of the hydrophobic domain of this enzyme in the biomimetic membrane

stabilizes it, decreasing the number of defects in its structure. Nevertheless, higher values of charge resistance have been reported for other supported lipid layers, i.e for tethered membranes (Jeuken, Connell et al. 2005, Jeuken, Bushby et al. 2007, Mårtensson and Agmo Hernández 2012). This indicates that the bilayer formed in our gold wires is not defect free.

The functional reconstitution of a Respiratory Complex I allows using a full arrange of electrochemical techniques to study its functional properties. The results presented in this chapter indicate that both activities of Complex I (NADH oxidation and proton transport) can be monitored in the same experiment by electrochemistry. It is important to note that the activity of the enzyme is only observable when the enzyme, the NADH and the quinone are present in the construction, which indicates that we are monitoring at the electrode the oxidation of the quinones that have been reduced previously by the CpI. The measurement temperature used (25ºC) is not ideal for monitoring the activity of the Respiratory Complex I, in fact the optimum temperature growth for *R. marinus* is 65ºC (Batista, Marreiros et al. 2011). This can explain the low current obtained in our measurements.

The oxidation of the 4-ATP generates a pH-dependent redox couple at the electrode surface that is not involved in the enzymatic activity. This redox probe allows monitoring quantitatively the changes of pH at the membrane/electrode interface. Therefore, a fast and simple electrochemical method is developed for studying proton translocation across supported membranes that does not require the use of the normally used fluorescence probes (Bogachev, Murtazina et al. 1996, Batista, Fernandes et al. 2010). It is important to note that the measured proton concentration in the interface is the net balance between proton translocation from the bulk solution to the electrode/membrane interface by CpI and the proton diffusion in the opposite direction through the supported membrane defects. The permeability of these supported bilayers to positively charged compounds through the defects was observed in a previous work done in our laboratory (Gutierrez Sanchez, Fernandez et al. 2011).

These results may open a new door in the technology used to study membrane proteins related with human health issues in their mimetic environment by electrochemistry. Furthermore, the proposed method to monitor both different activities will provide new

opportunities to circumvent the issues related with the development and screening of potential drugs that target and modulate the activity of membrane enzymes (Džafić, Klein et al. 2009, Preissl, Bick et al. 2011).

8. Study of reconstituted Respiratory Complex I by Surface Enhanced Infrared Spectroscopy (SEIRAS)

8.1 Introduction

In chapter 7 it has been demonstrated that we are able to reconstitute Respiratory Complex I from *Rhodotermus marinus* (CpI) on a biomimetic bilayer supported on gold electrodes. Due to this immobilization method on an electrode we can study by electrochemistry the activity properties of this enzyme in a configuration similar to the *in vivo* one. In this sense, this chapter presents an application of this method, combining electrochemistry with Surface Enhanced Infrared Spectroscopy (SEIRAS).

The results presented in this chapter were obtained during the short stay of the applicant in the laboratory of Professor Peter Hildebrandt at the Technische Universität Berlin, Germany.

It is important to note that the previous study of Chapter 7 was performed over two kinds of gold surfaces: (1) gold wires for the electrochemical studies and (2) gold plates used for the AFM study. Both were Au 1:1:1 surfaces, ideal to form a good bilayer without too many defects. In SEIRAs studies a rough gold surface at the nanoscale is used, which is necessary for obtaining the surface enhancement effect but it is not the ideal surface for supporting a perfect phospholipid bilayer.

The first goal of this chapter was to reproduce the electrochemistry results obtained over 1:1:1 gold surfaces (Gutierrez-Sanz, Olea et al. 2014) with a rough surface. The protocol used for reconstitution of CpI was the same as used previously in Chapter 7.

8.2 Results

The electrochemical measurements were performed in the SEIRAS cell at 25ºC under N_2 atmosphere in order to reproduce the conditions used in Chapter 7. Cyclic voltammetry was used to study the enzymatic activity of CpI reconstituted on the bilayer-modified electrode. Before the addition of NADH to the solution, the electrode was scanned 15 times between 0.1V to 0.7V vs. Ag/AgCl. The result of this treatment is shown in **Figure 8.1** (black line), in which a redox couple at 426 mV has been created from the partial oxidation of the 4-ATP SAM. Once achieved the redox couple, NADH was added into the solution another CV was measured. As expected, an increase of the oxidation current was measured (red dashed line). Two different parts in this voltammogram are observed. The first one is from 0.2 V to 0.55 V, where a plateau current of approximately 8 µA is reached that is asigned to the electroenzymatic oxidation of NADH. The second one (above 0.55 V), in which current increases exponentially is attributed to the direct and irreversible oxidation of NADH at the gold electrode (as observed in Fig. 7.6 (a) of Chapter 7 for a Au/4-ATP wire electrode).

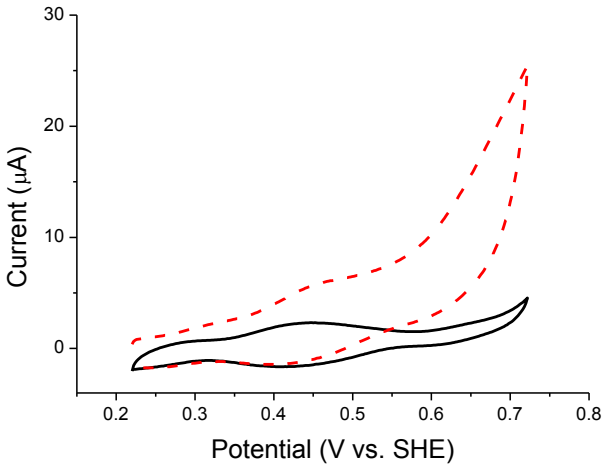

Figure 8.1: *CVs obtained from an Au/4-ATP/Bil-DMN/CpI electrode in pH 7.0, 0.1M phosphate buffer at 20 mV/s. The black solid line corresponds to the one obtained before the addition of 60 µM NADH to the solution (red dashed line).*

In order to verify that the oxidative current monitored was related with the activity of CpI, chronoamperometries in presence (red line) and in absence (black line) of the enzyme were performed. As shown in **Figure 8.2**, during each chronoamperometry aliquots of NADH were added sequentially into the solution. The addition of NADH

only generated an oxidative current when the enzyme was present in the construction (red line), which indicates that the oxidative current measured is directly related with the presence of CpI in the construction.

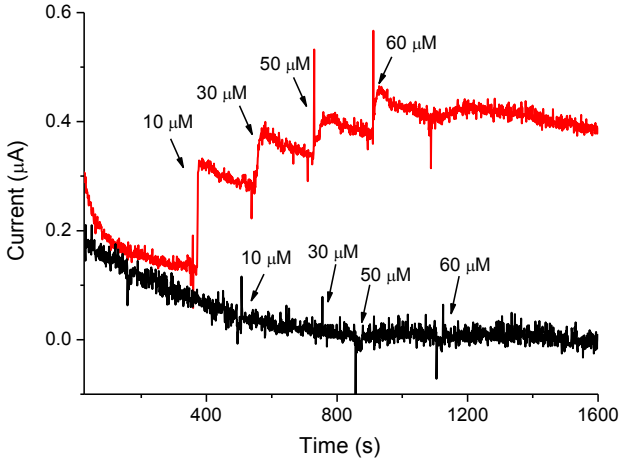

Figure 8.2: *Chronoamperometries obtained from an Au/4-ATP/Bil-DMN/CpI (red dashed line) and Au/4-ATP/Bil-DMN (black line) electrodes in pH 7.0, 0.1M phosphate buffer at + 475 mV.*

As commented in the previous chapter, DPV measurements were chosen to follow the shift of the proton concentration in the electrode/bilayer interface. In **Figure 8.3** are shown the measurements performed before (black line) and after the addition of 60 µM of NADH into the solution, in which a small shift of the peak potential is observed.

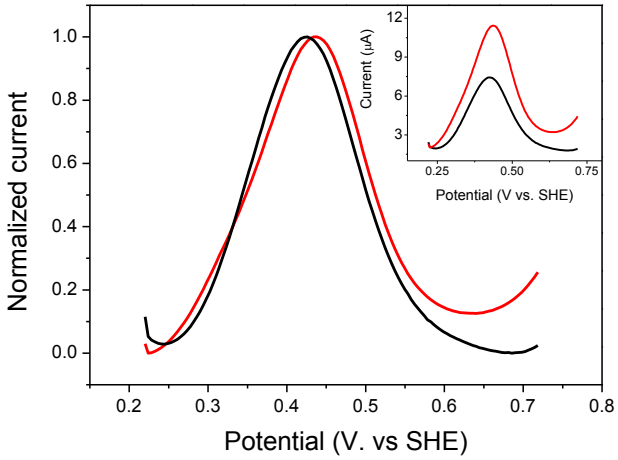

Figure 8.3: *DPVs of an Au/4-ATP/Bil-DMN/CpI electrode in 0.1 M phosphate buffer pH 7. Before addition of 60 µM NADH (black line) and after addition of 60 µM NADH (red line). Inset represents the same measurements without normalizing the current.*

Once the functionality of the biomimetic construction was checked on the rough gold surface used for SEIRAS measurements, an analysis of the different complexity levels of the construction by SEIRAS was performed. The surface enhancement effect causes that the compounds localized nearer to the metal surface give more intense infrared bands than the others. Because of this effect, the analysis has been done step-by step, beginning with the 4-ATP SAM formation on the gold electrode and following after with the bilayer and the CpI modification steps.

Using as reference spectrum the Au surface in 0.1 M phosphate buffer pH 7 before the SAM formation, a spectrum of the formed 4-ATP SAM in the same buffer was obtained (**Figure 8.4**). The main bands associated to the SAM are at 1630, 1593 and 1488 cm^{-1}. The bands at 1275, 1238, 1205 and 1110 cm^{-1} were less stable and are assigned to the replacement of ethanol adsorbed at the gold surface (coming from the 4-ATP solution for the SAM formation) by the phosphate present in the buffer solution.

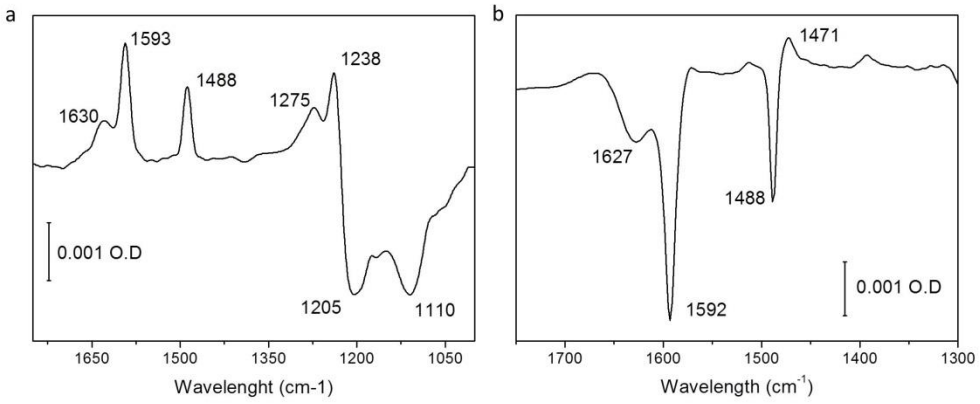

Figure 8.4: (a) *Spectrum of the Au/4-ATP in pH 7.0, 0.1 M phosphate buffer at 25ºC obtained using as reference the spectrum of the same gold surface before the modification. (b) Difference spectrum from a gold wire modified with 4-ATP between "after and before doing 15 CVs".*

The same Au/4-ATP electrode was scanned 15 times between 0.1 V and 0.7 V vs. Ag/AgCl. In the difference spectrum obtained after this treatment a decrease of the bands at 1627 cm^{-1}, 1592 cm^{-1}, and 1488 cm^{-1} is observed (**Figure 8.4** (b)). The latter one appeared to shift to a lower value frequency (1471 cm^{-1}).

Once the bands associated to the SAM of 4-ATP where identified, the formation of the phospholipid bilayer over the modified gold electrode was studied. For this purpose we incubated on the electrode two types of liposomes of PA:PC suspension (with and

without DMN). After an overnight incubation the liposome solution was removed and the cell was cleaned several times with phosphate buffer. The spectra obtained using as reference spectrum the gold modified with 4-ATP are shown in **Figure 8.5**. In both cases, two negative absorbance bands around 3300cm^{-1} and 1645 cm^{-1} were observed. Main bands associated to the presence of the bilayer are at 2958-6, 2925, 2854 and 1735-4 cm^{-1}. The presence of the DMN in the bilayer does not generate significant differences in the spectrum.

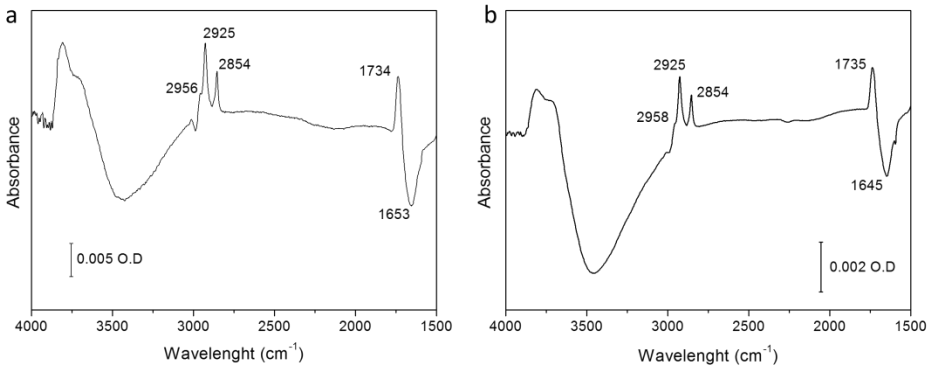

Figure 8.5: *Spectra of the gold surface modified with 4-ATP after overnight incubation of liposome suspension with (b) and without DMN (a) in pH 7.0, 0.1 M phosphate buffer at 25ºC obtained using as a reference spectrum that of the gold surface before the incubation.*

The reconstitution of CpI in the supported bilayer was studied by two different ways. The first one was the same as described in Chapter 7, i.e. inserting CpI in the liposomes and incubating the proteoliposome suspension on the electrode overnight at 4ºC. **Figure 8.6** (a) shows difference spectra obtained during the incubation using as a reference spectrum the Au/4-ATP at 4ºC. The most notable changes observed during the reconstitution process are the growth of the bands at 1630 and 1532 cm^{-1} correlated with the decrease of the 3500 cm^{-1} band. Taking an in depth look, bands associated with the presence of a bilayer on the electrode (2958, 2926, 2874, 2851 (inset of **Figure 8.6**(a)) and 1734 cm^{-1}) are also observed. A characteristic behaviour of CpI reconstitution was the way the amide I and amide II bands grew (1630 and 1532 cm^{-1} respectively).

In this sense, the change of the absorbance intensity ratio between these two bands during the incubation period is represented in **Figure 8.6** (b). The graph shows that the value of amide I/amide II ratio was 1.06 for the initial spectrum measured, and then it increased sequentially until reaching a stable value of 1.16 after 8 hours of incubation.

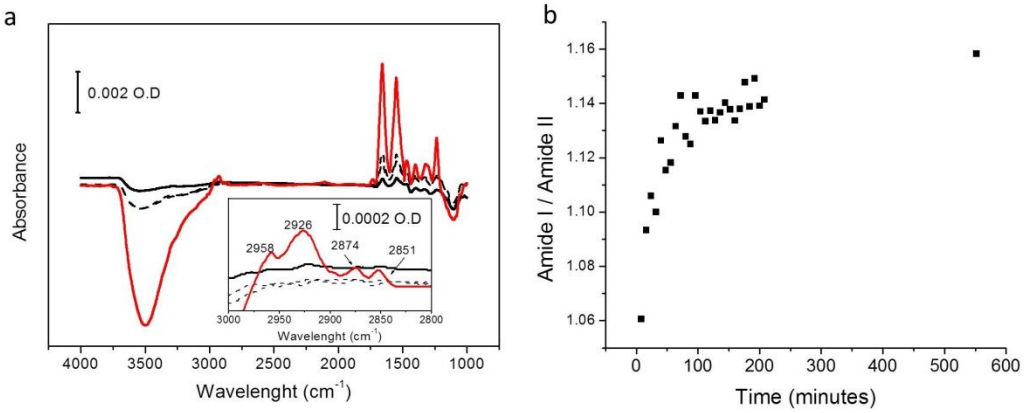

Figure 8.6: *Overnight incubation of a proteoliposome suspension on Au/4-ATP*. (a) *Spectra obtained at different times of the formation process in pH 5.0, 0.1M phosphate buffer at 4ºC using as reference spectrum that of Au/4-ATP. The first spectrum obtained after the addition of the proteoliposome suspension (black solid line) and the spectrum obtained after overnight incubation (red line) are shown. (b) Evolution of the intensity ratio of Amide I/Amide II bands during the incubation.*

Once the cell was cleaned several times in order to remove everything that was not attached to the surface, 60 µM of NADH was added into the solution to study the changes that the activity of CpI could generate in our system. In **Figure 8.7** are shown the spectra obtained from the biomimetic construction just before (black line) and after the addition of NADH (red line) in the solution. A control experiment was performed adding NADH in absence of CpI and changes were not observed (data not shown).

The orientation of all reconstituted CpI molecules was uncertain. As commented in the previous chapter, it is sure that there is a population of the enzyme that has the correct orientation shown in the scheme of **Figure 7.1**, but we cannot guarantee that 100% of the population is in the right configuration. In this sense, a step- by-step immobilization experiment was performed to force the protein orientation with its hydrophilic domain facing the solution (**Figure 8.8**).

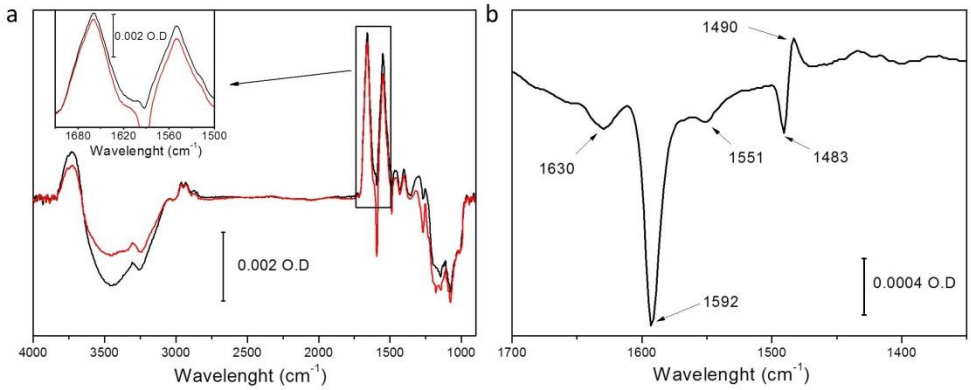

Figure 8.7: *Spectra of the complete construction obtained in pH 7.0 0.1M phosphate buffer at 25º C. (a) Spectra before (black line) and after the addition of NADH (red line). Inset shows a zoom of the amide bands region. (b) Difference Spectrum of "after NADH addition" minus "before NADH".*

CpI in detergent solution was inserted in the previously formed phospholipid bilayer over the Au electrode in presence of biobeads for removing the detergent. NADH was added into the solution and the same result was obtained than for the one-step immobilization of CpI and PhBL.

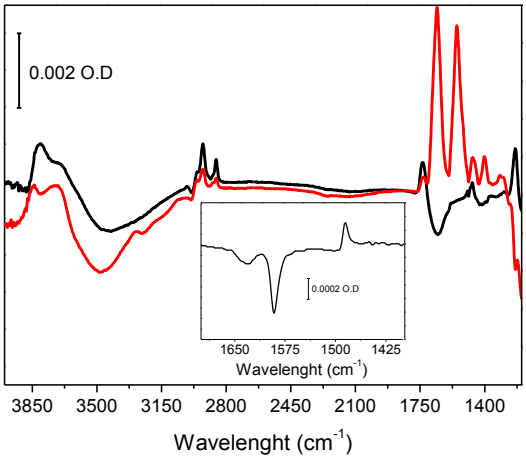

Figure 8.8: *Spectrum of the complete construction (red line) obtained by the step-by-step immobilization method in pH 7.0, 0.1 M phosphate buffer at 25º C. The spectrum corresponding to the bilayer formation step is represented with a black line. The difference spectrum for "after NADH addition" minus "before NADH" is shown in the inset graph.*

8.3 Discussion

The SEIRA-electrochemical study has demonstrated that we have been able to reproduce on a rough surface the results obtained in the previous chapter of CpI reconstitution. The addition of NADH into the solution produced an electrocatalytic wave in the CV due to DMN reduction by CpI and its reoxidation at the electrode. Therefore, the reconstituted CpI on the rough Au surface is also functional. However, the less smooth Au causes more defects in the supported phospholipid bilayer, as direct oxidation of NADH at the Au surface is observed in this case. The SEIRA results obtained of the 4-ATP SAM on the rough Au are in agreement with a previous work realized by Raj *et al*. (Raj, Fusao et al. 2001). The main bands associated to the 4-ATP are three; 1630 cm^{-1} (N-H deformation), 1593 cm^{-1} and 1488 cm^{-1} (C-C stretching). The scanning of the 4-ATP-modified electrode between the indicated potential values during 15 times in 0.1 M, pH 7 phosphate buffer has the same consequence as described by Raj *et al*. The difference spectrum shows the decrease of bands 1627 cm^{-1}, 1592 cm^{-1} and 1488 cm^{-1}, which correspond with the main vibrational bands associated to the SAM of 4-ATP. A notable feature is the growth of a vibrational band at 1471 cm^{-1}, which may be assigned to a C-C stretching mode from dimers of aniline formed upon oxidation of the 4-ATP SAM (Lukkari, Kleemola et al. 1998, Raj, Fusao et al. 2001).

The results obtained after incubation with the liposomes are in agreement with the formation of a phospholipid bilayer on the modified gold surface as commented in Chapter 7. Two types of membrane have been studied in the present chapter; (1) PA:PC bilayer and (2) PA:PC bilayer with DMN incorporated. In both cases, the difference spectrum shows two negative absorbance areas around 3300 cm^{-1} and 1645 cm^{-1}, that correspond to O-H vibration modes. This decrease in the absorbance indicates the replacement of water molecules adsorbed at the Au surface by the phospholipids. The adsorption of the phospholipids on the surface is associated with the growth of bands 2958/6 cm^{-1}, 2925 cm^{-1}, 2854 cm^{-1}, 1735/4 cm^{-1}. The broad bands at 2958/6 cm^{-1} and 2925 cm^{-1} are assigned to the asymmetrical stretching C−H modes of the methyl and methylene groups respectively of the phospholipids alkyl chains, whereas the 2854 cm^{-1} band is assigned to the symmetrical mode of the methylene group (Martin, Philippe et al. 2009). The band at 1742 cm^{-1} is assigned to the ester groups of the phospholipids from the bilayer, as previously reported (Ataka, Giess et al. 2004, Kozuch, Steinem et al. 2012).The presence of the DMN in the bilayer does not generate significant

differences in the spectrum. This behaviour can be due to the continuous diffusion of DMN inside the bilayer, thus its vibrational modes do not have a constant orientation relative to the Au surface normal that should allow the SEIRA effect.

The CpI embedded in the bilayer has been studied following two different strategies; (1) immobilization in one step and (2) immobilization in two steps.

(1) Strategy (1) consists in incubating proteoliposomes on a Au/4-ATP surface. As observed by AFM in the previous chapter, part of the CpI population is orientated with the peripheral arm looking to bulk solution, but we cannot reject the possibility of part of the population being in other orientations. The SEIRA study of this strategy clearly shows how the bilayer with the embedded CpI is forming during the incubation time (**Figure 8.6**(a)). The decrease of the absorbance in region 3000-3700 cm^{-1} is in agreement with the replacement of adsorbed water molecules by phospholipids as discussed above (**Figure 8.6**(a)). Furthermore, bands 2958, 2926 and 1734 cm^{-1} can be assigned without doubt to the bilayer formation, due to their presence also in the study of liposome deposition on Au/4-ATP. Bands assigned to CpI are at 1656 and 1550 cm^{-1}, which correspond to the Amide I and Amide II bands typical of proteins (Wharton 1986). **Figure 8.6** (b) shows the evolution of the intensity absorbance ratio between both bands. This evolution from a ratio of 1.06 to 1.16 indicates that the enzyme has suffered a reorientation during the incubation time (10 hours) until reaching a stable configuration. Furthermore, the increase of Amide I/Amide II ratio indicates that α-helices from the protein secondary structure are getting during the incubation a perpendicular orientation respect to the surface (Jiang, Zaitseva et al. 2008). This behaviour is the expected for the proposed configuration of the biomimetic construction (**Figure 7.1**), where the membrane domain of CpI contains multiple α-helices in perpendicular orientation to the surface.

(2) Strategy (2) consists in inserting the CpI after the phospholipid bilayer formation over Au/4-ATP. In this way, the peripheral arm of CpI cannot pass across the membrane and the only possible configuration is the expected one shown in **Figure 7.1**. As shown in **Figure 8.8**, the spectrum obtained from the first modification step (black line) indicates the presence of a phospholipid bilayer for the reasons commented above. The spectrum of the second step coincides with the one obtained with the "one step" strategy, suggesting that both strategies lead to the same final result. In strategy (2) the

decrease of the intensity of the bands assigned to the bilayer is observed when CpI is deposited onto Au/4-ATP/Bil, which can be caused by the insertion of CpI into the bilayer. It is also interesting to note that with both strategies the ratio between Amide I and II bands is quite reproducible, which suggests that the reconstituted CpI orientation is stable and is the same for both immobilization strategies.

Addition of NADH into the solution induces a clear change in the infrared spectrum as shown in **Figure 8.7** (a) and (b) and in the inset of **Figure 8.8**. In the spectrum represented in **Figure 8.7** (a) the first observable change is the increase of absorbance assigned to the vibration modes of O-H from adsorbed water molecules. In addition, small changes are observed in the region of the amide bands, more appreciable in **Figure 8.7** (b). A decrease of the bands at 1630, 1592, 1551 and 1483 cm^{-1} and the growth of a band at 1490 cm^{-1} is also evident. The addition of NADH into the solution implicates the reduction of DMN and the transport of protons from the bulk to the interface electrode/bilayer due to the activity of CpI. Therefore, we can hypothesize that the high proton concentration at the bilayer/electrode interface generated by CpI may cause the entering of water to the electrode/membrane interface in order to get homeostasis, explaining the increase of water molecule absorbance. But this hypothesis would suppose an increased distance of the bilayer from the electrode, which would implicate the decrease of the absorbance of its assigned bands, which we do not observe. Furthermore, this hypothesis would also suppose the increase of the absorbance at 1700-1400 cm^{-1} due to water adsorption, which we do not observe it. Another possibility could be that the reduction of the DMN generates a semiquinone radical that can attack the 4-ATP SAM molecules, leading to aniline dimerization. This hypothesis is supported by the fact that the observed changes upon NADH addition are very similar to those detected when the 4-ATP SAM is oxidized electrochemically, causing aniline dimerization (**Figure 8.4** (b)) (Lukkari, Kleemola et al. 1998, Raj, Fusao et al. 2001). However, there is a change upon NADH addition that is not observed in the case of the SAM oxidation, which is the decrease of the band at 1551 cm^{-1}. This change can be associated to a conformational change of CpI, as the band frequency corresponds with the Amide II one. The existence of a conformational change during CpI activity has been proposed (Baradaran, Berrisford et al. 2013). This conformational change could explain the coupling mechanism of both activities of CpI (NADH oxidation and proton translocation), which is an open question nowadays (Sazanov 2014) .

9. Global discussion

Each chapter of this thesis is subdivided in two main parts; results and discussion. This chapter has been made with the aim of making a general discussion of these five chapters.

To immobilize in a functional and oriented way membrane proteins on gold electrodes on supported phospholipid bilayers has been the main goal of this thesis. In this sense, two proteins were chosen: NiFeSe hydrogenase from *Desulfovibrio vulgaris* Hildenborough and Respiratory Complex I from *Rhodotermus marinus*. Both enzymes are functionally related. Both of them control the proton concentration and both contribute to the reduction of the quinone pool (Fontecilla-Camps, Fontecilla Camps et al. 2007, Marreiros, Batista et al. 2013, Tengölics, Mészáros et al. 2014).

The firsts three chapters of this thesis are focused in the immobilization of the membrane bound NiFeSe hydrogenase on gold electrodes modified with a supported phospholipid bilayer. The reasons of the substitution of S atom by the Se atom in the active of this type of hydrogenases, and its role in the catalytic properties of this type of hydrogenases are not elucidated nowadays. Multiple hypothesis has been done attending to the relevant properties of Se compared to S, such as the higher nucleophilicity of selenium, the lower potential of Sec-containing redox couples and the increased acidity of Sec, which allows selenols to be active at lower pHs (Baltazar, Teixeira et al. 2012).

In this sense, a first characterization of the activity of this enzyme was performed (Chapter 4). The isotope exchange activity of NiFeSe Hase was analysed by mass spectrometry in order to obtain intrinsic measurements of the catalytic activity independently of the presence of a redox mediator (Alvin 1979). As commented in the discussion of this chapter, the pH dependence of the isotope exchange activity of this enzyme (Figure 4.2), the higher K_m value found in the H_2/D_2O activity than for the D_2/H_2O together with the similar V_{max} values for both activities indicate that double isotope exchange activity mechanism involves two catalytic cycles at the active site. These results and the MD calculations (Oscar, Marta et al. 2013) support that the protein structure surrounding the active site modulates its catalytic function, known as

the “cage effect” (Tamiya and Miller 1963, Alvin 1979, Bernhard, Buhrke et al. 2001). On the other hand, the experimental results of H/D exchange obtained suggest that the effect on the catalytic mechanism of Se presence instead of S in the active site is minor. The U489C mutant, in whom the SeCys at the active site was replaced by a Cys as in standard NiFe hydrogenases gave a very similar double/single exchange ratio to that of the native enzyme. Therefore, it seems that the main role of the Se-Cys in the active site is the protection against oxygen inactivation (Snider, Ruggles et al. 2013), allowing the fast reactivation under reducing conditions as shown in the chronoamperometric results of Chapter 6 of the immobilized NiFeSe Hase.

The method for immobilising this membrane-bound NiFeSe Hase was developed in our laboratory by Cristina Gutiérrez-Sánchez *et al*. in two different configurations shown in **Figure 5.1** (Gutierrez Sanchez, Fernandez et al. 2011). These constructions were characterized by electrochemistry and AFM. In Chapter 5 of this thesis is presented a chemical characterization of the biomimetic construction by SEIRAS combined with electrochemistry. SEIRAS has been reported to be a very useful technique to characterize and study membrane proteins (Wang, Jiang Xiu et al. 2012, Ataka, Stripp et al. 2013, Kriegel, Uchida et al. 2014). Our results are agreement with these mentioned works and confirm the two different configurations that can be built on the electrodes, with either the enzyme on top of the phospholipid bilayer or viceversa. Moreover, for one of the configurations we have shown for the first time in a SEIRA-electrochemical setup direct electron transfer to an electrode of a membrane-bound enzyme in presence of a biomimetic membrane.

This configuration was used to study the inhibition of this Hase by common inhibitors of hydrogenases: CO and O_2 (Gutiérrez-Sánchez, Rüdiger et al. 2010). In Chapter 6 we conclude that the NiFeSe Hase from *D. vulgaris* is tolerant to oxygen inhibition, but quite sensitive to CO inhibition while producing H_2 electroenzymatically. These results are in consonance with those observed for other NiFeSe Hases (Parkin, Goldet et al. 2008). As shown in **Figure 5.1** (a) a delimitated space is created between the electrode and the biomimetic bilayer in this configuration. This characteristic of the configuration was used to create a membrane potential between the interface bilayer/electrode and the bulk solution based on the hydrogenase activity (as shown in **Figure 6.1**). In order to probe that the local proton concentration shifted due to the hydrogenase activity, the

redox couple formed from the partial oxidation of 4-ATP SAM, which is pH-dependent, was used (Lukkari, Kleemola et al. 1998, Raj, Fusao et al. 2001).

This pH probe at the electrode surface has also allowed us to develop a method to immobilize the Respiratory Complex I from *Rhodotermus marinus* on a gold electrode embedded in a supported phospholipid bilayer and to monitor in the same experiment both activities of this enzyme for the first time (as shown in Chapter 7). Until now different methods have been used to measure the activity of CpI, but none of them monitor proton transport and electron transport in the same experiment (Walker 1992, Batista, Marreiros et al. 2012, Santidrian, Matsuno-Yagi et al. 2013, Verkhovskaya and Bloch 2013). The construction of the CpI embedded in a supported phospholipid bilayer has been characterized in this thesis by AFM (7.2.1), Impedance Spectroscopy (7.2.2) and by SEIRAS combined with electrochemistry (Chapter 8). These studies have demonstrated that with the developed method we have achieved the configuration shown in **Figure 7.1**, which represents clear advantages compared to a configuration in which the protein is attached directly to the electrode and the bilayer is formed over the protein (Kriegel, Uchida et al. 2014). This latter configuration does not allow studying by electrochemical methods the functional properties of CpI of quinone reduction inside a membrane and proton translocation across it.

The methodology developed during this thesis demonstrates the possibility of reconstituting functionally and in orientated way different redox membrane proteins in biomimetic environments on electrodes. Immobilization of proteins on electrodes has multiple uses, from basic studies of the immobilized proteins to its application in biosensors, biofuel cells or in nanotechnology (Noll and Noll 2011). The development of the immobilization on electrodes has advanced faster for globular proteins than for membrane proteins (Jeuken 2009) although the important roles they play in cell life. In this sense, this thesis contribute to this field opening doors to new fundamental studies of both studied enzymes and to the possible future development of biosensors, drug discovery or to other applications (Džafić, Klein et al. 2009, Noll and Noll 2011, Preissl, Bick et al. 2011).

10. Conclusions

- The catalytic mechanism for the H/D exchange activity of hydrogenases requires the unbinding of the HD intermediate from the bimetallic active site, followed by its re-coordination before it is released towards the solution, to obtain the double exchange of protons, and not the exchange of two protons in the same catalytic cycle as occurs with some inorganic catalysts.

- The dependence of single/double exchange activity on the pH, together with the different affinity constants measured for D_2 and H_2 while the V_{max} for both molecules is the same, indicate the existence of a "cage effect" in NiFeSe hydrogenases due to the structural surroundings of the active site capable of tuning the catalytic properties of these enzymes.

- Surface Enhance Infrared Spectroscopy (SEIRAS) combined with electrochemistry confirms the possibility of immobilizing the membrane-bound NiFeSe hydrogenase from *D. vulgaris* (NiFeSe Hase) on to a gold electrode in two different configurations: (a) one in which the enzyme is attached to a supported phospholipid membrane formed on the gold electrode and (b) other in which the enzyme is covalently bound to the electrode and the bilayer is formed over the top of the enzyme film.

- The orientated and functional immobilization of the NiFeSe Hase on an electrode allows creating and controlling a proton gradient across the supported phospholipid bilayer formed on the top of the enzyme film.

- Respiratory Complex I from *Rhodotermus marinus* (CpI) has been functionally reconstituted for the first time embedded on a supported phospholipid bilayer over a gold electrode. Both activities of this enzyme (proton transport across the membrane and electron transport from NADH to a quinone) can be measured electrochemically in the same experiment.

- SEIRAS combined with electrochemical detection confirms the oriented and functional reconstitution of CpI, with the membrane domain inserted in the supported phospholipid bilayer and the peripheral arm pointing out towards the solution.

- The SEIRAS difference spectra indicate that the addition of NADH to the reconstituted CpI on Au generates; a) a change in the ratio of amide I and amide II bands of CpI; b) a chemical modification of the 4-ATP SAM and c) an increase of the intensity in O-H frequency range. These results suggest: a) a reorientation of the enzyme structure takes place during activity; b) the SAM monolayer may be attacked by the quinones reduced by CpI; c) a reorientation of water molecules adsorbed at the gold surface occurs due to the enzymatic activity.

10. Conclusiones

- El mecanismo catalítico de la actividad de intercambio D/H de las hidrogenasas para obtener el doble intercambio de protones requiere la liberación del producto intermediario HD del centro activo bimetálico seguido de su re-coordinación antes de que su liberación hacia la solución, y no el intercambio de dos protones en el mismo ciclo catalítico como ocurre en algunos catalizadores inorgánicos.

- La dependencia de pH de la actividad simple/doble intercambio, junto con los diferentes valores de las constantes de afinidad medidos para D_2 y H_2 mientras que la V_{max} para ambas moléculas es la misma, indica la existencia del llamado "efecto jaula" en las hidrogenasas NiFeSe. Este efecto es debido a la estructura del entorno del centro activo, capaz de modular las propiedades catalíticas de estas enzimas.

- La técnica de espectroscopía vibracional, SEIRAS, combinada con electroquímica confirma la posibilidad de inmovilizar la hidrogenasa de membrana NiFeSe de *D. vulgaris* (NiFeSe Hase) sobre un electrodo de oro en dos configuraciones diferentes: (a) una en el que se une la enzima a una membrana de fosfolípidos formada previamente sobre el electrodo de oro y (b) otra en la que la enzima se une covalentemente al electrodo y la bicapa se forma sobre la enzima ya unida al electrodo.

- La inmovilización orientada y funcional de la NiFeSe Hase en un electrodo permite la creación y el control de un gradiente de protones a través de una bicapa fosfolipídica formada sobre la capa de enzimas previamente inmovilizadas en un electrodo.

- El Complejo Respiratorio I de Rhodotermus marinus (CrI) ha sido funcionalmente reconstituido por primera vez insertado en una bicapa de fosfolípidos soportada sobre un electrodo de oro. Ambas actividades de esta enzima (transporte de protones a través de la membrana y el transporte de electrones del NADH a una quinona) se pueden medir electroquímicamente en el mismo experimento.

- La técnica SEIRAS combinada con electroquímica confirma la reconstitución orientada y funcional de CrI, con el dominio de membrana insertado en la bicapa y el brazo hidrofílico señalando hacia la solución.

- Los espectros de diferencia obtenidos mediante SEIRAS indican que la adición de NADH al CrI reconstituido sobre Au modificado con una SAM de 4-ATP genera; a) un cambio en la proporción de las intensidades de las bandas amida I y amida II del CrI; b) una modificación química de la SAM 4-ATP y c) un aumento de la intensidad en el intervalo de frecuencia en el que absorbe el enlace OH. Estos resultados sugieren: a) que una reorientación de la estructura de la enzima tiene lugar con la actividad; b) la SAM puede ser atacada por las quinonas reducidas por el CrI; c) una reorientación de las moléculas de agua adsorbidas en la superficie de oro se produce debido a la actividad enzimática.

11. Bibliography

Adamska, A., A. Silakov, C. Lambertz, O. Rüdiger, T. Happe, E. Reijerse and W. Lubitz (2012). "Identification and Characterization of the "Super-Reduced" State of the H-Cluster in [FeFe] Hydrogenase: A New Building Block for the Catalytic Cycle?" Angewandte Chemie International Edition **51**(46): 11458-11462.

Alvin, I. K. (1979). "Hydrogenase: Properties and applications." Enzyme and Microbial Technology.

Asimov, I. (1978). The Bicentennial Man, Panther.

Ataka, K., F. Giess, W. Knoll, R. Naumann, S. Haber Pohlmeier, B. Richter and J. Heberle (2004). "Oriented Attachment and Membrane Reconstitution of His-Tagged CytochromecOxidase to a Gold Electrode: In Situ Monitoring by Surface-Enhanced Infrared Absorption Spectroscopy." Journal of the American Chemical Society **126**(49): 16199-16206.

Ataka, K., S. T. Stripp and J. Heberle (2013). "Surface-enhanced infrared absorption spectroscopy (SEIRAS) to probe monolayers of membrane proteins." Biochimica et Biophysica Acta (BBA) - Biomembranes **1828**(10): 2283-2293.

Bagatolli, L. (2009). Membranes and Fluorescence Microscopy. Reviews in Fluorescence 2007, Springer New York. **2007:** 33-51.

Baldwin, R. L. (2000). "Structure and mechanism in protein science. A guide to enzyme catalysis and protein folding, by A. Fersht. 1999. New York: Freeman. 631 pp. $67.95 (hardcover)." Protein Science **9**(1): 207-207.

Baltazar, C. S., V. H. Teixeira and C. M. Soares (2012). "Structural features of [NiFeSe] and [NiFe] hydrogenases determining their different properties: a computational approach." Journal of biological inorganic chemistry : JBIC : a publication of the Society of Biological Inorganic Chemistry **17**(4): 543-555.

Baltazar, C. S. A., M. C. Marques, C. M. Soares, A. M. DeLacey, I. A. C. Pereira and P. M. Matias (2011). "Nickel–Iron–Selenium Hydrogenases – An Overview." European Journal of Inorganic Chemistry **2011**(7): 948-962.

Baradaran, R., J. M. Berrisford, G. S. Minhas and L. A. Sazanov (2013). "Crystal structure of the entire respiratory complex I." Nature **494**(7438): 443-448.

Barker, C. D., T. Reda and J. Hirst (2007). "The Flavoprotein Subcomplex of Complex I (NADH:Ubiquinone Oxidoreductase) from Bovine Heart Mitochondria: Insights into the

Mechanisms of NADH Oxidation and NAD+ Reduction from Protein Film Voltammetry†." Biochemistry **46**(11): 3454-3464.

Batista, A. P., A. S. Fernandes, R. O. Louro, J. Steuber and M. M. Pereira (2010). "Energy conservation by Rhodothermus marinus respiratory complex I." Biochim Biophys Acta **1797**(4): 509-515.

Batista, A. P., B. C. Marreiros, R. O. Louro and M. M. Pereira (2012). "Study of ion translocation by respiratory complex I. A new insight using (23)Na NMR spectroscopy." Biochim Biophys Acta **1817**(10): 1810-1816.

Batista, A. P., B. C. Marreiros and M. M. Pereira (2011). "Decoupling of the Catalytic and Transport Activities of Complex I from Rhodothermus marinus by Sodium/Proton Antiporter Inhibitor." ACS Chemical Biology **6**(5): 477-483.

Batista, A. P. and M. M. Pereira (2011). "Sodium influence on energy transduction by complexes I from Escherichia coli and Paracoccus denitrificans." Biochim Biophys Acta **1807**(3): 286-292.

Berlier, Y., P. A. Lespinat and B. Dimon (1990). "A gas chromatographic-mass spectrometric technique for studying simultaneous hydrogen-deuteron exchange and para-orthohydrogen conversion in hydrogenases of Desulfovibrio vulgaris Hildenborough." Analytical biochemistry **188**(2): 427-431.

Bernhard, M., T. Buhrke, B. Bleijlevens, A. L. De Lacey, V. M. Fernandez, S. P. Albracht and B. Friedrich (2001). "The H2 sensor of Ralstonia eutropha. Biochemical characteristics, spectroscopic properties, and its interaction with a histidine protein kinase." The Journal of biological chemistry **276**(19): 15592-15597.

Bertrand, P., F. Dole, M. Asso and B. Guigliarelli (2000). "Is there a rate-limiting step in the catalytic cycle of Ni-Fe hydrogenases?" Journal of biological inorganic chemistry : JBIC : a publication of the Society of Biological Inorganic Chemistry **5**(6): 682-691.

Binnig, G., C. F. Quate and C. Gerber (1986). "Atomic Force Microscope." Physical Review Letters **56**(9): 930-933.

Bippes, C. A. and D. J. Muller (2011). "High-resolution atomic force microscopy and spectroscopy of native membrane proteins." Reports on Progress in Physics **74**(8): 086601.

Blaedel, W. J. and R. A. Jenkins (1975). "Electrochemical oxidation of reduced nicotinamide adenine dinucleotide." Analytical Chemistry **47**(8): 1337-1343.

Blanford, C. F. (2013). "The birth of protein electrochemistry." Chemical Communications **49**(95): 11130-11132.

Bogachev, A. V., R. A. Murtazina and V. P. Skulachev (1996). "H+/e- stoichiometry for NADH dehydrogenase I and dimethyl sulfoxide reductase in anaerobically grown Escherichia coli cells." Journal of Bacteriology **178**(21): 6233-6237.

Buoninsegni, F. T., R. Herrero and M. R. Moncelli (1998). "Alkanethiol monolayers and alkanethiol|phospholipid bilayers supported by mercury: an electrochemical characterization." Journal of Electroanalytical Chemistry **452**(1): 33-42.

Carroll, J., I. M. Fearnley, J. M. Skehel, R. J. Shannon, J. Hirst and J. E. Walker (2006). "Bovine complex I is a complex of 45 different subunits." The Journal of biological chemistry **281**(43): 32724-32727.

Coldrick, Z., P. Steenson, P. Millner, M. Davies and A. Nelson (2009). "Phospholipid monolayer coated microfabricated electrodes to model the interaction of molecules with biomembranes." Electrochimica Acta **54**(22): 4954-4962.

De-Lacey, A. L., V. M. Fernandez, A. De Lacey, V. Fernández, M. Rousset and R. Cammack (2007). "Activation and Inactivation of Hydrogenase Function and the Catalytic Cycle: Spectroelectrochemical Studies." Chemical Reviews **107**(10): 4304-4330.

De Lacey, A. L., V. M. Fernández, M. Rousset and R. Cammack (2007). "Activation and Inactivation of Hydrogenase Function and the Catalytic Cycle: Spectroelectrochemical Studies." Chemical Reviews **107**(10): 4304-4330.

De Lacey, A. L., C. Gutiérrez-Sánchez, V. M. Fernández, I. Pacheco and I. A. Pereira (2008). "FTIR spectroelectrochemical characterization of the Ni-Fe-Se hydrogenase from Desulfovibrio vulgaris Hildenborough." Journal of biological inorganic chemistry : JBIC : a publication of the Society of Biological Inorganic Chemistry **13**(8): 1315-1320.

Demchenko, A. P., Y. Mély, G. Duportail and A. S. Klymchenko (2009). "Monitoring Biophysical Properties of Lipid Membranes by Environment-Sensitive Fluorescent Probes." Biophysical journal **96**(9): 3461-3470.

Dementin, S., V. Belle, P. Bertrand, B. Guigliarelli, G. Adryanczyk-Perrier, A. L. De Lacey, V. M. Fernandez, M. Rousset and C. Léger (2006). "Changing the Ligation of the Distal [4Fe4S] Cluster in NiFe Hydrogenase Impairs Inter- and Intramolecular Electron Transfers." Journal of the American Chemical Society **128**(15): 5209-5218.

Džafić, E., O. Klein, P. Goswami, W. Kühlbrandt and W. Mäntele (2009). "Infrared spectroscopic study of the structural and functional properties of the Na+/H+ antiporter MjNhaP1 from Methanococcus jannaschii." Biochimica et Biophysica Acta (BBA) - Bioenergetics **1787**(6): 730-737.

Džafić, E., O. Klein, E. Screpanti, C. Hunte and W. Mäntele (2009). "Flexibility and dynamics of NhaA Na+/H+-antiporter of Escherichia coli studied by Fourier transform infrared spectroscopy." Spectrochimica Acta Part A: Molecular and Biomolecular Spectroscopy **72**(1): 102-109.

Efremov, R. G. and L. A. Sazanov (2012). "The coupling mechanism of respiratory complex I — A structural and evolutionary perspective." Biochimica et Biophysica Acta (BBA) - Bioenergetics **1817**(10): 1785-1795.

Fauque, G., Y. Berlier, M. Czechowski, B. Dimon, P. Lespinat and J. LeGall (1987). "A proton-deuterium exchange study of three types ofDesulfovibrio hydrogenases." Journal of Industrial Microbiology **2**(1): 15-23.

Fauque, G., H. D. Peck, J. J. G. Moura, B. H. Huynh, Y. Berlier, D. V. DerVartanian, M. Teixeira, A. E. Przybyla, P. A. Lespinat, I. Moura and J. LeGall (1988). "The three classes of hydrogenases from sulfate-reducing bacteria of the genus Desulfovibrio." FEMS Microbiology Letters **54**(4): 299-344.

Fernandes, A. S., F. L. Sousa, M. Teixeira and M. M. Pereira (2006). "Electron paramagnetic resonance studies of the iron-sulfur centers from complex I of Rhodothermus marinus." Biochemistry **45**(3): 1002-1008.

Fontecilla-Camps, J. C., J. Fontecilla Camps, A. Volbeda, C. Cavazza and Y. Nicolet (2007). "Structure/Function Relationships of [NiFe]- and [FeFe]-Hydrogenases." Chemical Reviews **107**(10): 4273-4303.

Forzi, L., J. Koch, A. M. Guss, C. G. Radosevich, W. W. Metcalf and R. Hedderich (2005). "Assignment of the [4Fe-4S] clusters of Ech hydrogenase from Methanosarcina barkeri to individual subunits via the characterization of site-directed mutants." FEBS Journal **272**(18): 4741-4753.

Gutiérrez-Sánchez, C., O. Rüdiger, V. M. Fernández, A. L. De Lacey, M. Marques and I. A. Pereira (2010). "Interaction of the active site of the Ni-Fe-Se hydrogenase from Desulfovibrio vulgaris Hildenborough with carbon monoxide and oxygen inhibitors." Journal of biological inorganic chemistry : JBIC : a publication of the Society of Biological Inorganic Chemistry **15**(8): 1285-1292.

Gutierrez-Sanz, O., D. Olea, M. Pita, A. P. Batista, A. Alonso-Caballero, M. M. Pereira, M. Vélez and A. L. De Lacey (2014). "Reconstitution of Respiratory Complex I on a Biomimetic Membrane Supported on Gold Electrodes." Langmuir.

Gutierrez Sanchez, C., V. M. Fernandez, M. Velez, A. L. De-Lacey, C. Gutiérrez Sánchez, D. Olea, M. Marques, V. Fernández, I. s. A. C. Pereira, M. Vélez and A. De Lacey (2011). "Oriented Immobilization of a Membrane-Bound Hydrogenase onto an Electrode for Direct Electron Transfer." Langmuir **27**(10): 6449-6457.

Hellwig, P., D. Scheide, S. Bungert, W. Mäntele and T. Friedrich (2000). "FT-IR Spectroscopic Characterization of NADH:Ubiquinone Oxidoreductase (Complex I) from Escherichia coli: Oxidation of FeS Cluster N2 is Coupled with the Protonation of an Aspartate or Glutamate Side Chain†." Biochemistry **39**(35): 10884-10891.

Hiromoto, T., E. Warkentin, J. Moll, U. Ermler and S. Shima (2009). "The Crystal Structure of an [Fe]-Hydrogenase–Substrate Complex Reveals the Framework for H2 Activation." Angewandte Chemie International Edition **48**(35): 6457-6460.

Inagaki, S., R. Ghirlando and R. Grisshammer (2013). "Biophysical characterization of membrane proteins in nanodiscs." Methods **59**(3): 287-300.

Jennifer, L. C., S. W. Paul, A. H. Mitra and E. F. Patrick (2007). "Transition metal catalyzed D2/H2O exchange: Distinguishing between the single and double exchange pathways." Journal of Molecular Catalysis A: Chemical **267**.

Jeuken, L. J. C. (2009). "Electrodes for integral membrane enzymes." Natural product reports **26**(10): 1234.

Jeuken, L. J. C., R. J. Bushby and S. D. Evans (2007). "Proton transport into a tethered bilayer lipid membrane." Electrochemistry Communications **9**(4): 610-614.

Jeuken, L. J. C., S. D. Connell, M. Nurnabi, J. O'Reilly, P. J. F. Henderson, S. D. Evans and R. J. Bushby (2005). "Direct Electrochemical Interaction between a Modified Gold Electrode and a Bacterial Membrane Extract." Langmuir **21**(4): 1481-1488.

Jeuken, L. J. C., S. A. Weiss, P. J. F. Henderson, S. D. Evans and R. J. Bushby (2008). "Impedance Spectroscopy of Bacterial Membranes: Coenzyme-Q Diffusion in a Finite Diffusion Layer." Analytical Chemistry **80**(23): 9084-9090.

Jiang, X., E. Zaitseva, M. Schmidt, F. Siebert, M. Engelhard, R. Schlesinger, K. Ataka, R. Vogel and J. Heberle (2008). "Resolving voltage-dependent structural changes of a membrane photoreceptor by surface-enhanced IR difference spectroscopy." Proceedings of the National Academy of Sciences of the United States of America **105**(34): 12113-12117.

Keller, C. A. and B. Kasemo (1998). "Surface Specific Kinetics of Lipid Vesicle Adsorption Measured with a Quartz Crystal Microbalance." Biophysical journal **75**(3): 1397-1402.

Khan, M., N. Dosoky and J. Williams (2013). "Engineering Lipid Bilayer Membranes for Protein Studies." International Journal of Molecular Sciences **14**(11): 21561-21597.

Kriegel, S., T. Uchida, M. Osawa, T. Friedrich and P. Hellwig (2014). "A biomimetic environment to study E. coli Complex I through Surface Enhanced IR Absorption Spectroscopy (SEIRAS)." Biochemistry.

Le Gall, J., W. J. Payne, L. Chen, M. Y. Liu and A. V. Xavier (1994). "Localization and specificity of cytochromes and other electron transfer proteins from sulfate-reducing bacteria." Biochimie **76**(7): 655-665.

Lee, C.-S., S. Kim and M. Kim (2009). "Ion-Sensitive Field-Effect Transistor for Biological Sensing." Sensors **9**(9): 7111-7131.

Léger, C., S. J. Elliott, K. R. Hoke, L. J. C. Jeuken, A. K. Jones and F. A. Armstrong (2003). "Enzyme Electrokinetics: Using Protein Film Voltammetry To Investigate Redox Enzymes and Their Mechanisms†." Biochemistry **42**(29): 8653-8662.

Leroux, F., S. Dementin, B. Burlat, L. Cournac, A. Volbeda, S. Champ, L. Martin, B. Guigliarelli, P. Bertrand, J. Fontecilla-Camps, M. Rousset and C. Léger (2008). "Experimental approaches to kinetics of gas diffusion in hydrogenase." Proceedings of the National Academy of Sciences of the United States of America **105**(32): 11188-11193.

Liebgott, P.-P. P., F. Leroux, B. Burlat, S. Dementin, C. Baffert, T. Lautier, V. Fourmond, P. Ceccaldi, C. Cavazza, I. Meynial-Salles, P. Soucaille, J. C. Fontecilla-Camps, B. Guigliarelli, P. Bertrand, M. Rousset and C. Léger (2010). "Relating diffusion along the substrate tunnel and oxygen sensitivity in hydrogenase." Nature chemical biology **6**(1): 63-70.

Linnett, N. (1970). PH Measurements in Theory and Practice, Radiometer.

Lipkowski, J. (2010). "Building biomimetic membrane at a gold electrode surface." PCCP. Physical chemistry chemical physics **12**(42): 13874.

Lubitz, W., H. Ogata, O. Rüdiger and E. Reijerse (2014). "Hydrogenases." Chemical Reviews **114**(8): 4081-4148.

Lubitz, W. and W. Tumas (2007). "Hydrogen: An Overview." Chemical Reviews **107**(10): 3900-3903.

Lukkari, J., K. Kleemola, M. Meretoja, T. Ollonqvist and J. Kankare (1998). "Electrochemical Post-Self-Assembly Transformation of 4-Aminothiophenol Monolayers on Gold Electrodes." Langmuir **14**(7): 1705-1715.

MacDonald, R. C., R. I. MacDonald, B. P. Menco, K. Takeshita, N. K. Subbarao and L. R. Hu (1991). "Small-volume extrusion apparatus for preparation of large, unilamellar vesicles." Biochim Biophys Acta **1061**(2): 297-303.

Marques, M. C., R. Coelho, A. L. De Lacey, I. A. Pereira and P. M. Matias (2010). "The three-dimensional structure of [NiFeSe] hydrogenase from Desulfovibrio vulgaris Hildenborough: a hydrogenase without a bridging ligand in the active site in its oxidised, "as-isolated" state." Journal of molecular biology **396**(4): 893-907.

Marreiros, B. C., A. P. Batista, A. M. S. Duarte and M. M. Pereira (2013). "A missing link between complex I and group 4 membrane-bound [NiFe] hydrogenases." Biochim Biophys Acta **1827**(2): 198-209.

Mårtensson, C. and V. Agmo Hernández (2012). "Ubiquinone-10 in gold-immobilized lipid membrane structures acts as a sensor for acetylcholine and other tetraalkylammonium cations." Bioelectrochemistry **88**(0): 171-180.

Martin, B., B. Philippe and P. Ernö (2009). Structure Determination of Organic Compounds Tables of Spectral Data.

Mathiesen, C. and C. Hägerhäll (2003). "The 'antiporter module' of respiratory chain Complex I includes the MrpC/NuoK subunit – a revision of the modular evolution scheme." FEBS letters **549**(1–3): 7-13.

Matias, P. M., I. A. C. Pereira, C. M. Soares and M. A. Carrondo (2005). "Sulphate respiration from hydrogen in Desulfovibrio bacteria: a structural biology overview." Progress in Biophysics and Molecular Biology **89**(3): 292-329.

McMillan, D. G. G., S. J. Marritt, J. N. Butt and L. J. C. Jeuken (2012). "Menaquinone-7 Is Specific Cofactor in Tetraheme Quinol Dehydrogenase CymA." Journal of Biological Chemistry **287**(17): 14215-14225.

Mitchell, P. and J. Moyle (1967). "Chemiosmotic hypothesis of oxidative phosphorylation." Nature **213**(5072): 137-139.

Noll, T. and G. Noll (2011). "Strategies for "wiring" redox-active proteins to electrodes and applications in biosensors, biofuel cells, and nanotechnology." Chemical Society Reviews **40**(7): 3564-3576.

Noy, A. (2011). "Bionanoelectronics." Advanced Materials **23**(7): 807-820.

Olejnik, P., B. Palys, A. Kowalczyk and A. Nowicka (2012). "Orientation of Laccase on Charged Surfaces. Mediatorless Oxygen Reduction on Amino- and Carboxyl-Ended Ethylphenyl Groups." The journal of physical chemistry. C **116**(49): 25911-25918.

Oscar, G.-S., C. M. Marta, S. A. B. Carla, M. F. Víctor, M. S. Claudio, A. C. P. Ines and L. D. L. Antonio (2013). "Influence of the protein structure surrounding the active site on the catalytic activity of [NiFeSe] hydrogenases." Journal of biological inorganic chemistry : JBIC : a publication of the Society of Biological Inorganic Chemistry **18**(4): 419-427.

P, V. (2002). "Continuous monitoring of the activation and activity of 6NiFe9-hydrogenases by membrane-inlet mass spectrometry." International Journal of Hydrogen Energy.

Page, C. C., C. C. Moser, X. Chen and P. L. Dutton (1999). "Natural engineering principles of electron tunnelling in biological oxidation-reduction." Nature **402**(6757): 47-52.

Parkin, A., G. Goldet, C. Cavazza, J. C. Fontecilla-Camps and F. A. Armstrong (2008). "The difference a Se makes? Oxygen-tolerant hydrogen production by the [NiFeSe]-hydrogenase

from Desulfomicrobium baculatum." Journal of the American Chemical Society **130**(40): 13410-13416.

Paulette, M. V., H. Michele-France, B. Yves and L. Paul Antoine (1982). "Effect of pH on H-2H exchange, H2 production and H2 uptake, catalysed by the membrane-bound hydrogenase of Paracoccus denitrificans." Biochimica et Biophysica Acta (BBA) - Bioenergetics.

Pereira, M. M., J. N. Carita and M. Teixeira (1999). "Membrane-bound electron transfer chain of the thermohalophilic bacterium Rhodothermus marinus: a novel multihemic cytochrome bc, a new complex III." Biochemistry **38**(4): 1268-1275.

Preissl, S., I. Bick, P. Obrdlik, K. Diekert, S. Gul and P. Gribbon (2011). "Development of an assay for Complex I/Complex III of the respiratory chain using solid supported membranes and its application in mitochondrial toxicity screening in drug discovery." Assay Drug Dev Technol **9**(2): 147-156.

Raj, C. R., K. Fusao and O. Takeo (2001). "Electrochemical and in Situ FTIR Spectroscopic Investigation on the Electrochemical Transformation of 4-Aminothiophenol on a Gold Electrode in Neutral Solution." Langmuir **17**.

Ruediger, O., C. Gutierrez Sanchez, I. A. C. Pereira, M. Velez, V. M. Fernandez, O. Rüdiger, C. Gutiérrez Sánchez, D. Olea, I. Pereira, M. Vélez, V. Fernández and A. De-Lacey (2010). "Enzymatic Anodes for Hydrogen Fuel Cells based on Covalent Attachment of Ni-Fe Hydrogenases and Direct Electron Transfer to SAM-Modified Gold Electrodes." Electroanalysis **22**(7-8): 776-783.

Salamon, Z., Y. Wang, G. Tollin and H. A. Macleod (1994). "Assembly and molecular organization of self-assembled lipid bilayers on solid substrates monitored by surface plasmon resonance spectroscopy." Biochim Biophys Acta **1195**(2): 267-275.

Santidrian, A. F., A. Matsuno-Yagi, M. Ritland, B. B. Seo, S. E. LeBoeuf, L. J. Gay, T. Yagi and B. Felding-Habermann (2013). "Mitochondrial complex I activity and NAD+/NADH balance regulate breast cancer progression." The Journal of clinical investigation **123**(3): 1068-1081.

Sazanov, L. (2014). "The mechanism of coupling between electron transfer and proton translocation in respiratory complex I." Journal of bioenergetics and biomembranes: 1-7.

Sazanov, L. A. and P. Hinchliffe (2006). "Structure of the Hydrophilic Domain of Respiratory Complex I from Thermus thermophilus." Science (New York, N Y) **311**(5766): 1430-1436.

Schäfer, G. (2004). Membrane-Associated Energy Transduction in Bacteria and Archaea. Encyclopedia of Biological Chemistry. W. J. L. D. Lane. New York, Elsevier**:** 637-645.

Schiller, S. M., R. Naumann, K. Lovejoy, H. Kunz and W. Knoll (2003). "Archaea Analogue Thiolipids for Tethered Bilayer Lipid Membranes on Ultrasmooth Gold Surfaces." Angewandte Chemie International Edition **42**(2): 208-211.

Siebert, F. and P. Hildebrandt (2008). Introduction. Vibrational Spectroscopy in Life Science, Wiley-VCH Verlag GmbH & Co. KGaA**:** 1-10.

Snider, G. W., E. Ruggles, N. Khan and R. J. Hondal (2013). "Selenocysteine Confers Resistance to Inactivation by Oxidation in Thioredoxin Reductase: Comparison of Selenium and Sulfur Enzymes." Biochemistry **52**(32): 5472-5481.

Tamagnini, P., R. Axelsson, P. Lindberg, F. Oxelfelt, R. Wünschiers and P. Lindblad (2002). "Hydrogenases and Hydrogen Metabolism of Cyanobacteria." Microbiology and Molecular Biology Reviews **66**(1): 1-20.

Tamiya, N. and S. L. Miller (1963). "Kinetic studies on hydrogenase." The Journal of biological chemistry **238**: 2194-2198.

Teixeira, M., G. Fauque, I. Moura, P. A. Lespinat, Y. Berlier, B. Prickril, H. D. Peck, A. V. Xavier, J. Le Gall and J. J. G. Moura (1987). "Nickel-[iron-sulfur]-selenium-containing hydrogenases from Desulfovibrio baculatus (DSM 1743)." European Journal of Biochemistry **167**(1): 47-58.

Tengölics, R., L. Mészáros, E. Győri, Z. Doffkay, K. L. Kovács and G. Rákhely (2014). "Connection between the membrane electron transport system and Hyn hydrogenase in the purple sulfur bacterium, Thiocapsa roseopersicina BBS." Biochimica et Biophysica Acta (BBA) - Bioenergetics(0).

Thauer, R. K., A.-K. Kaster, M. Goenrich, M. Schick, T. Hiromoto and S. Shima (2010). "Hydrogenases from Methanogenic Archaea, Nickel, a Novel Cofactor, and H2 Storage." Annual Review of Biochemistry **79**(1): 507-536.

Todorovic, S., A. Verissimo, N. Wisitruangsakul, I. Zebger, P. Hildebrandt, M. M. Pereira, M. Teixeira and D. H. Murgida (2008). "SERR-Spectroelectrochemical Study of a cbb(3) Oxygen Reductase in a Biomimetic Construct." J Phys Chem B **112**(51): 16952-16959.

Utesch, T., D. Millo, M. Castro, P. Hildebrandt, I. Zebger and M. Mroginski (2013). "Effect of the Protonation Degree of a Self-Assembled Monolayer on the Immobilization Dynamics of a [NiFe] Hydrogenase." Langmuir **29**(2): 673-682.

Valente, F. M., P. M. Pereira, S. S. Venceslau, M. Regalla, A. V. Coelho and I. A. Pereira (2007). "The [NiFeSe] hydrogenase from Desulfovibrio vulgaris Hildenborough is a bacterial lipoprotein lacking a typical lipoprotein signal peptide." FEBS letters **581**(18): 3341-3344.

Valente, F. M., L. M. Saraiva, J. LeGall, A. V. Xavier, M. Teixeira and I. A. Pereira (2001). "A membrane-bound cytochrome c3: a type II cytochrome c3 from Desulfovibrio vulgaris Hildenborough." Chembiochem : a European journal of chemical biology **2**(12): 895-905.

Valente, F. M. A., A. S. F. Oliveira, N. Gnadt, I. Pacheco, A. V. Coelho, A. V. Xavier, M. Teixeira, C. M. Soares and I. A. C. Pereira (2005). "Hydrogenases in Desulfovibrio vulgaris Hildenborough: Structural and physiologic characterisation of the membrane-bound [NiFeSe] hydrogenase." Journal of Biological Inorganic Chemistry **10**(6): 667-682.

Verkhovskaya, M. and D. A. Bloch (2013). "Energy-converting respiratory Complex I: on the way to the molecular mechanism of the proton pump." Int J Biochem Cell Biol **45**(2): 491-511.

Vignais, P. M., B. Billoud and J. Meyer (2001). "Classification and phylogeny of hydrogenases1." FEMS Microbiology Reviews **25**(4): 455-501.

Vignais, P. M., L. Cournac, E. C. Hatchikian, S. Elsen, L. Serebryakova, N. Zorin and B. Dimon (2002). "Continuous monitoring of the activation and activity of [NiFe]-hydrogenases by membrane-inlet mass spectrometry." International Journal of Hydrogen Energy **27**(11-12): 1441-1448.

Vogt, S., E. Lyon, S. Shima and R. Thauer (2008). "The exchange activities of [Fe] hydrogenase (iron–sulfur-cluster-free hydrogenase) from methanogenic archaea in comparison with the exchange activities of [FeFe] and [NiFe] hydrogenases." JBIC Journal of Biological Inorganic Chemistry **13**(1): 97-106.

Volbeda, A., L. Martin, E. Barbier, O. Gutiérrez-Sanz, A. De Lacey, P.-P. Liebgott, S. Dementin, M. Rousset and J. Fontecilla-Camps (2014). "Crystallographic studies of [NiFe]-hydrogenase mutants: towards consensus structures for the elusive unready oxidized states." JBIC Journal of Biological Inorganic Chemistry: 1-12.

Walker, J. E. (1992). "The NADH:ubiquinone oxidoreductase (complex I) of respiratory chains." Q Rev Biophys **25**(3): 253-324.

Wang, L. X., E. Jiang Xiu, L.-X. Wang and X.-E. Jiang (2012). "Bioanalytical Applications of Surface-enhanced Infrared Absorption Spectroscopy." Current Opinion in Structural Biology **40**(7): 975-982.
Wharton, C. W. (1986). "Infra-red and Raman spectroscopic studies of enzyme structure and function." Biochem J **233**(1): 25-36.

Yang, X. and M. B. Hall (2009). "Monoiron Hydrogenase Catalysis: Hydrogen Activation with the Formation of a Dihydrogen, Fe−Hδ−···Hδ+−O, Bond and Methenyl-H4MPT+ Triggered Hydride Transfer." Journal of the American Chemical Society **131**(31): 10901-10908.

Zheng, D., M. Wang, L. Chen, N. Wang and L. Sun (2014). "Redox Reactions of [FeFe]-Hydrogenase Models Containing an Internal Amine and a Pendant Phosphine." Inorganic Chemistry **53**(3): 1555-1561.

Zorin, N. A., B. Dimon, J. Gagnon, J. Gaillard, P. Carrier and P. M. Vignais (1996). "Inhibition by iodoacetamide and acetylene of the H-D-exchange reaction catalyzed by Thiocapsa roseopersicina hydrogenase." European journal of biochemistry / FEBS **241**(2): 675-681.

Zoski, C., Ed. (2006). Handbook of Electrochemistry, Elsevier Science.

Output of publications derived from this thesis

JACS
JOURNAL OF THE AMERICAN CHEMICAL SOCIETY

Communication

pubs.acs.org/JACS

Understanding and Tuning the Catalytic Bias of Hydrogenase

Abbas Abou Hamdan,[†] Sébastien Dementin,[†] Pierre-Pol Liebgott,[†] Oscar Gutierrez-Sanz,[‡] Pierre Richaud,[§] Antonio L. De Lacey,[‡] Marc Rousset,[†] Patrick Bertrand,[†] Laurent Cournac,[§,∥,*] and Christophe Léger[†,*]

[†]Laboratoire de Bioénergétique et Ingénierie des Protéines, Institut de Microbiologie de la Méditerranée, CNRS and Aix-Marseille Université, 31 chemin Joseph Aiguier, 13402 Marseille Cedex 20, France

[‡]Instituto de Catalisis y Petroleoquimica (CSIC), 28049 Madrid, Spain

[§]CEA, DSV, IBEB, Laboratoire de Bioénergétique et Biotechnologie des Bactéries & Microalgues, Saint Paul Lez Durance/CNRS, UMR Biologie Végétale & Microbiologie Environnementales, Saint Paul lez Durance, France/Aix-Marseille Université, Saint Paul lez Durance, France

Supporting Information

ABSTRACT: When enzymes are optimized for biotechnological purposes, the goal often is to increase stability or catalytic efficiency. However, many enzymes reversibly convert their substrate and product, and if one is interested in catalysis in only one direction, it may be necessary to prevent the reverse reaction. In other cases, reversibility may be advantageous because only an enzyme that can operate in both directions can turnover at a high rate even under conditions of low thermodynamic driving force. Therefore, understanding the basic mechanisms of reversibility in complex enzymes should help the rational engineering of these proteins. Here, we focus on NiFe hydrogenase, an enzyme that catalyzes H_2 oxidation and production, and we elucidate the mechanism that governs the catalytic bias (the ratio of maximal rates in the two directions). Unexpectedly, we found that this bias is not mainly determined by redox properties of the active site, but rather by steps which occur on sites of the proteins that are remote from the active site. We evidence a novel strategy for tuning the catalytic bias of an oxidoreductase, which consists in modulating the rate of a step that is limiting only in one direction of the reaction, without modifying the properties of the active site.

The four Michaelis parameters (two maximal rates and two values of K_m) which characterize the forward and reverse reactions of a one-substrate one-product enzyme are related to each other and to the equilibrium constant of the reaction by the Haldane equation.[1] The forward and reverse maximal rates sometimes differ so much that certain enzymes were designated as "one-way enzymes".[2] The origin of such kinetic asymmetry, referred to as "catalytic bias", has rarely been investigated. Jencks proposed that directionality may result from the destabilization of the enzyme−substrate complex, which would decrease the energy required to reach the transition state in the forward direction.[2] This "Circe effect" is controversial[3] and has found no echo in the case of oxidoreductases, whose directionality is always discussed by comparing the potential of the substrate/product redox couple with the potential of either the active site or the redox centers of the electron transfer (ET) chain, when there is one (see examples in Supporting Information (SI)).

In trying to explain the catalytic bias from a single property of the enzyme (the potential of either the active site or the ET chain), one implicitly assumes that a single redox step, ET either between the substrate and active site or to/from an electron relay, determines both maximal rates. However, the catalytic cycle of oxidoreductases involves various steps (substrate binding, product release, proton and electron transfers, active-site chemistry) and it may occur that the rate limiting step (rls) is not the same when the enzyme works forward or backward. Two different steps may define the two maximal rates, and their ratio. Demonstrating that this can occur requires that the rls be defined in both directions in a series of variants that exhibit different catalytic preferences. Hereafter, we do so by characterizing a series of *Desulfovibrio fructosovorans* (*Df*) NiFe hydrogenase mutants. Figure 1 shows the structure of the wild type (WT) enzyme and illustrates the idea that its catalytic mechanism involves sites of the protein that are far apart from one another. Previously, we have shown that the WT enzyme catalyzes H_2 production and oxidation at similar maximal rates and that narrowing the substrate channel (Figure 1d) using site directed mutagenesis has no effect on the maximal rate of H_2 oxidation.[4,5] Here we show that these mutations slow H_2 production up to 100-fold. In redox titrations, the active site of the mutants that have little reductive activity behaves as that of the WT enzyme. We use a novel method based on the isotope-exchange assay to determine the rates of H_2 release from the active site to the solvent, and we conclude that this step limits H_2 production whereas H_2 entry does not determine the maximal rate of H_2 oxidation. Conversely, the previous observation[5] that modifying the ET chain selectively slows H_2 oxidation shows that ET limits the rate of H_2 oxidation but not H_2 production.[6] This is the first demonstration, on a specific example, that slowing a step that is rate limiting only when the enzyme works in one direction is a general mechanism for biasing the enzyme in the other

Received: March 3, 2012
Published: April 27, 2012

Relation between anaerobic inactivation and oxygen tolerance in a large series of NiFe hydrogenase mutants

Abbas Abou Hamdan[a], Pierre-Pol Liebgott[b], Vincent Fourmond[a], Oscar Gutiérrez-Sanz[c], Antonio L. De Lacey[c], Pascale Infossi[a], Marc Rousset[a], Sébastien Dementin[a], and Christophe Léger[a,1]

[a]Laboratoire de Bioénergétique et Ingénierie des Protéines, Centre National de la Recherche Scientifique, Aix-Marseille Université, Institut de Microbiologie de la Méditerranée, 13402 Marseille Cedex 20, France; [b]Laboratoire de Microbiologie, Institut de Recherche pour le Développement, Aix Marseille Université, Unité Mixte de Recherche D180, Microbiologie et Biotechnologie des Environnements Chauds, Ecole Supérieure d'Ingénieurs de Luminy, 13288 Marseille Cedex 09, France; and [c]Laboratorio de Bioelectrocatalisis, Departamento de Biocatalisis, Instituto de Catalisis y Petroleoquimica, Consejo Superior de Investigaciones Cientificas, 28049 Madrid, Spain

Edited* by Jean-Michel Savéant, Université Paris Diderot (Paris 7), Paris, France, and approved October 19, 2012 (received for review July 29, 2012)

Nickel-containing hydrogenases, the biological catalysts of H_2 oxidation and production, reversibly inactivate under anaerobic, oxidizing conditions. We aim at understanding the mechanism of (in)activation and what determines its kinetics, because there is a correlation between fast reductive reactivation and oxygen tolerance, a property of some hydrogenases that is very desirable from the point of view of biotechnology. Direct electrochemistry is potentially very useful for learning about the redox-dependent conversions between active and inactive forms of hydrogenase, but the voltammetric signals are complex and often misread. Here we describe simple analytical models that we used to characterize and compare 16 mutants, obtained by substituting the position-74 valine of the O_2-sensitive NiFe hydrogenase from *Desulfovibrio fructosovorans*. We observed that this substitution can accelerate reactivation up to 1,000-fold, depending on the polarity of the position 74 amino acid side chain. In terms of kinetics of anaerobic (in)activation and oxygen tolerance, the valine-to-histidine mutation has the most spectacular effect: The V74H mutant compares favorably with the O_2-tolerant hydrogenase from *Aquifex aeolicus*, which we use here as a benchmark.

electrocatalysis | direct electron transfer | protein film voltammetry | hydrogen

The nickel–iron hydrogenases that have been crystallized and/or thoroughly studied so far are very similar from a structural point of view: They all are either soluble heterodimers or heterodimers isolated from a membrane-associated complex. The amino acids that surround the NiFe active site are conserved (1) and yet the kinetic properties of these enzymes are diverse. For example, some NiFe hydrogenases can oxidize and produce H_2, whereas others preferentially catalyze one direction of the reaction (2–4). Another property of some hydrogenases that has attracted considerable interest is their sensitivity (and sometimes their resistance) to O_2. This interest stems from the fact that hydrogenases could be used for H_2 oxidation in fuel cells or H_2 production in photo-electrochemical cells if they were functional under aerobic conditions (5).

The NiFe hydrogenases that have been studied first, referred to as "standard," were purified from *Allochromatium vinosum* or *Desulfovibrio* species. Upon exposure to O_2, they convert into two inactive forms called NiA and NiB, where an oxygenated ligand bridges the Ni and the Fe. The NiB and NiA states can be reactivated by reduction, the former more quickly than the latter (6). The membrane-bound NiFe hydrogenases from, e.g., *Ralstonia eutropha* or *Aquifex aeolicus* are reversibly inhibited by O_2 and termed "O_2 resistant." Apparently, this resistance results from (*i*) the enzyme reacting with O_2 to form only the NiB state and (*ii*) this NiB state reactivating much more quickly than in standard hydrogenases (4, 7). The most patent differences between O_2-resistant and O_2-sensitive hydrogenases are the structures and redox properties of the FeS cluster that is proximal to the active site. Recent structural and spectroscopic investigations have shown that in O_2-resistant enzymes, it is an unprecedented 4Fe3S cluster (8–10) that has a high reduction potential and the ability to cycle through three redox states in a narrow range of potential (11).

The rate of reactivation of NiB partly determines O_2 tolerance, but the reason this reaction is orders of magnitude faster in oxygen-resistant hydrogenases than in standard hydrogenases has not been investigated. The hypothesis that fast reactivation may result from a thermodynamic advantage (that is, NiB having a higher reduction potential) (7) has found no experimental support: The redox potential of the NiB state in the NiFe hydrogenase from *A. aeolicus* is not significantly greater than in standard hydrogenases (4), and the V74C mutation in *Desulfovibrio fructosovorans* has no effect on the spectral and redox properties of the NiB state, whereas it does increase significantly its rate of reduction (12).

The anaerobic conversion between active enzyme and the NiB state is often studied in protein film voltammetry experiments, where the enzyme is adsorbed or attached to a rotating-disk electrode and electron transfer is direct. The value of the electrode potential (E) is set to drive the catalytic reaction while the turnover rate (the activity) is simultaneously measured as a current (13). Changing the electrode potential also triggers the conversion between active and inactive states. In chronoamperometry (CA) experiments, the (in)activation is seen as current transients following potential steps (14, 15). In cyclic voltammetry (CV) experiments, the oxidative inactivation gives the electrochemical response the complex shape that is shown in Fig. 1*A* (14–16). Starting from the low potential limit, the current initially increases as the electrode potential increases (and so does the driving force for H_2 oxidation) and then bends down or even decreases at high potential, as a result of the oxidative formation of the inactive state. As the potential is lowered back on the reverse scan, the reactivation produces an increase in current, which is eventually outcompeted by the decrease in steady-state activity that results from the potential being less oxidizing. Hysteresis occurs because the conversion between (in)active states is slow on the voltammetric timescale (16), irrespective of scan rate in the experimentally accessible range of scan rate ($\nu > 0.1$ mV/s). The wave shape is defined by the steady-state electrochemical response of the active enzyme (17) and the potential-dependent kinetics of conversion between active and inactive states, but the latter, crucial information is not easily disclosed. In particular, the position of the first inflection point on the reverse

Author contributions: V.F., M.R., S.D., and C.L. designed research; A.A.H., P.-P.L., V.F., O.G.-S., A.L.D.L., P.I., S.D., and C.L. performed research; A.A.H., P.-P.L., V.F., O.G.-S., A.L.D.L., and C.L. analyzed data; and V.F., S.D., and C.L. wrote the paper.

The authors declare no conflict of interest.

*This Direct Submission article had a prearranged editor.

[1]To whom correspondence should be addressed. E-mail: christophe.leger@imm.cnrs.fr.

This article contains supporting information online at www.pnas.org/lookup/suppl/doi:10.1073/pnas.1212258109/-/DCSupplemental.

nature chemical biology

BRIEF COMMUNICATION

PUBLISHED ONLINE: 11 NOVEMBER 2012 | DOI: 10.1038/NCHEMBIO.1110

O_2-independent formation of the inactive states of NiFe hydrogenase

Abbas Abou Hamdan[1], Bénédicte Burlat[1], Oscar Gutiérrez-Sanz[2], Pierre-Pol Liebgott[1], Carole Baffert[1], Antonio L De Lacey[2], Marc Rousset[1], Bruno Guigliarelli[1], Christophe Léger[1] & Sébastien Dementin[1]*

We studied the mechanism of aerobic inactivation of *Desulfovibrio fructosovorans* nickel-iron (NiFe) hydrogenase by quantitatively examining the results of electrochemistry, EPR and FTIR experiments. They suggest that, contrary to the commonly accepted mechanism, the attacking O_2 is not incorporated as an active site ligand but, rather, acts as an electron acceptor. Our findings offer new ways toward the understanding of O_2 inactivation and O_2 tolerance in NiFe hydrogenases.

Hydrogenases are complex metalloenzymes that catalyze the reversible conversion between H_2 and protons. A substantial portion of the literature on these enzymes focuses on their inactive forms, in part because most hydrogenases are inhibited under oxidizing (aerobic or anaerobic) conditions, and this is an obstacle for the use of these enzymes in fuel cells, photoelectrochemical cells or 'hydrogen farms' that exploit photosynthetic microorganisms (green algae and cyanobacteria). The mechanism of inactivation of NiFe hydrogenases has been studied for over 30 years. After aerobic oxidation, they are reversibly converted into two chemically distinct inactive forms, NiA and NiB (**Fig. 1a**), which are recognized by their spectroscopic signatures and rates of reactivation under reducing conditions[1]. NiA reactivates more slowly than NiB, and, hence, the names 'unready' and 'ready' are often used synonymously with NiA and NiB, respectively[1]. The resolution of the structure of aerobically purified enzymes from *Desulfovibrio* species shows that an oxygenated ligand bridges the dinuclear NiFe active site[2,3]. The oxidation of the cysteines that ligate the nickel is also detected in several crystals of O_2-exposed NiFe hydrogenases[4]. Whereas it is now held that NiB contains a hydroxyl bridging group, the nature of the bridging ligand in NiA is still under debate (see ref. 5 for a review).

The current model of aerobic inactivation has emerged from electrochemical protein film voltammetry (PFV) studies in which the O_2-sensitive enzyme from *Allochromatium vinosum* is adsorbed onto an electrode, and its activity is detected as a current[6]. In a typical experiment, the enzyme, the redox state of which is determined by the value of the electrode potential (E), is first inactivated by adding oxygen. The electrode potential is then stepped to a value that is low enough that the enzyme reactivates, and the resulting biphasic increase in current can be analyzed to determine how much NiA and NiB species have been formed under particular inactivation conditions (**Fig. 1b**). The NiA-to-NiB ratio increases when exposure to O_2 has taken place under more oxidizing conditions (that is, at a higher electrode potential and a lower H_2 concentration)[6]. This finding led to the current hypothesis that NiFe hydrogenases are inactivated because their active site has trapped the product of completely or partially reduced O_2, resulting in the formation of the ready and unready forms, respectively. This mechanism would also apply to O_2-tolerant enzymes (found in, for example, *Ralstonia eutropha*, *Aquifex aeolicus* or *Escherichia coli*), but the original properties of the iron-sulfur cluster that is proximal to the active site in these enzymes would favor 'backward electron transfer' and complete reduction of the attacking O_2 so that NiB is selectively formed[7–10].

To investigate the role of O_2 in this process, we used the O_2-sensitive NiFe enzyme from *D. fructosovorans* covalently attached (rather than adsorbed) to a rotating disc graphite electrode (see **Supplementary Results**, **Supplementary Fig. 1** for a description of the procedure and advantages of covalent attachment). The signals shown in **Supplementary Figure 2** are reactivation traces obtained at $E = -90$ mV, a pressure of 0.1 bar H_2, pH 5.5, 40 °C, after the enzyme has been inactivated either aerobically or anaerobically, in the presence or absence of H_2 and at $E = +65$, +215 or +400 mV. The proportions of the inactive forms deduced by fitting these traces (as described in the captions of **Supplementary Figs. 2** and **3**) are reported in **Table 1**. First, we noted that, in all cases, a certain fraction of enzyme (noted as 'inert' in **Table 1**) could never be reactivated. This form was more abundant when the enzyme had been inactivated at a higher potential, in the absence of H_2 and in the presence of O_2. This is reminiscent of the so-called 'lost phase' found in previous studies of *A. vinosum* NiFe hydrogenase[6], which probably results from irreversible damage of the active site[11]. Second,

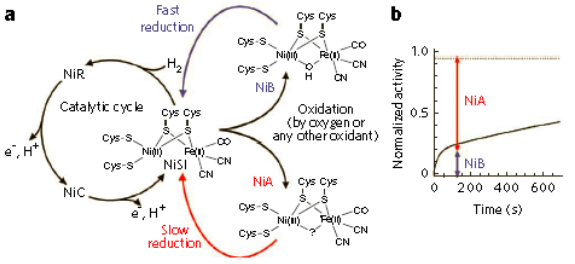

Figure 1 | Active and inactive forms of the NiFe hydrogenase. (**a**) The catalytic cycle includes the active NiSI, NiR and NiC states. After oxidation, the enzyme is converted into the inactive NiA and NiB states. NiA, NiB and NiC are in the Ni(III) state; NiSI and NiR are in the Ni(II) state, making them EPR silent. (**b**) Typical reactivation trace obtained by PFV after the enzyme has been inactivated. The activity is normalized by the initial current measured before inactivation. The dashed line indicates the activity measured after reactivation (**Supplementary Fig. 3**). The difference between the initial and final activities represents the proportion of an inert form detected only in PFV experiments.

[1]Aix-Marseille Université, Centre National de la Recherche Scientifique (CNRS), Laboratoire de Bioénergétique et Ingénierie des Protéines, Unité Mixte de Recherche 7281, Institut de Microbiologie de la Méditerranée, Marseille, France. [2]Consejo Superior de Investigaciones Científicas (CSIC), Instituto de Catalisis y Petroleoquímica (ICP), Laboratorio de Bioelectrocatálisis, Madrid, Spain. *e-mail: dementin@imm.cnrs.fr

J Biol Inorg Chem (2013) 18:419–427
DOI 10.1007/s00775-013-0986-4

ORIGINAL PAPER

Influence of the protein structure surrounding the active site on the catalytic activity of [NiFeSe] hydrogenases

Oscar Gutiérrez-Sanz · Marta C. Marques · Carla S. A. Baltazar · Víctor M. Fernández · Claudio M. Soares · Ines A. C. Pereira · Antonio L. De Lacey

Received: 14 December 2012 / Accepted: 6 February 2013 / Published online: 7 March 2013

Abstract A combined experimental and theoretical study of the catalytic activity of a [NiFeSe] hydrogenase has been performed by H/D exchange mass spectrometry and molecular dynamics simulations. Hydrogenases are enzymes that catalyze the heterolytic cleavage or production of H_2. The [NiFeSe] hydrogenases belong to a subgroup of the [NiFe] enzymes in which a selenocysteine is a ligand of the nickel atom in the active site instead of cysteine. The aim of this research is to determine how much the specific catalytic properties of this hydrogenase are influenced by the replacement of a sulfur by selenium in the coordination of the bimetallic active site versus the changes in the protein structure surrounding the active site. The pH dependence of the D_2/H^+ exchange activity and the high isotope effect observed in the Michaelis constant for the dihydrogen substrate and in the single exchange/double exchange ratio suggest that a "cage effect" due to the protein structure surrounding the active site is modulating the enzymatic catalysis. This "cage effect" is supported by molecular dynamics simulations of the diffusion of H_2 and D_2 from the outside to the inside of the protein, which show different accumulation of these substrates in a cavity next to the active site.

Keywords Hydrogenase · Selenocysteine · Enzyme kinetics · Isotope exchange · Molecular dynamics

O. Gutiérrez-Sanz · V. M. Fernández · A. L. De Lacey (✉)
Instituto de Catálisis y Petroleoquímica, CSIC, c/Marie Curie 2, 28049 Madrid, Spain
e-mail: alopez@icp.csic.es

M. C. Marques · C. S. A. Baltazar · C. M. Soares · I. A. C. Pereira
Instituto de Tecnologia Química e Biológica, Universidade Nova de Lisboa, Av. da Republica, 2780-157 Oeiras, Portugal

Introduction

Hydrogenases have emerged as attractive enzymes for biotechnological applications [1, 2], but most importantly as a source of inspiration for the development of biomimetic catalysts for H_2 production or for its oxidation in fuel cells [3–5]. Hydrogenases can catalyze this reaction in a reversible way with high turnover, under mild conditions and with almost no overpotential [1, 6]. The active site of hydrogenases contains nickel and/or iron as the only metals [7]; thus nature shows us that efficient catalysis of H_2 production and oxidation is possible without using noble metals. In most [NiFe] hydrogenases the nickel atom is coordinated by the thiol groups of four cysteine amino acids, two of them in a terminal position and the other two forming bridges with the iron atom of the active site [7]. However, in some [NiFe] hydrogenases one of the cysteines is replaced by a selenocysteine, as shown in Fig. 1a. The interesting aspect of these [NiFeSe] hydrogenases is that, although the chemical properties of selenium and sulfur are similar, the change of coordination caused by replacement of one cysteine by a selenocysteine modifies considerably the catalytic and spectroscopic features of the active site [8]. Some of the most notable catalytic properties of [NiFeSe] hydrogenases are (a) they become active immediately upon reduction, whereas most [NiFe] hydrogenases isolated under aerobic conditions require a slow reductive activation process, (b) they have higher H_2-production activity than H_2-oxidation activity, in contrast to most [NiFe] hydrogenases, and (c) they are more tolerant towards oxygen in the H_2-production activity than [FeFe] hydrogenases and most [NiFe] hydrogenases [8–12]. However, it is not yet clear if these differences are only due to the replacement of sulfur by

THE JOURNAL OF PHYSICAL CHEMISTRY Letters

Letter

pubs.acs.org/JPCL

Orientation and Function of a Membrane-Bound Enzyme Monitored by Electrochemical Surface-Enhanced Infrared Absorption Spectroscopy

Oscar Gutiérrez-Sanz,[‡] Marta Marques,[§] Inês A. C. Pereira,[§] Antonio L. De Lacey,[‡] Wolfgang Lubitz,[†] and Olaf Rüdiger*[,†]

[†]Max-Planck-Institut für Chemische Energiekonversion, Stiftstrasse 34-36, 45470 Mülheim an der Ruhr, Germany

[‡]Instituto de Catálisis y Petroleoquímica, CSIC, c/Marie Curie 2, 28049 Madrid, Spain

[§]Instituto de Tecnologia Química e Biológica, Universidade Nova de Lisboa Oeiras, Portugal

ABSTRACT: Electrochemical SEIRA is the method of choice for characterizing a lipid-bilayer-anchored, membrane-bound hydrogenase immobilized on a gold electrode. This setup allows the study of the enzyme under conditions mimicking its natural environment. A single experiment provides all of the crucial spectroscopic information relating to the protein orientation, active site of the protein, and the lipid bilayer and also direct electrochemical determination of the catalytic H_2 oxidation by the enzyme.

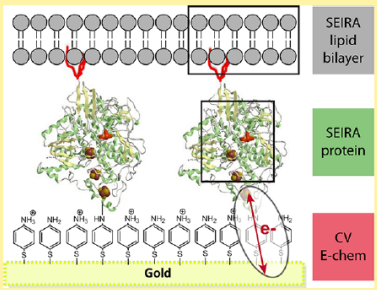

SECTION: Biophysical Chemistry and Biomolecules

Integration of redox proteins into nanostructured systems is of great interest for their application in biosensors, biofuel cells, nanobioelectronic devices, and nanobiocatalytic processes.[1] In this context, current research has focused on developing suitable interfaces able to link chemical reactions catalyzed by redox enzymes to electrochemical processes.[2] The goal is to optimize the immobilization of the enzyme on the conductive support while maintaining the biocatalyst's native structure and function and at the same time assuring the charge transport between both elements of the biodevice. This aim is especially challenging for membrane proteins due to their higher structural complexity and instability in the absence of their native lipid environment.[3] To deal with this problem several strategies have been developed for building biomimetic membranes on conductive supports.[4] Furthermore, these supported model membranes allow the study of membrane protein function.[5] One of the most useful techniques for studying the combination of membrane redox enzymes with biomimetic membranes supported on conductive surfaces is surface-enhanced infrared absorption (SEIRA) spectroelectrochemistry.[6−8] This technique allows the sensitive characterization of the chemical structure at the electrode interface while driving the electrocatalytic activity of the membrane enzyme. Moreover, it allows monitoring the step-by-step immobilization of a redox enzyme on an electrode by monitoring difference spectra.[6,9]

In this work we have studied the chemical structure and function of a membrane-attached hydrogenase coimmobilized with a phospholipid bilayer on a gold electrode, by SEIRA spectroelectrochemistry. Hydrogenases are redox metalloenzymes (containing Ni and/or Fe) that catalyze the reversible oxidation of H_2 to protons.[10−12] The study of hydrogenases is currently one of the most interesting areas of science from both the fundamental and application point of view. This is due to the worldwide growing interest in using H_2 for energy-conversion processes; therefore, the study of hydrogenases is important for developing alternative electrocatalysts to Pt in H_2 energy conversion technology. We have shown in a previous combined electrochemical and atomic force microscopy (AFM) study that the membrane-bound hydrogenase from *Desulfovibrio vulgaris* Hildenborough can be immobilized onto gold electrodes with its lipid tail inserted into a supported phospholipid bilayer.[13]

Moreover, the orientation of the enzyme relative to the electrode surface can be controlled by the immobilization procedure, either by inserting the hydrogenase on top of the phospholipid bilayer supported on the electrode or by forming the phospholipid bilayer on top of a hydrogenase monolayer covalently bound to the electrode (Figure 1). In the absence of phospholipids or detergents, the lipidic group located at the N terminus of the protein can be spontaneously cleaved, decreasing the catalytic activity of the resulting soluble enzyme. This suggested that the lipidic tail plays an important structural role in catalysis.[14] In the present work, for the first time we present data of the chemical structure of a membrane-bound hydrogenase immobilized at the electrode surface for both

Received: July 2, 2013
Accepted: August 5, 2013
Published: August 5, 2013

Langmuir

Article

pubs.acs.org/Langmuir

Reconstitution of Respiratory Complex I on a Biomimetic Membrane Supported on Gold Electrodes

Oscar Gutiérrez-Sanz,[†] David Olea,[†] Marcos Pita,[†] Ana P. Batista,[‡] Alvaro Alonso,[†] Manuela M. Pereira,[‡] Marisela Vélez,[†,§] and Antonio L. De Lacey*[,†]

[†]Instituto de Catalisis y Petroleoquímica, CSIC, c/Marie Curie 2, L10, 28049 Madrid, Spain

[‡]Instituto de Tecnologia Química e Biológica, Universidade Nova de Lisboa, Apartado 127, 2781-901 Oeiras, Portugal

[§]Instituto Madrileño de Estudios Avanzados en Nanociencia (IMDEA-Nanociencia), Facultad de Ciencias, C-IX-3ª Cantoblanco, 28049 Madrid, Spain

Supporting Information

ABSTRACT: For the first time, respiratory complex I has been reconstituted on an electrode preserving its structure and activity. Respiratory complex I is a membrane-bound enzyme that has an essential function in cellular energy production. It couples NADH:quinone oxidoreduction to translocation of ions across the cellular (in prokaryotes) or mitochondrial membranes. Therefore, complex I contributes to the establishment and maintenance of the transmembrane difference of electrochemical potential required for adenosine triphosphate synthesis, transport, and motility. Our new strategy has been applied for reconstituting the bacterial complex I from *Rhodothermus marinus* onto a biomimetic membrane supported on gold electrodes modified with a thiol self-assembled monolayer (SAM). Atomic force microscopy and faradaic impedance measurements give evidence of the biomimetic construction, whereas electrochemical measurements show its functionality. Both electron transfer and proton translocation by respiratory complex I were monitored, simulating in vivo conditions.

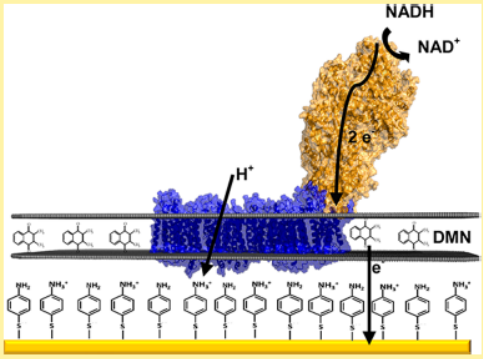

INTRODUCTION

Life depends on continuous flow of energy and on mechanisms that control this energy flow. Respiratory complex I (E.C.1.6.5.3) is an energy transducing enzyme present in the three domains of life. This enzyme catalyzes the oxidation of NADH and the reduction of quinone coupled to ion translocation across the membrane. In this way, it contributes to the establishment of the transmembrane difference of electrochemical potential which is used for the synthesis of adenosine triphosphate, solute transport, and motility. Deficiencies in this complex have been shown to be implicated in several pathologies, namely, neurodegenerative diseases such as Leber's hereditary optic neuropathy, Parkinson's, and dystonia disorders.[1]

In mitochondria, the enzyme is composed of 45 subunits with a total molecular mass of 1 MDa, whereas the bacterial complex I, considered to comprise the minimal functional unit, has in general 14 subunits (named Nqo1-14 or NuoA-N) with a total mass of 550 kDa. The subunits are arranged in an L-shaped structure, consisting of peripheral and membrane arms as shown in Figure 1.[2−5] The peripheral part contains the prosthetic groups (iron−sulfur centers and FMN),[2] while the membrane part is, most likely, involved in quinone reduction and charge translocation.[5] The nature of the ion(s) translocated by this enzyme is still a highly discussed issue, being H^+ and Na^+ possible candidates. It is generally accepted that H^+ is the coupling ion in complex I;[6,7] however, in the case of some bacterial complexes I, Na^+ has been proposed to have that role.[8,9] It was also shown that some bacterial complexes I are capable of H^+ and Na^+ translocation, but in opposite directions, with H^+ being the coupling ion.[10−12]

The study of this enzyme is currently a hot topic in bioenergetics, stimulated by recently structural and functional data.[2,5] Still, the mechanisms of quinone reduction, ion translocation and their coupling are unknown. To our knowledge, the study of both redox and ion translocation activities in the same experimental setup was not full achieved yet. Different strategies and techniques have been employed to study NADH oxidation, mostly working with soluble subcomplexes or partially solubilized proteins for using electrochemical and spectroscopic techniques.[13−16] To study proton translocation, the complex I has to be inserted in a lipid bilayer that provides the enzyme with the appropriate lipid environment and separates two compartments needed to maintain the proton gradient. Protein orientation and compartmentalization can be achieved by working with intact

Received: May 12, 2014
Revised: June 26, 2014
Published: July 2, 2014

J Biol Inorg Chem
DOI 10.1007/s00775-014-1203-9

ORIGINAL PAPER

Crystallographic studies of [NiFe]-hydrogenase mutants: towards consensus structures for the elusive unready oxidized states

Anne Volbeda · Lydie Martin · Elodie Barbier · Oscar Gutiérrez-Sanz · Antonio L. De Lacey · Pierre-Pol Liebgott · Sébastien Dementin · Marc Rousset · Juan C. Fontecilla-Camps

Received: 21 July 2014 / Accepted: 1 October 2014

Abstract Catalytically inactive oxidized O_2-sensitive [NiFe]-hydrogenases are characterized by a mixture of the paramagnetic Ni-A and Ni-B states. Upon O_2 exposure, enzymes in a partially reduced state preferentially form the unready Ni-A state. Because partial O_2 reduction should generate a peroxide intermediate, this species was previously assigned to the elongated Ni–Fe bridging electron density observed for preparations of [NiFe]-hydrogenases known to contain the Ni-A state. However, this proposition has been challenged based on the stability of this state to UV light exposure and the possibility of generating it anaerobically under either chemical or electrochemical oxidizing conditions. Consequently, we have considered alternative structures for the Ni-A species including oxidation of thiolate ligands to either sulfenate or sulfenic acid. Here, we report both new and revised [NiFe]-hydrogenases structures and conclude, taking into account corresponding characterizations by Fourier transform infrared spectroscopy (FTIR), that the Ni-A species contains oxidized cysteine and bridging hydroxide ligands instead of the peroxide ligand we proposed earlier. Our analysis was rendered difficult by the typical formation of mixtures of unready oxidized states that, furthermore, can be reduced by X-ray induced photoelectrons. The present study could be carried out thanks to the use of *Desulfovibrio fructosovorans* [NiFe]-hydrogenase mutants with special properties. In addition to the Ni-A state, crystallographic results are also reported for two diamagnetic unready states, allowing the proposal of a revised oxidized inactive Ni-SU model and a new structure characterized by a persulfide ion that is assigned to an Ni-'S_{ox}' species.

An Interactive 3D Complement page in Proteopedia is available at: http://proteopedia.org/wiki/index.php/Journal:JBIC:28

Electronic supplementary material The online version of this article (doi:10.1007/s00775-014-1203-9) contains supplementary material, which is available to authorized users.

A. Volbeda (✉) · L. Martin · E. Barbier · Juan. C. Fontecilla-Camps
University Grenoble Alpes, IBS, 38044 Grenoble, France
e-mail: anne.volbeda@ibs.fr

A. Volbeda · L. Martin · E. Barbier · Juan. C. Fontecilla-Camps
CEA, IBS, 38044 Grenoble, France

A. Volbeda · L. Martin · E. Barbier · Juan. C. Fontecilla-Camps
CNRS, IBS, 38044 Grenoble, France

Present Address:
E. Barbier
CEA, MINATEC, 38044 Grenoble, France

O. Gutiérrez-Sanz · A. L. De Lacey
Instituto de Catálisis y Petroleoquímica, CSIC, 28049 Madrid, Spain

P.-P. Liebgott · S. Dementin · M. Rousset
Aix-Marseille Université, CNRS, IMM, 13402 Marseille, France

Present Address:
P.-P. Liebgott
Aix-Marseille Université, CNRS/INSU, MIO, 13288 Marseille, France

Present Address:
M. Rousset
Consulate General of France, 205 N Michigan Ave, Chicago, IL 60601, USA

Published online: 15 October 2014

FTIR Spectroscopy of Metalloproteins

Oscar Gutiérrez-Sanz, Olaf Rüdiger, and Antonio L. De Lacey

Abstract

Absorption of infrared radiation by proteins gives important information about their structure and function. The most intense infrared bands correspond to the overlap of all the peptide bond absorption. Additionally, in many metalloproteins their prosthetic groups have intrinsic ligands or bind substrates/inhibitors that absorb intensively in the infrared. Here, we describe thoroughly several Fourier transform infrared methods for studying structure–function relationships in metalloproteins, using hydrogenases as an example.

Key words Metalloenzymes, Infrared, Spectroelectrochemistry, SEIRA, Hydrogenase

1 Introduction

Absorption of infrared radiation by proteins gives important information about their structure and function. Functional groups of proteins are detected in the infrared spectra when they are changes of the dipole moment of one or more of their vibrational modes [1]. The most intense infrared bands of a protein correspond to the amide I and amide II ones, which correspond to the overlap of all the peptide bond absorption. The amide I band is mostly due to the carbonyl stretching vibrations, which have frequencies in the range of 1,630–1,680 cm^{-1} dependent on the protein secondary structure [2]. The amide II band is mostly due to the bending mode of N-H in peptide bonds, their frequency being around 1,550 cm^{-1} [2]. Some functional groups of amino acid residues can also be detected by infrared absorption, such as thiols, carboxylic acids, and aromatic rings, although their band intensities are very weak. A further complication for infrared spectroscopy of proteins in solution is the strong absorption by water, which leaves only a narrow window of the spectrum for analysis [2]. This problem can be tackled in different ways. Dissolving the protein in deuterated water allows shifting the operational spectral window

Juan C. Fontecilla-Camps and Yvain Nicolet (eds.), *Metalloproteins: Methods and Protocols*, Methods in Molecular Biology, vol. 1122, DOI 10.1007/978-1-62703-794-5_7,